Progress in bioplastics blends, compatibilization, modifications, and AI-driven innovations for material applications

Shorey, Rohan; Esmizadeh, Elnaz; Mekonnen, Tizazu H.

Publisher's version / Version de l'éditeur:
https://doi.org/10.1016/j.progpolymsci.2025.102064
Progress in Polymer Science, 173, C, pp. 1-31, 2025-12-10

Progress in Polymer Science 173 (2026) 102064

Contents lists available at ScienceDirect

Progress in Polymer Science

journal homepage: www.elsevier.com/locate/progpolymsci

Progress in bioplastics blends, compatibilization, modifications, and AI-driven innovations for material applications

Rohan Shorey[a], Elnaz Esmizadeh[b], Tizazu H. Mekonnen[a,*]

[a] Department of Chemical Engineering, Institute of Polymer Research, Waterloo Institute of Nanotechnology, University of Waterloo, Waterloo, ON, Canada
[b] Facade Systems and Products group, Construction Research Centre, National Research Council Canada, 1200 Montreal Rd, Ottawa, ON, K1A0R6, Canada

ARTICLE INFO

Article history:
Received 26 May 2025
Revised 7 November 2025
Accepted 9 December 2025
Available online 10 December 2025

Keywords:
Bioplastic blends
Compatibilization
Biodegradability
Recyclability
Artificial intelligence

ABSTRACT

Many bioplastics offer potential advantages over petroleum-based plastics, such as renewability, improved sustainability, and, in some cases, biodegradability or lower toxicity. However, in most cases, their limited mechanical performance, processing stability, or higher production costs hinder widespread adoption. Blending is a key strategy to overcome these limitations; however, the inherent immiscibility of most biopolymers leads to challenges like coarse morphology and poor interfacial adhesion. This review aims to provide an in-depth analysis of bioplastic blends by examining the fundamental principles (thermodynamic interactions, process kinematics, and morphology development) that control their behavior. It critically evaluates a broad spectrum of compatibilization strategies that span non-reactive and reactive methods and those utilizing nanofillers, aimed at stabilizing blend microstructures and enhancing material performance. A novel aspect of this work is its integration of these material science concepts with important end-of-life considerations, including biodegradability and recyclability challenges. Furthermore, it highlights the transformative role of artificial intelligence (AI) and machine learning (ML) as novel instruments for accelerating the design and optimization of next-generation bioplastic formulations. Overall, this review concludes that unlocking the full potential of bioplastics for high-performance industrial applications necessitates a holistic approach that integrates tailored blending strategies with advanced computational design, thus paving the way for the realization of a circular bioeconomy.

1. Introduction

Bioplastics, novel materials of the 21st century, play a crucial role in transitioning towards a more sustainable and circular economy [1,2] . Concerns associated with environmental degradation and efforts to reduce the carbon footprint of conventional plastics are catalyzing an interest in the development and utilization of bio-based and biodegradable plastics [3]. Bioplastics encompass a diverse family of polymers, from bio-based and biodegradable plastics like polylactic acid (PLA), starch, and polyhydroxyalkanoates (PHAs) [4], to bio-based non-biodegradable polymers such as biopolypropylene (Bio-PP), bio-polyethylene (Bio-PE), and further on to petrochemical-sourced but biodegradable bioplastics like polybutylene adipate co-terephthalate (PBAT) [3].

While the bioplastics market has grown steadily in recent years, their current production volume remains relatively small compared to the vast output of conventional plastics. However, Fig. 1b displays that bioplastic production is expected to hit a five-fold increase (4605 thousand metric tons) by 2028 [5–7]. Furthermore, the growth in the utilization of bio-based/non-biodegradable plastics has been projected to be triple (2827 t) in 2028 from its pro-

List of abbreviations: AI, Artificial Intelligence; ANN, Artificial Neural Networks; Bio-PE, Bio-Polyethylene; Bio-PET, Bio-Polyethylene Terephthalate; Bio-PP, Bio-Polypropylene; Bio-PTT, Bio-Polytrimethylene Terephthalate; Ca, Capillary Number; CNT, Carbon Nanotube; De, Deborah Number; ΔG_m, Gibbs Free Energy of Mixing; ΔH_m, Enthalpy of Mixing; ΔS_m, Entropy of Mixing; EPDM, Ethylene Propylene Diene Monomer; ESAO, Epoxy-based Styrene-Acrylic Oligomer; GCT, Group Contribution Theory; IFR, Imbedded Fiber Retraction; IPN, Interpenetrating Network; LSSVR, Least-Squares Support Vector Regression; MA, Maleic Anhydride; MFI, Melt Flow Index; ML, Machine Learning; MLP-ANN, Multilayer Perceptron Artificial Neural Network; MLPNN, Multilayer Perceptron Neural Network; Mw, Molecular weight; MWCNT, Multiwalled Carbon Nanotubes; NR, Natural Rubber; OWK, Owens-Wendt-Kaelble; PA-11, Polyamide-11; PBAT, Polybutylene Adipate-co-Terephthalate; PBSA, Poly(butylene succinate-co-adipate); PC, Polycarbonate; PCL, Polycaprolactone; PE, Polyethylene; PEBA, Poly (ether-b-amide); PEF, Polyethylene Furanoate; PEO, Polyethylene Oxide; PGA, Polyglycolic Acid; PGMA, Poly(glycidyl methacrylate); PHB, Poly(3-hydroxybutyrate); PHBV, Poly(3-hydroxybutyrate-co-3-hydroxyvalerate); PLA, Polylactic Acid; PLLA, Poly(L-lactic acid); PVA, Polyvinyl Alcohol; PUR, Polyurethane; SP, Sepiolite; T_g, Glass Transition Temperature; TPS, Thermoplastic Starch; UDC, Universal Dynamic Crosslinker; USC, Universal Static Crosslinker; Re, Reynolds Number; s, Interfacial Tension; ?, Viscosity.

* Corresponding author.
E-mail address: tmekonnen@uwaterloo.ca (T.H. Mekonnen).

https://doi.org/10.1016/j.progpolymsci.2025.102064

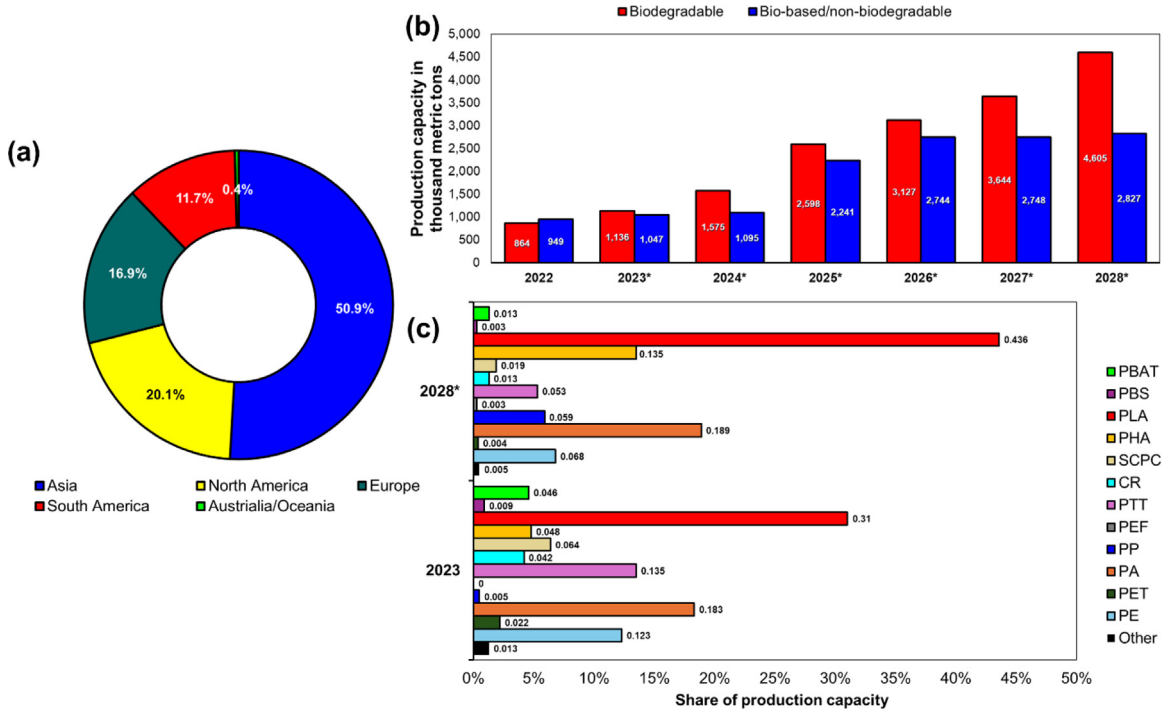

Fig. 1. Worldwide production capacity of bioplastics. (a) Regional distribution [8], Copyright 2023. Adapted with permission from Statista. (b) Classification by biodegradability [7], Copyright 2023. Adapted with permission from Statista. (c) Breakdown by polymer type [6], Copyright 2022. Adapted with permission from Statista.

duction capacity in 2022. Geographically, the bioplastics industry in being led by Asia, accounting for 50.9 % of the total production capacity. The dominating share (around 30 %) of PLA in the present market has been predicted to be maintained through 2028, whereas, PHAs have been predicted to exhibit significant growth (Fig. 1c) [5–7]. This growing trajectory of bioplastics highlights the urgent need to address the technical challenges that are limiting the wide-scale application of these promising materials across industries.

Despite the numerous advantages, a significant gap exists between the theoretical potential of the bioplastics and their practical large-scale employment. This gap stems from the challenges associated with bioplastic production and utilization, including cost-effectiveness in comparison to conventional plastics, inferior thermal stability, narrow processing window [9], slow crystallization [10]. Thus, research and innovation aimed at overcoming these limitations via blending with each other [11,12], development of biocomposites and nanocomposites [13,14], as well as strategies for enhancing compatibility, plasticization [15] is critical for advancing the performance, scalability, and industrial viability of bioplastics.

Among the various efforts, blending bioplastics offers a flexible and versatile approach to creating sustainable materials with tailored material properties and optimal cost structure [16,17]. However, this solution introduced a thermodynamic challenge inherent to traditional polymer blends, where polymer blend miscibility or compatibility is an exception [18,19]. The inherent immiscibility between different biopolymers often leads to phase separation, which adversely affects the mechanical properties and stability of the resulting materials [20]. Further, to mitigate the challenges of immiscibility, compatibilization approaches are extensively employed to effectively reduce the interfacial tension between the disparate biopolymers [21]. This promotes better adhesion and dispersion within the polymer matrix, thus enhancing the morphology development and flow properties of the resulting blends [22].

The novelty of this work lies in its integrated approach, combining fundamental polymer science, compatibilization techniques, end-of-life considerations (biodegradability and recyclability), and cutting-edge AI-driven design paradigms. The primary objective of this work is to provide academic researchers and industrial practisioners with a comprehensive roadmap. By covering the current state of knowledge and highlighting future pathways, this work aims to empower the scientific community to design next-generation, high-performance cost-effective bioplastic blends tailored for specific applications.

2. Fundamentals of polymer blending

Polymer blends are vital for optimizing properties and reducing costs in the plastics industry. Commercially successful traditional polymer blend examples include Santoprene® (ExxonMobil), a polypropylene (PP) matrix with dispersed ethylene propylene diene monomer (EPDM) [23], and Zytel® ST-801 (DuPont), where sub-micron EPDM rubber droplets enhance Nylon 6,6 toughness [24]. Examples of commercial bioplastic blends include Ecoflex® (BASF, Germany), which is based on confidential biopolymer blends including PLA and PBAT, and Mater-Bi (Novamont, S.p.a, Italy), a blend of biodegradable thermoplastics (corn starch, vegetable oil derivatives, and biodegradable synthetic polyester) [25].

Most polymer blends are immiscible in the melt state or may phase separate (i.e., undergo coarsening) during solidification [26]. The blend microstructure, established during compounding, can further evolve during secondary processing steps such as injection and compression molding, fiber spinning, and film forming. As described in D. R. Paul's seminal textbook on polymer blends, "immiscibility is the rule and miscibility is the exception", highlighting the rarity of miscible melt-processed blends that do not form phase-separated microstructures [20].

This immiscibility exhibited by the polymeric fractions stems from their high molecular weights reducing the entropy of mixing, incompatible chemistries limiting chain interactions, and unfavorable enthalpy changes (ΔH_m), leading to a positive Gibbs free

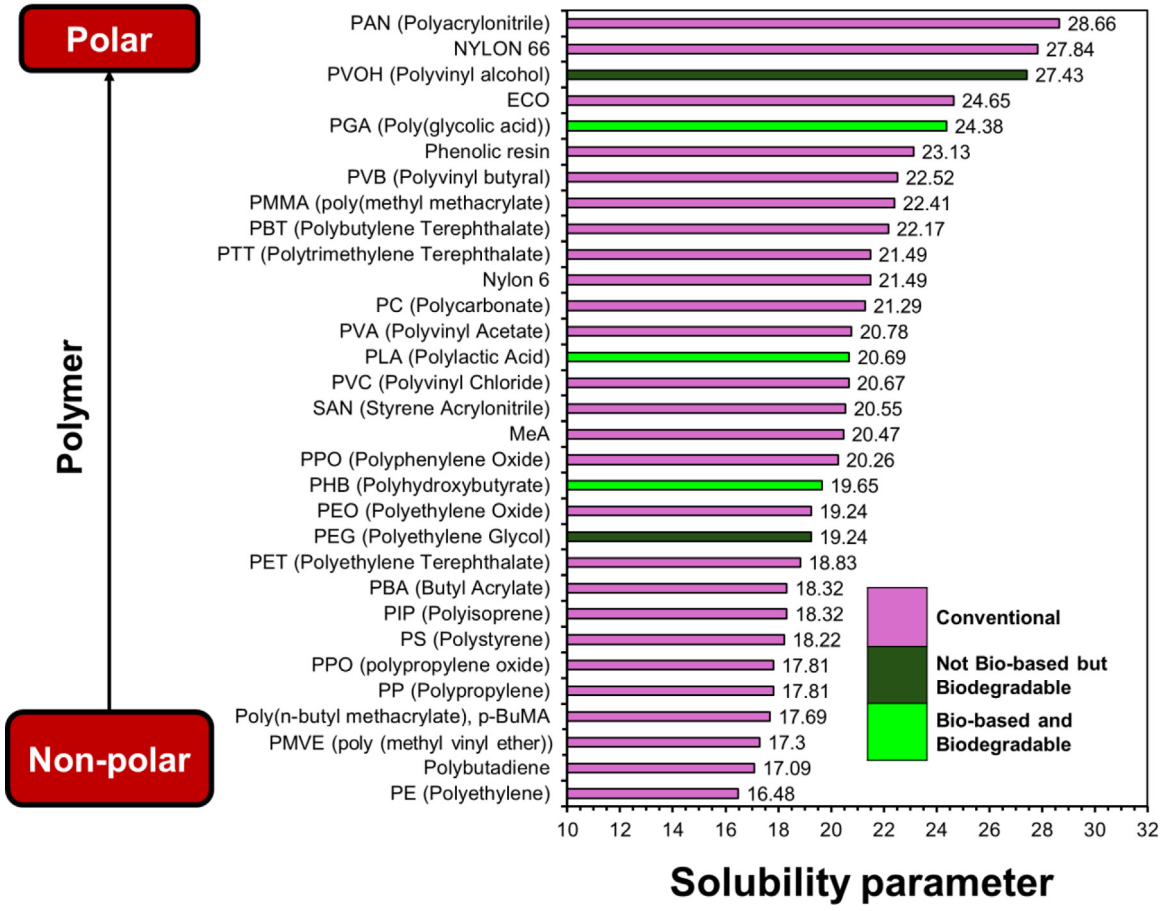

Fig. 2. Solubility parameter values for polymers calculated using GCT [27], Copyright 2006. Adapted with permission from Destech Publications Inc.

energy of mixing (ΔG_m), as described by Eq. (1):

$$\mathbf{\Delta G_m = \Delta H_m - T\Delta S_m} \quad (1)$$

where T is the temperature, ΔH_m is the enthalpy of mixing, and ΔS_m is the entropy of the mixture. Miscibile polymer blends are indicated when $\Delta G_m \langle$ 0, while $\Delta G_m \rangle$ 0 indicates immiscibility. For nonpolar polymers, ΔH_m is typically positive, making miscibility reliant on the entropy term.

2.1. Solubility parameter for predicting polymer miscibility

Various methods have been developed to predict the miscibility of polymer components in a blend. Mike Coleman and Paul Painter were leaders in the advancing the use of Group Contribution Theory (GCT) for estimating solubility parameters and interaction parameters (Hansen or Hildebrand) based on the chemical structures of polymers, accounting for hydrogen bonding and other molecular interactions [27]. These parameters can then be used to quantify the ability of one polymer to interact with another. To compare the solubility of polymers, the classical GCT developed by Hildebrand can be employed [28] . In this approach, the solubility parameter (δ) is calculated (Eq. (2)) as:

$$\delta = 4.1\left(\frac{\gamma}{(M/\rho)^{1/3}}\right)^{0.43} \quad (2)$$

where ρ is density, M is molecular weight and γ is surface tension. The solubility parameters values of several polymer systems employing GCT have been calculated and illustrated in Fig. 2. The respective systems have been ordered from non-polar polymers to their polar counterparts [41]. It can be noted from Fig. 2 that polyolefins like polyethylene (PE) and polypropylene (PP) are highly non-polar, with weak specific interaction values of 16.48 $(J/cm^3)^{1/2}$ and 17.81 $(J/cm^3)^{1/2}$, respectively. On the other hand, polyacrylonitrile (PAN) and nylon 6,6 are polar, with strong specific interaction values of 28.66 $(J/cm^3)^{1/2}$ and 27.84 $(J/cm^3)^{1/2}$, respectively. Among the biopolymers, poly(glycolic acid) (PGA), a biodegradable and thermoplastic aliphatic polyester, displays strong polarity with an interaction parameter of 24.38 $(J/cm^3)^{1/2}$ compared to polyhydroxybutyrate, a bacterial polyester exhibiting a characteristic nonpolar interaction parameter of 19.65 $(J/cm^3)^{1/2}$. While no definitive miscibility parameter value guarantees polymer blend miscibility, proximity in the parameter values of the blend constituents is considered favorable for miscibility and compatibility.

2.2. Importance of interfacial energy

Polymer blend miscibility is influenced by interfacial energy between the components. A miscible system forms a single phase with near-zero free energy of mixing, while immiscible blends form two phases, which may be either “compatible” or “incompatible” with high interfacial tension as illustrated in

$$\frac{\mathbf{\Delta G_m}}{\mathbf{V}} = \mathbf{RT}\left[\frac{\rho_A\phi_A}{M_A}\ln\phi_A + \frac{\rho_B\phi_B}{M_B}\ln\phi_B\right] + \chi_{AB}\frac{\mathbf{RT}}{\mathbf{V_{ref}}}\phi_A\phi_B \quad (3)$$

In the above equation, the first two logarithmic terms denote combinational entropy of mixing, while the third term represents the enthalpy of mixing. For polymers with infinite molar mass, the entropy contribution is small, making the system’s miscibility primarily dependent on the enthalpy of mixing. If the parameter χ

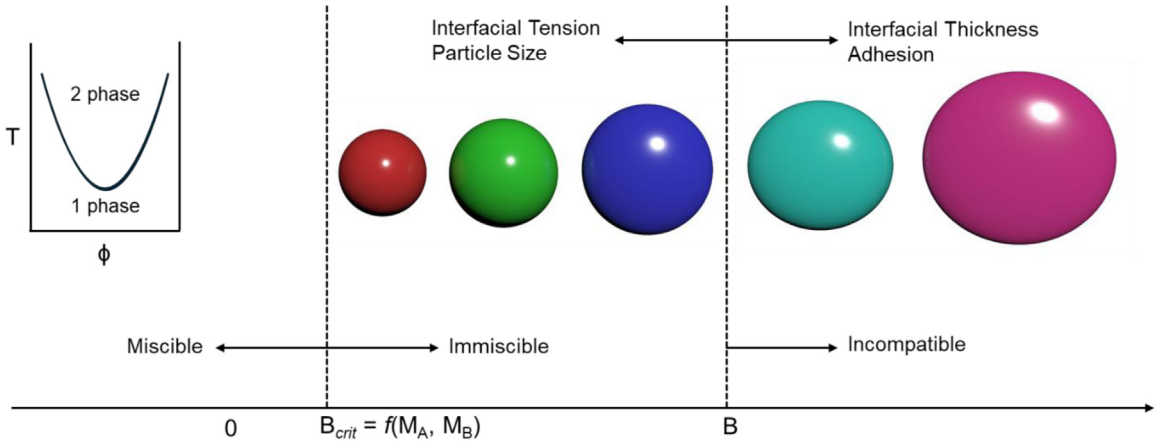

Fig. 3. Miscibility and polymer-polymer interaction energy [20], Copyright 2012. Adapted with permission from Elsevier Science Ltd.

is negative, the system exhibits miscibility ($\Delta H_m < 0$). Miscibility occurs when $\chi < \chi_{crit}$, where χ_{crit} is the critical χ value which is a function of the molecular weight of the components and it can be expressed as (Eq. (4)) [30] :

$$\chi_{crit} = \frac{1}{2}\left(\frac{1}{\sqrt{r_1}} + \frac{1}{\sqrt{r_2}}\right)^2 \tag{4}$$

where r denotes the number of polymer segments, which is proportional to the degree of polymerization.

As shown in Fig. 3, higher interfacial tension (σ_{12}) typically increases the dispersed-phase particle size. Interfacial tension, which defines interaction energy, can be measured directly using the pendant drop method or estimated from the surface tensions of the blend components. The pendant drop method is widely employed for its accuracy and time-consuming nature [31]. Empirical equations and surface tension-based models are alternative methods for interfacial tension estimates [32–34]. The interfacial tension can be influenced by several factors during melt blending, including phase miscibility between the dispersed phase and the matrix phase, the effects of compatibilizing additives that migrate to the interface, and interfacial reactions (e.g. in situ grafting and transesterification). Further, experimental errors, model assumptions, and empirical parameters can impact the design and performance of polymer blends [35,36]. For instance, Biresaw et al. reported an interfacial tension value of 5.4 ± 1.3 dyn/cm for a PLA/PS blend using the imbedded fiber retraction (IFR) method [45], consistent with Luciani's solubility parameter-based empirical equation (4.4 dyn/cm) and Antonoff's equation (3.0 ± 1.4 dyn/cm), respectively [37–41]. Interfacial tension can also be calculated from the surface tensions of the two polymers in a blend. For nonpolar-polar systems, the Owens-Wendt-Kaelble (OWK) equation (Eq. (5)), based on the Geometric mean, is commonly used:

$$\gamma_{12} = \gamma_1 + \gamma_2 - 2\left[\sqrt{\gamma_1^D \gamma_2^D} + \sqrt{\gamma_1^P \gamma_2^P}\right] \tag{5}$$

Wu's equation utilizes the harmonic or "reciprocal" mean (Eq. (6)) [42] :

$$\gamma_{12} = \gamma_1 + \gamma_2 - 4\left[\frac{\gamma_1^D \gamma_2^D}{\gamma_1^D + \gamma_2^D} + \frac{\gamma_1^P \gamma_2^P}{\gamma_1^P + \gamma_2^P}\right] \tag{6}$$

In a study by Tadele et al., OWK and Wu's equations were utilized for calculating the interfacial tension values of corn zein protein (modified and baseline) blends with PBAT, as presented in Table 1 [12].

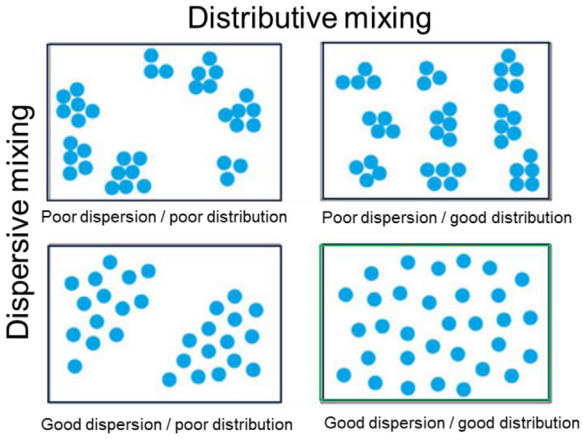

Fig. 4. Dispersive and distributive mixing [43], Copyright 1997. Adapted with permission from John Wiley & Sons Inc.

2.3. Impact of kinematics (Rheology and processing)

The morphology development of polymer melt blends strongly depends on mixing process efficiency in an extruder or forming process. As illustrated in Fig. 4, dispersive mixing is where particles or droplets break up into daughter particles or droplets when deformed or subjected to critical stress. Distributive mixing on the other hand, is the movement of particles or droplets in the matrix toward a more uniform or random arrangement. Melt compounding systems accomplish both types of mixing through shear and extensional flows. Process time, temperature, and the shear or extension history (imparted by the extrusion) for all processing steps is critical in the quantification of dispersive and distributive mixing performance. Minor phase droplet breakup occurs in fluids in shear or extensional flows when there is sufficient deformational strain and stress. Flow-induced coalescence can also occur as droplets collide in the flow field [43].

Even miscible blends in melt processing require dispersive breakup of domains and distributive mixing. Most systems are diffusion-limited within process residence times and miscible polymer blends may not be molecularly mixed at the exit of polymer processing equipment, such as an extruder or in a mold cavity. To diffusion limitation can be overcome by utilizing advanced compounding techniques like reactive extrusion, high-shear mixing, and compatibilizers [44,45]. Further, subjecting the extrudate to post-processing techniques (thermal or solvent annealing) could aid in enhancing diffusion [46,47]. Mixing design, including the ex-

Table 1
mZein/PBAT interfacial tension values [12].

Sample	Zein (wt %)	mZein (wt %)	PBAT (wt %)	OWK equation (mN/m)	Wu equation (mN/m)
Zein/PBAT (70/30)	70	-	30	6.12	3.614
Zein/PBAT (50/50)	50	-	50	5.571	1.673
Zein/PBAT (30/70)	30	-	70	1.896	3.022
mZein/PBAT (70/30)	-	70	30	0.352	1.663
mZein/PBAT (50/50)	-	50	50	1.029	0.495
mZein/PBAT (30/70)	-	30	70	1.975	0.037

truder screw length to height of flight, helix angle, ratio of pressure flow and drag flow, and the direction of the shearing plane is critical to achieve efficient dispersion and distribution of component polymers in blends [48].

3. Morphology of bioplastic blends

The morphology of polymer blends plays a crucial role in determining their mechanical, thermal, and barrier properties. For miscible blends, a single-phase homogeneous morphology is typically observed, resulting in uniform properties throughout the material. However, in partially miscible or immiscible blends, phase separation often leads to a heterogeneous morphology with distinct domains corresponding to each component. In general, the morphology of an immiscible polymer blend formed during melt processing is governed by constituent material properties, thermodynamic interactions between components and the kinematics of the process. The critical factors that control morphological development and stability are viscosity and volume ratio of component polymers, interfacial tension or energy between phases, and processing methods and conditions that drive the dispersion and coalescence of components [49–51].

In the case of bioplastic blends, miscibility is rare due to the inherent chemical and structural differences between many biopolymers. Certain grades of PHA, such as poly(3-hydroxybutyrate) (PHB) can mix homogeneously with PLA, leading to improved ductility and thermal properties. PHAs are biodegradable linear polyesters derived from microorganisms, with PHB being the most common form. The miscibility of PLA/atactic PHB blends typically depends on the molecular weight of PHB, with lower molecular weight PHB leading to better miscibility and enhanced crystallization of PLA, while higher molecular weight PHB causes immiscibility [52,53]. Iannace et al. studied PLLA/PHBV blends, finding that higher PHBV content reduced tensile strength but increased elongation at break [54].

Further, some hybrid bioplastic blends composed of a bioplastic and non-bioplastic component have been studied. A few of them have been discussed as follows:

- Poly(ε-caprolactone) (PCL) and Poly(vinyl acetate) (PVAc): The miscibility of PCL with PVAc was investigated using DSC, revealing a single transition temperature across the entire composition range. This blend forms transparent material with improved flexibility and processability [55,56].
- Poly(3-hydroxybutyrate) (PHB) and poly (vinyl acetate) (PVAc): This blend is miscible across the entire composition range, exhibiting a single glass transition temperature that varies with composition. The addition of PVAc increases nucleation density and crystallization rates at higher temperatures, while reducing crystallization and toughening the composite at temperatures near the glass transition, enhancing its resistance to embrittlement at room temperature [57,58].
- Poly(lactic acid) (PLA) and polyethylene glycol (PEG): PEG acts as an effective plasticizer for PLA, due to its biocompatibility, low cost, and ability to enhance PLA's ductility and flexibility. However, the miscibility of PEG depends on its molecular weight and concentration. Molecular dynamic simulations revealed that PLA and PEG are miscible at low PEG concentrations (10–30 wt %) but become immiscible at higher concentrations (>50 wt %) [59–61].

Melt blending of two immiscible polymers commonly leads to two main types of blend morphologies, i.e. dispersed and co-continuous (Fig. 5). The morphology of blends also depends on the blend concentration. Dispersed morphology occurs in asymmetric compositions, where the lower-viscosity major component forms the continuous phase (or matrix), and the higher-viscosity minor component forms the dispersed phase [62,63]. Dispersed morphology can form various structures like droplets for enhanced toughness or fiber-like and lamellar structures for improved barrier properties [64]. During blending, pellets of the dispersed phase stretch into sheets, which then break into fibers, and eventually into particles. Stopping the process at different stages can yield various morphologies, such as laminar, fiber/matrix, or particle/matrix [65]. The dispersed phase usually forms a droplet morphology characterized by an average diameter (D_d) or a particle size distribution (PSD).

In contrast, a co-continuous morphology forms near-symmetric blend compositions (e.g., 55/45, 50/50, 45/55) and is suitable for electrical and many other high-performance material applications [64]. Co-continuous morphology can also form a 3D network of both phases, providing continuous pathways through the entire blend, known as an interpenetrating network (IPN). Co-continuous morphology emerges at or near the phase inversion point of dispersed morphology during melt compounding, where the dispersed phase transitions into a continuous network [20,66] . This phenomenon typically occurs within a narrow range of approximately ±5 vol. % around the phase inversion point (Fig. 6). This morphology is particularly appealing due to its ability to combine the properties of individual components effectively. However, it is a non-equilibrium structure therefore inherently unstable, undergoing filament break-up and retraction as soon as the polymer melt blend exits the mixer. To preserve the co-continuous morphologies, interfacial tension between phases need to be reduced. This can be achieved by utilization of compatibilizers that reduce interfacial energies and suppress coalescence. Also, the use of nanoparticles as stabilizers for preserving co-continuous structures has been reported in literature [67]. Further, rapid quenching after mixing can help "freeze" the co-continuous structure, before filament breakup occurs [68,69].

Paul and Barlow defined the phase inversion point as the condition where the viscosity ratio of the components equals the volume ratio [20]. It was refined by Kitayama and Paul [66], as follows (Eq. (7)):

$$\frac{\phi_A}{\phi_B} = 0.887\left(\frac{\eta_A(\dot{\gamma}, T)}{\eta_B(\dot{\gamma}, T)}\right)^{0.29} \quad (7)$$

where ϕ is the volume fraction. The morphology of an immiscible polymer blend fabricated by melt processing is governed by constituent material properties, volume ratio, interfacial tension, and processing conditions, requiring careful consideration.

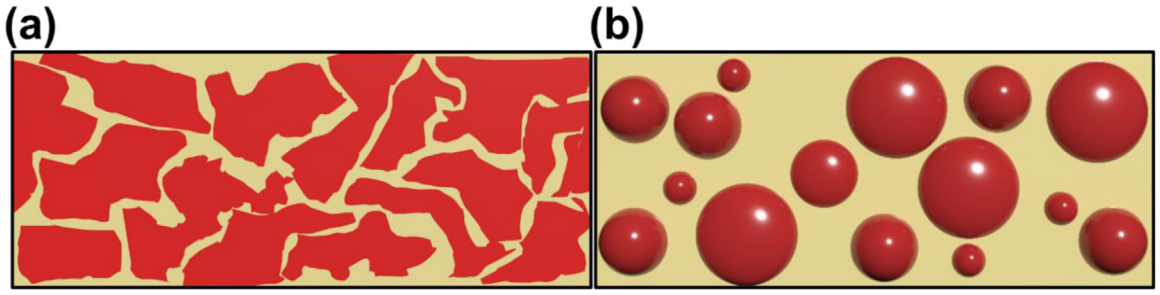

Fig. 5. Morphologies of immiscible blends with (a) Co-continuous and (b) Dispersed.

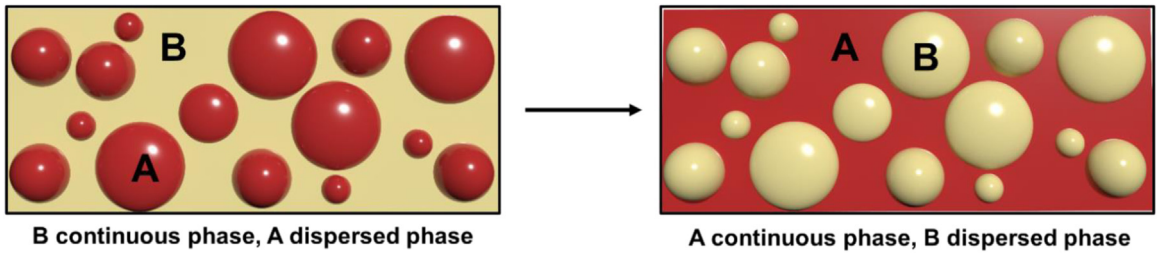

Fig. 6. Phase inversion in immiscible polymer blends.

3.1. Morphology development and mixing regimes

Morphology development strongly depends on the mixing conditions in the extruder or subsequent forming processes. During the mixing, the domains of each component are deformed by the applied flow field, resulting in elongated particles of the dispersed phase, which are essential for forming a fully continuous phase (when the volume fraction of the minor phase is below 0.7). The stability of these elongated structures depends on their aspect ratio ($^{l}/_{d}$) and the local Capillary number (Ca), which is described by Eq. (8) [68].

$$\mathbf{Ca} = {}^{\boldsymbol{\gamma}\,\boldsymbol{\eta}_{\mathbf{m}}\mathbf{d}}/_{\boldsymbol{\sigma}_{12}} \tag{8}$$

where the process kinematics are captured with the shear stress $\tau = \gamma \eta_m$, and the thermodynamic interactions with the interfacial tension σ_{12}.

During mixing, when Ca is high, shear stress dominates interfacial stress, causing particles to stretch. The elongation of dispersed-phase particles is governed by the conservation of volume, with the diameter of the resulting elongated cylinder being a function of deformation. As the elongation progresses, the Ca decreases with increasing $^{l}/_{d}$. Once the critical capillary number (Ca_{crit}) is reached, interfacial stress destabilizes the elongated particles, leading to break up. This behavior divides the mixing process into two distinct regimes:

- Distributive mixing ($Ca < Ca_{crit}$) occurs where shear stress significantly exceeds interfacial stress, allowing droplets to stretch into stable, slender threads without breaking. This enables the formation of co-continuous morphologies over a broad range of compositions.
- Dispersive mixing ($Ca >> Ca_{crit}$) occurs when interfacial stress becomes significant, causing surface disturbances on the threads to grow, leading to droplet break-up. As a result, co-continuous morphologies are only achievable at high-volume fractions.

Compounding systems accomplish both types of mixings through shear and extensional flows. Key factors include process time, temperature, and the shear or extension history. Minor phase breakup occurs under sufficient deformational strain, while flow-induced coalescence may occur as dispersed phases collide in the flow field [20,70]. Even miscible blends in melt processing require both dispersive and distributive mixing types. However, diffusion limitations during typical process residence times often prevent full molecular mixing upon exiting processing equipment.

3.2. Evolution of morphology

3.2.1. Dispersed-phase morphology structure breakup/coalescence

The flow of polymer melts in a compounding or shaping/forming system is laminar, typically with a very low Reynolds number ($Re << 1$). Under shear or extension, droplets undergo an affine deformation, stretching into a thread or sheet (as illustrated in Fig. 7) and Rayleigh instability occurs, and the thread breaks into daughter droplets.

Grace et al. explored and quantified the dispersive mixing of immiscible Newtonian fluids [72]. The classical breakup mechanisms were studied extensively, and the famous Grace curve was established as shown in Fig. 8**.** The Grace curve illustrated the relationship between droplet breakup in simple shear, the Capillary number, Ca, and the viscosity ratio. Grace showed that droplet breakup occurs when the Ca versus viscosity ratio falls within or above the curves. The rule of thumb from Grace's research on immiscible Newtonian model fluids is that if the viscosity ratio exceeds 3.5, no breakup occurs (Fig. 8). This explains why twin-screw compounding extruders are highly effective and efficient in dispersive mixing of immiscible polymers or rubbers.

Wu investigated droplet breakup in non-Newtonian viscoelastic polymer melts during extrusion compounding [74]. The results revealed that for non-Newtonian systems the dispersion window broadened, and the dispersed phase droplet breakup occurred even at viscosity ratios above 3.5, unlike Newtonian systems. This work shows that twin-screw compounding is very effective in dispersing immiscible, incompatible polymers. A predictive equation for droplet size (Eq. (9)) incorporating viscosity ratio, interfacial tension, and stress was also developed [74].

$$\mathbf{D_d} = \frac{4\boldsymbol{\gamma_{dm}}(\boldsymbol{\eta_d}/\boldsymbol{\eta_m})^{\pm 0.84}}{\boldsymbol{\eta_m}\boldsymbol{\gamma}} \tag{9}$$

where the power-law sign is + for $\eta_r > 1$ and – for $\eta_r < 1$ ($\eta_r = \eta_d/\eta_m$).

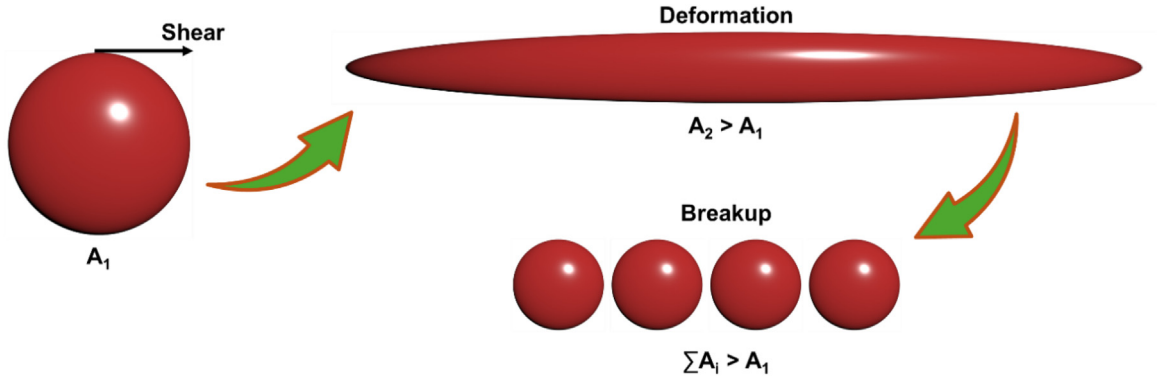

Fig. 7. Rayleigh instability and breakup, where A1 refers to the diameter of the initial (big) droplet and A2 is the transverse diameter of the thread or sheet under shear [71], Copyright 2004. Adapted with permission from American Physical Society.

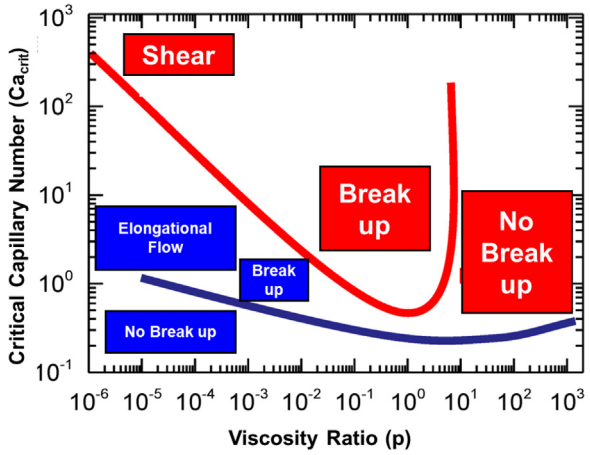

Fig. 8. Relation between Ca_{crit} and viscosity ratio (p) in polymer blends [73], Copyright 2020. Adapted with permission from Multidisciplinary Digital Publishing Institute.

Sundararaj et al. investigated the fundamentals of melting and dispersion of immiscible polymer blends using model polymers (polycarbonate (PC) in polyethylene (PE) matrix) with Couette cell experiments (Fig. 9) [75,76]. For a dispersed phase (polycarbonate) within a continuous (polyethylene) matrix, a surface erosion mechanism was observed, where droplets from the dispersed phase shed fragments into the surrounding matrix, as displayed in Fig. 9b

Fig. 10a shows the kinetics of erosive dispersion (PC in PE matrix), plotting relative droplet volume as a function of shear time [77]. The reduction in droplet volume exhibits fitting a first or second-order type kinetic expression. As is apparent from Fig. 10a, the system experienced minimal surface erosion and shedding under specific shear and temperature conditions [77].

They also studied stress behavior using the Deborah number ($De = \lambda \gamma$) defined as the ratio of the relaxation time and the characteristic process time, establishing criteria for breakup (Fig. 10b). Moreover, Sundararaj also observed another dispersion mechanism, vorticity alignment, and breakup, where normal force may develop at the north and south poles of a rotating droplet causing breakup or erosion perpendicular to the shear direction. Fig. 11 summarizes the four droplet breakup mechanisms: sheet breakup, erosion, tip-streaming, and vorticity-induced breakup.

Flow-induced coalescence is a kinematic process where droplets collide and merge within a flow field, as illustrated in Fig. 12. The process involves three steps: 1) droplets moving at different velocities collide or come into proximity with one another at some small distance (h_0), 2) the fluid drains between the drop to a critical gap (h_{crit}), and 3) the droplets join and form a larger droplet. Droplet breakups and coalescence often occur simultaneously. The evolution of the particle size distribution during the mixing process reflects the balance between dispersive mixing and coalescence.

Chester's classical model defines the probability that the coalescence of a blend in a shear flow will occur with the expression [72]:

$$\mathbf{Probability_c} \propto \mathbf{exp}\left(-\frac{\mathbf{D_d}\boldsymbol{\eta}_\mathbf{d}}{\mathbf{2h_c}\boldsymbol{\eta}_\mathbf{m}}\mathbf{Ca}^{3/2}\right) \tag{10}$$

where h_c is the critical gap height for draining (~5 nm). Coalescence is more likely when D_d is small, and η_d and Ca are low. Low Ca is associated with low η_m, low shear rate, and high interfacial tension. While Chester's model effectively relates material properties, particle size, and process kinematics to coalescence, it neglects the effect of dispersed phase concentration and interparticle distance [72,80]. Later advancements, particularly by Han Meijer et al. incorporated these additional variables, offering a comprehensive model for flow-induced coalescence [78–83]. The probability of coalescence of colliding droplets is described as the product of the probabilities of droplet collision and fluid drainage (Eq. (11)):

$$\mathbf{Probability_c} = \mathbf{P_{collision}P_{Drain}} = \mathbf{exp}\left(-\frac{\mathbf{t_{collision}}}{\mathbf{t_{process}}}\right) \mathbf{exp}\left(-\frac{\mathbf{t_{drain}}}{\mathbf{t_{interaction}}}\right) \tag{11}$$

where $t_{collision}$ is the kinematic time of a collision, $t_{process}$ is the characteristic process time interval, t_{drain} is the time for matrix fluid drainage between droplets, and $t_{ineraction}$ is the time of droplet interaction. Meijer modeled immobile, partially mobile, and fully mobile interfaces, thus, predicting the extent of deformation possible in droplets. Moreover, various empirical relations can be utilized for predicting the material properties of polymer blends, a few of which have been presented in Table 2.

In a work by Pesaranhajiabbas et al., the thermal, mechanical, and viscoelastic properties of various blend formulations of BioPBSA and PBAT were studied. The formulation with a homogeneous distribution of PBAT fractions demonstrated better material properties than its counterparts incorporating larger, nonhomogeneous PBAT particles. This improvement could be attributed to a higher interfacial area and improved interphase adhesion, which resulted in better stress transfer [91].

3.2.2. Evolution of co-Continuous morphology

The formation of co-continuous structures likely involves sheet formation, break-up, and local coalescence of the minor phase,

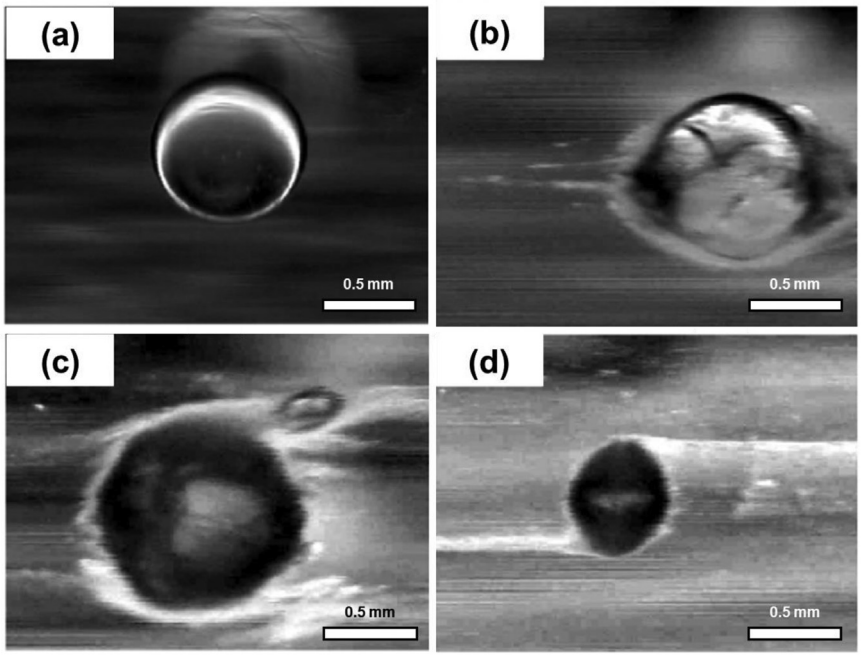

Fig. 9. Erosive dispersion process. (a) droplet rotation in a shear field, (b) droplet breakup by surface erosion and shedding, (c) fragment separation, and (d) incorporation of eroded film into the matrix [75], Copyright 2004. Adapted with permission from John Wiley & Sons Inc.

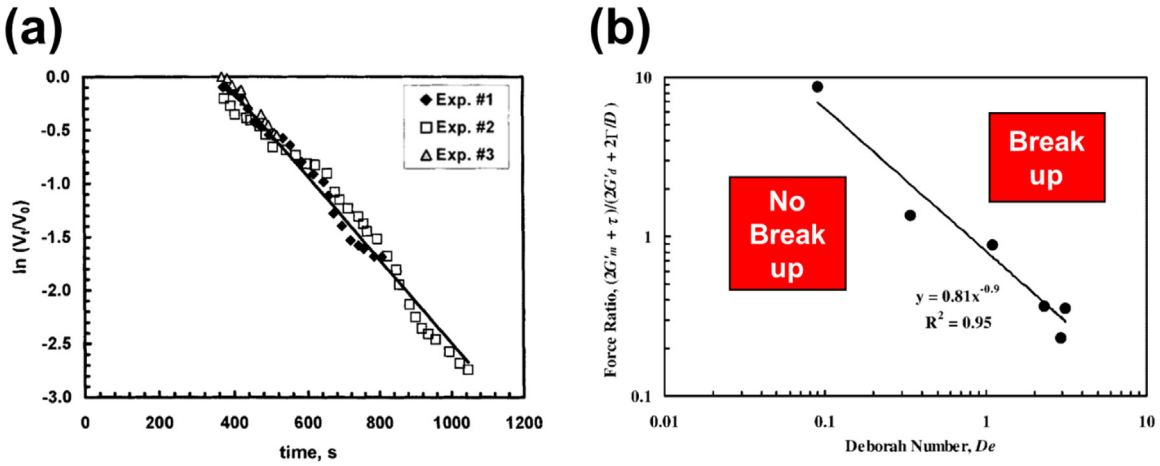

Fig. 10. (a) Erosion mechanism kinematics in an immiscible blend [77], Copyright 2004. Adapted with permission from John Wiley & Sons Inc. (b) Relationship between stress and Deborah number (De) [76], Copyright 2003. Adapted with permission from John Wiley & Sons Inc.

rather than simply packing elongated droplets into a continuous network. The condition Ca > 1 applies to the stability of elongated structures, regardless of their origin. These structures must remain stable during processing to achieve co-continuity [68]. Willemse et al. modeled a co-continuous morphology as densely packed elongated particles [68]. The lower limit of the volume fraction for co-continuity ($\phi_{d,cc}$) is expressed as:

$$\frac{1}{\phi_{\mathbf{d,cc}}} = 1.38 + 0.0213\left(\frac{\eta_{\mathbf{m}}\dot{\gamma}}{\sigma}\mathbf{R}_0\right)^{4.2} \quad (12)$$

where η_m is the viscosity of the matrix and R_0 is the equivalent sphere radius of the minor component. The equation suggested that the co-continuity is achievable at low-volume fractions when $\frac{\eta_m \dot{\gamma}}{\sigma}$ and R_0 parameters are sufficiently high. Increasing matrix viscosity stabilizes the filaments of the minor phase, enabling co-continuity at lower volume fractions.

In immiscible polymer blends with constant dispersed-phase viscosity, the onset of co-continuity is influenced by the viscosity of the matrix. For example, in PE/PS traditional blend, in series A with higher matrix viscosity, co-continuity occurs at 27 vol % PS, while in series B with lower matrix viscosity, co-continuity does not start until 56 vol % PS (Fig. 13).

In another study, they showed that increasing interfacial tension shifts the critical composition for the onset of co-continuity to higher concentrations, thereby narrowing the composition range. This effect arises from two counteracting factors: the stability of the co-continuous morphology and the phase dimensions, with stability playing a more significant role [68].

One application of co-continuous morphology is the production of porous structures from polymer blends for membrane and other applications. Sarazin et al. developed porous PLLA scaffolds from co-continuous bioplastic blends of PLLA and PCL using melt processing [93]. By controlling blend composition and annealing conditions, a wide range of co-continuous phase sizes was achieved (Fig. 14). Extracting the PCL phase resulted in fully interconnected porous PLLA, exhibiting high mechanical integrity. These scaffolds

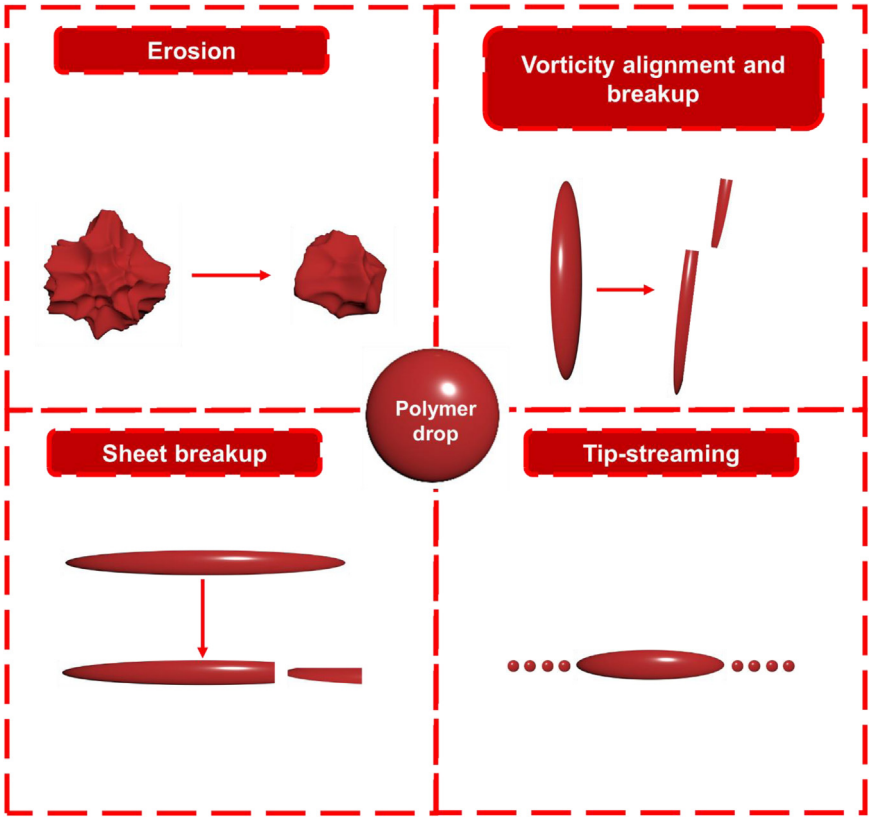

Fig. 11. Droplet breakup mechanisms in polymer melt.

Table 2
Empirical mixing rules for predicting material properties [86].

Property	Equation	Equation number	Ref.
Density (blend)	$\rho_{blend} = \sum_i w_i \rho_i$	(12)	[84,85]
Viscosity (blend)	$\eta^n_{blend} = \phi_A \eta^n_A + (1-\phi_A)\eta^n_B$	(13)	[86]
Viscosity (blend)	$\eta_{blend} = \phi_A^2 \eta_A + (1-\phi_A)^2 \eta_B + 2\phi_A(1-\phi_A)\eta_{AB}$	(14)	[87]
Viscosity (immiscible polymer blends)	$\log \eta = \log \eta_L + \Delta \log \eta^E$	(15)	[88]
	$\log \eta_L = -\log(1+\beta[\phi_A(1-\phi_A)]^{\frac{1}{2}}) - \log(\frac{\phi_A}{\eta_A} + \frac{1-\phi_A}{\eta_B})$	(16)	[88]
	$\Delta \log \eta^E = \eta_{max}[1 - \frac{(\phi-\phi_i)^2}{\phi(1-\phi_i)^2+\phi_i^2(1-\phi)}]$	(17)	[88]
Melt flow index	$MFI = \frac{k\pi\sigma PR^4}{8\eta L}$	(18)	[89]
M_w	$\frac{1}{MFI} = GM_w$	(19)	[90]

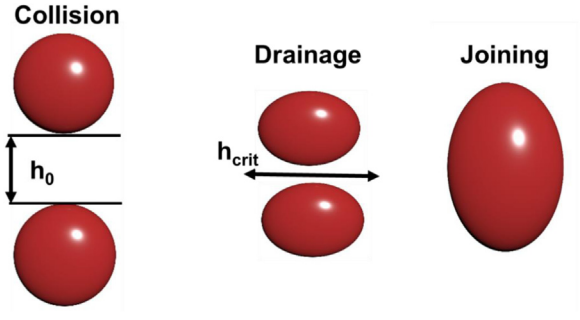

Fig. 12. Flow-induced coalescence in immiscible polymer blends.

demonstrated the ability to absorb up to 80 % of their porosity with water and successfully incorporate significant amounts of a model drug, bovine serum albumin (BSA), showcasing their accessibility to aqueous solutions and potential for controlled drug release. These findings highlight the suitability of this method for creating scaffolds for tissue engineering and drug delivery applications [93].

3.3. Effects of interfacial reactions and compatibilizers on morphology

Polymer systems with reactive components exhibit profoundly different morphology evolution and stability compared to non-reactive systems. In non-reactive systems, compatibilizers are intended to migrate to the interface, reducing interfacial tension to facilitate droplet breakup and minimizing the probability of coalescence [94]. Blends with interfacial reactions, including grafting and transesterification, can create a compatibilizing copolymer or moiety during the melt blending process [14,95,96]. Since viscous polymers are usually diffusion-limited, *in-situ* grafting depends on dispersive mixing, (i.e., deformation and breakup), to increase the interfacial area available for the reaction to occur [97]. The reaction "kinetics" is a function of the chemical reaction kinematic rate and the extent of interfacial area generation [97]. In many systems, the reaction rates are fast, so grafting "kinetics" are dominated by the dispersive mixing process [98]. Phase inversion can generate high

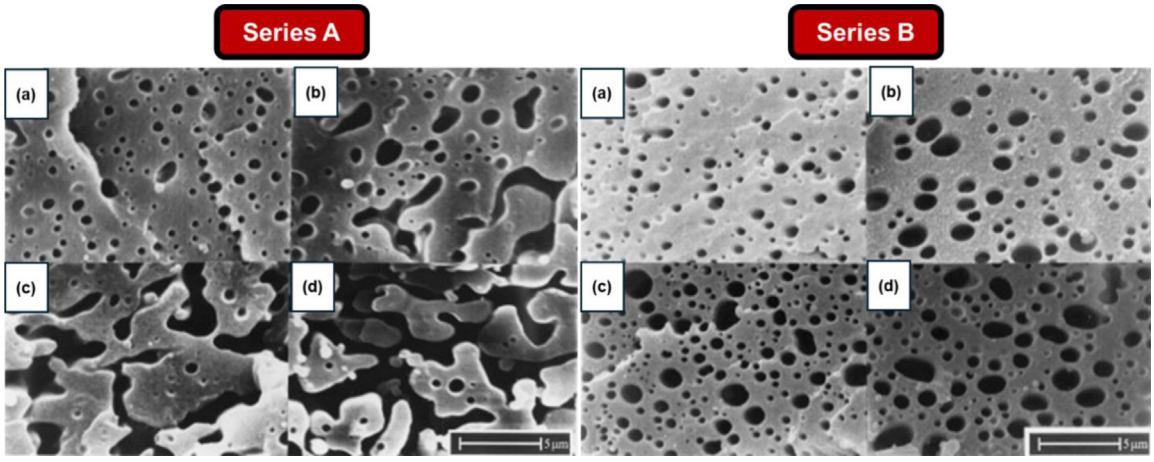

Fig. 13. SEM of PE/PS blends. (a) contains 17 vol % PS, (b) contains 27 vol % PS, (c) contains 35 vol % PS, and (d) contains 46 vol % PS [92], Copyright 1998. Adapted with permission from Elsevier Science Ltd.

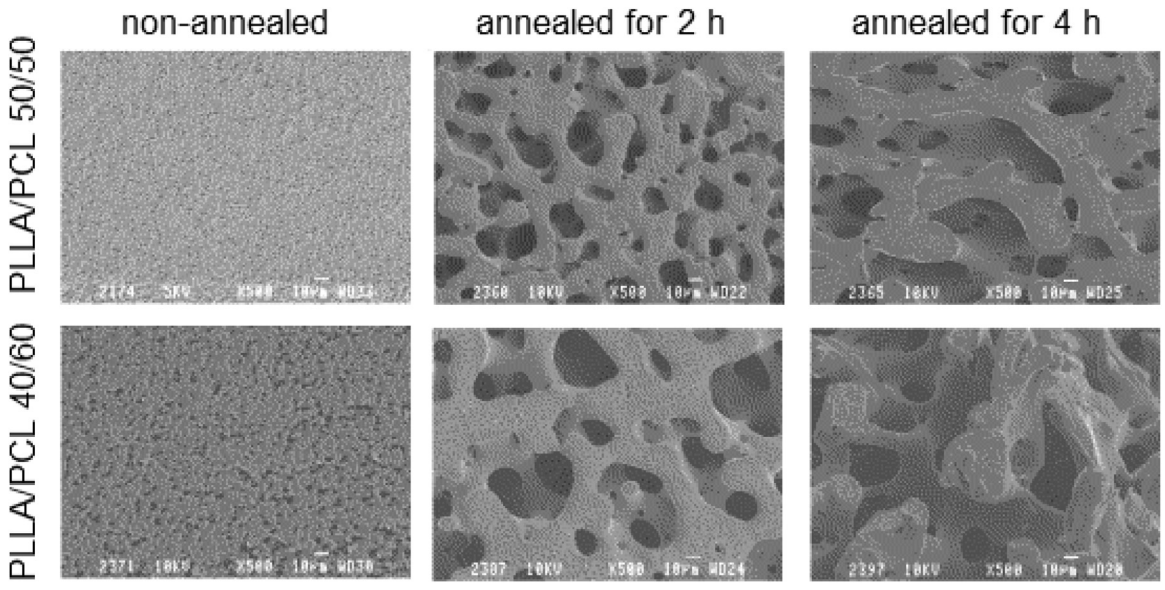

Fig. 14. Effect of annealing on the morphology of the PLLA scaffold from blends (after extraction of the PCL phase) [93], Copyright 2004. Adapted with permission from Elsevier Science Ltd.

interfacial areas efficiently, increasing the extent of the reaction. Grafting alters the melt viscosity, usually increasing it by retarding droplet rotation, which in turn influences morphology evolution.

Both deformation and breakup in a flow field increase the interfacial area, increasing the effective rate of reaction [49]. For rapid interfacial reactions, such as the amine–anhydride reaction, the overall grafting rate is primarily governed by interfacial area (Fig. 15). In contrast, if the reaction is slow, the grafting rate is controlled by both reactivity and mixing (Fig. 15) [99]. Slow systems are problematic in extrusion and compounding operations, making it essential to complete the grafting before the material exits the extruder.

4. Compatibilization strategies for bioplastic blends

Blending biopolymers offers a time-efficient and economical approach for developing novel materials with enhanced material properties, especially when compared to creating new polymers with new monomeric units and polymerization pathways [100]. The properties of biopolymer blends depend on the miscibility of their components, with strong interactions leading to homogeneity and weak interactions resulting in heterogeneous structures with agglomeration sites [101–107]. Like other polymeric blends, bioplastic blends can be categorized into three types based on their miscibility – completely miscible blends (which exhibit nanoscale homogeneity), partially miscible blends (which display a fine phase morphology with homogeneous individual phases), and fully immiscible blends (exhibit coarse morphology, poor interfacial adhesion, and sharp interfaces) [100]. They can also be classified according to the number of constituent polymers as binary, ternary, and quaternary blends, comprising two, three, and four different biopolymers, respectively. In literature, extensive work has been done on blending biopolymer and a few of the studies have been tabulated (Table 3).

However, the blends of bioplastics often exhibit inherent phase separations, coarse morphologies, and weak interfacial adhesion, leading to instability, poor tensile properties, and phase coarsening [117,118]. Hence, to overcome these challenges, compatibilization strategies are employed to stabilize the microstructure and enhance performance [119].

Hence, the utilization of compatibilizers results in a reduction of interfacial tension, enhancement of interfacial adhesion between

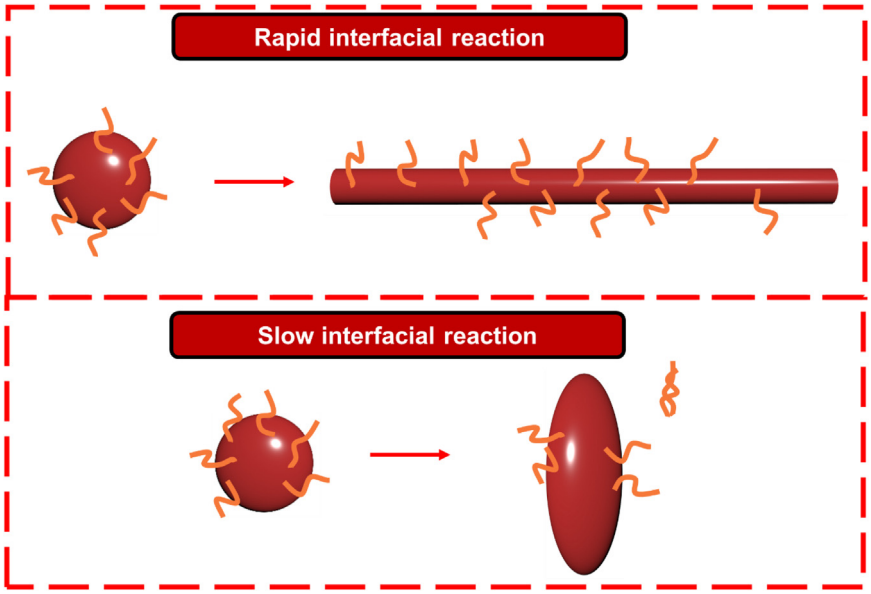

Fig. 15. Droplet breakup with interfacial grafting.

Table 3
Other studies on blending biopolymers.

Primary polymer	Secondary/Ternary/ Quaternary polymer phase	Material properties to enhance	Ref.
PLLA	Starch (corn)	Tensile strength, elongation at break	[108]
PLA	PCL and PBS	Interfacial nucleation of PLA droplets at the PCL/PBS interface	[109]
PHBV	TPS (Starch (corn), acetyl tributyl citrate)	Tensile strength, interfacial adhesion	[110]
PLA modified by PEO	Polyamide-11 (PA-11) and Poly (ether-b-amide) (PEBA)	Impact toughness	[111]
PLA	NR	Impact strength	[112]
PLA	PBAT and MWCNT	Electrical conductivity	[113]
PCL	TPS (corn starch, glycerol)	Viscoelastic properties	[108]
PLLA	NR	Tensile and impact strength	[114]
PLA	PHBV	Elongation at break, tensile strength	[115]
PLA	PHB	Mechanical properties, biodegradability	[116]

the different phases, and stabilization of the blend's morphology (i.e., reduce coarsening), transforming heterogeneous blends into stable formulations with synergistic properties [94,118,120–127]. Strategies for compatibilization include non-reactive compatibilization, which enhances physical interactions, reactive compatibilization, which promotes chemical reactions at the interface; and nanofiller-induced compatibilization, which uses nanoscale fillers to bridge phases [118]. The extent of stabilization and achievement of long term compatibility depend on processing conditions, polymer fraction properties, employed compatibilization strategy, and the specific interactions between the formulation components [128–130]. Reactive compatibilization is generally more effective than additive methods because it forms stronger interfacial bonds [131].

4.1. Non-reactive compatibilization via block- and graft-copolymers

In non-reactive compatibilization, a third polymeric fraction is incorporated into the immiscible polymer blend. The mechanism of this compatibilization depends on the chemical functionality of the third, compatibilizing polymeric fraction, which needs to have some similarity to the original constituent polymers of the immiscible blend [29,118]. The third polymer fraction should interact with the constituent fractions. As illustrated in Fig. 16, the compatibilizer should migrate to the interface between the original constituents and reduce interfacial tension. This, in turn, minimizes the coalescence of the dispersed phase, hence stabilizing the morphology (Fig. 16) [114,118,133].

The property changes achieved by compatibilization should be pertinent to the application of the compatibilized blend [118]. As illustrated in Fig. 17, in a work by Rosli et al., the effect of the addition of *A. angustifolia* cellulose on the material properties of compatibilized PLA-NR blends was studied [114]. The biodegradability of the cellulose-added specimens increased proportionally with the amount of cellulose added to the compatibilized blend (Fig. 17d). However, the 7.5 wt % and 10 wt % cellulose-added specimens exhibited instances of fiber pull-out, attributed to weak interfacial adhesion, as illustrated in Fig. 17b–c. In another work, the compatibilization effect of PLA-g-TPU fraction on PLA/TPU blend was studied [134]. It was apparent from SEM micrographs (Fig. 18a) that the addition of the grafted copolymer enhanced the phase compatibility of the PLA/TPU blend. Further, the improved tensile strength and elongation at break exhibited by PGU-constituting specimens signified an enhanced interfacial adhesion between PLA and TPU fractions (Fig. 18b–c).

Overall, block and graft copolymers are still widely accepted as one of the most effective compatibilizers of immiscible polymer blends. The ability of a block copolymer to adsorb at and stabilize the interface of a polymer blend against coalescence primarily depends on its molecular weight, the ratio of its constituent blocks, the structure, viscoelastic properties, and molecular weights of the blend components [135]. In most cases, low-molecular-weight block-polymer compatibilizers are more likely to migrate to the interface, while high-molecular-weight block-polymers are generally more effective at preventing coalescence. However, low-molecular-weight polymers are typically more solu-

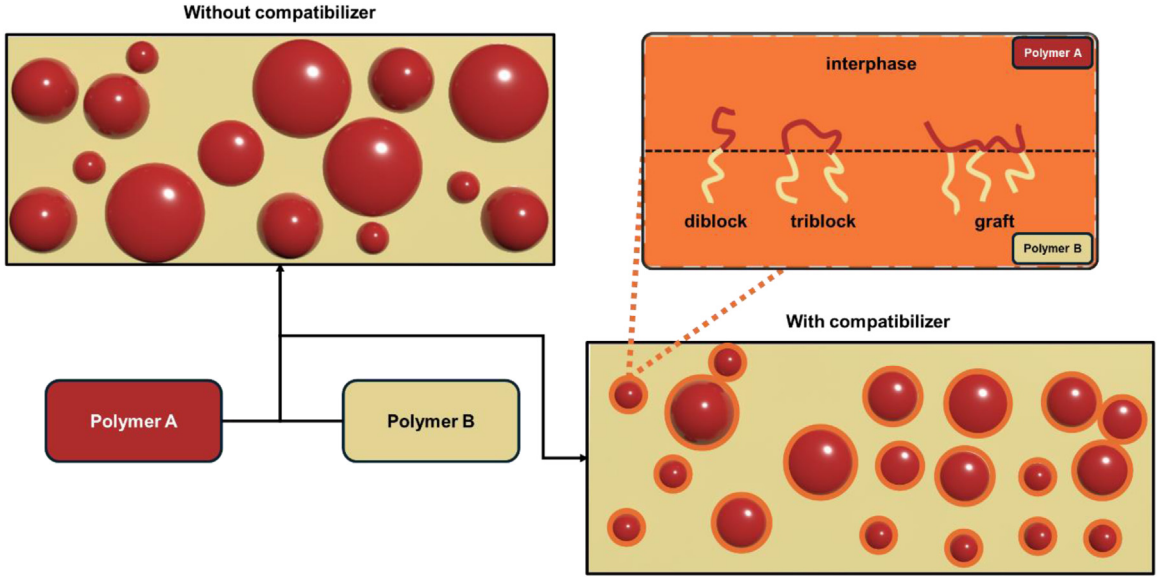

Fig. 16. Compatibilization of a polymer blend with graft and block copolymers [132], Copyright 2019. Adapted with permission from Elsevier Science Ltd.

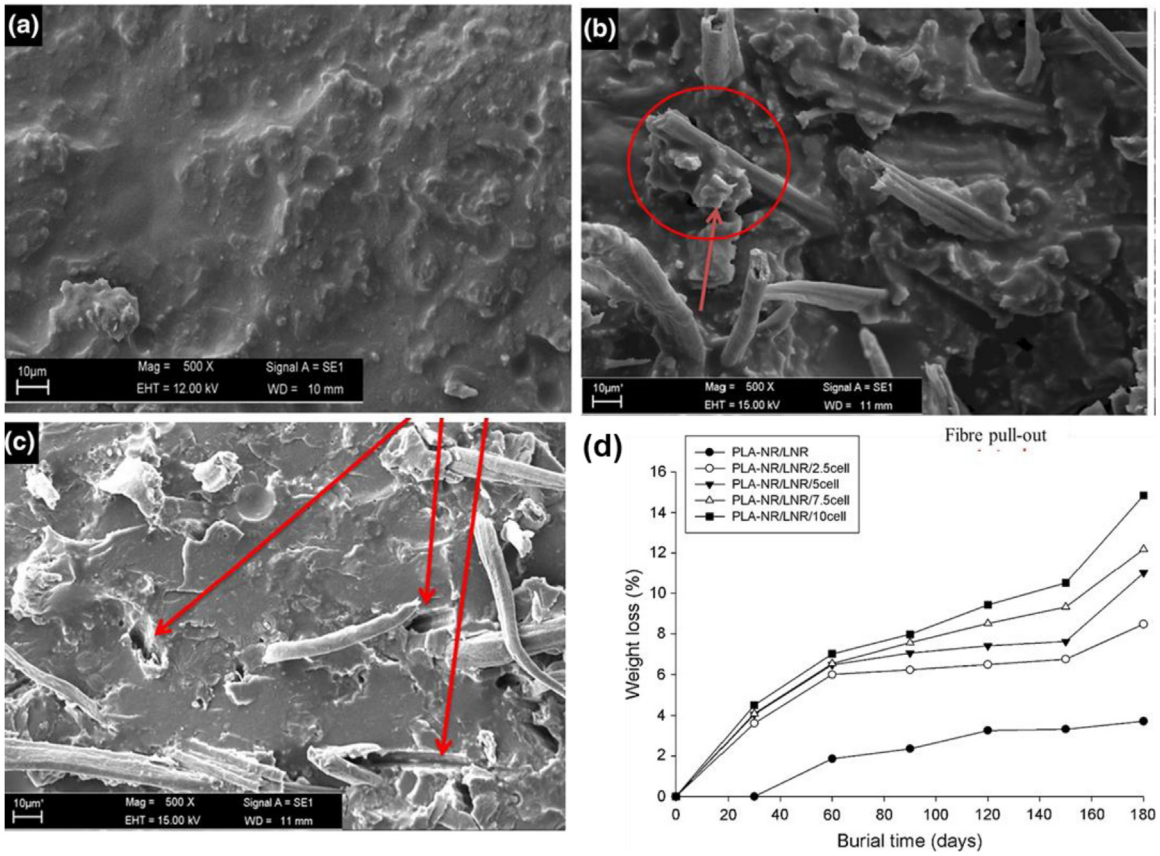

Fig. 17. SEM micrographs (impact fracture surface), (a) baseline (compatibilized PLA-NR blend), (b) cellulose added blend (7.5 wt %), (c) cellulose added blend (10 wt %), and (d) Percent weight loss of specimens (post burial) [114], Copyright 2019. Adapted with permission from Springer Nature.

ble in the blend components, whereas high-molecular-weight polymers often form micelles, which can hinder their effectiveness as compatibilizers [135,136]. Some studies have shown that stability of block and graft copolymer compatibilized blends can be considerably affected by the molecular structures, which subsequently determines the microstructure morphology and compatibilization efficiency [137,138]. Thus, an optimization and balancing act is needed to achieve the best compatibilization impact.

The employment of branched or comb copolymers as compatibilizers of polymers and biopolymers has also been studied and reported [139–141]. Prof. Yongjin Li's group from Hangzhou Normal University have a number of excellent contributions in this area. For instance, Dong et al. synthesized reactive linear (RL) and reactive comb (RC) co-polymers by copolymerizing methyl methacrylate (MMA) with glycidyl methacrylate (GMA) and a type of MMA macromer (Fig. 19), which were then used as compatibi-

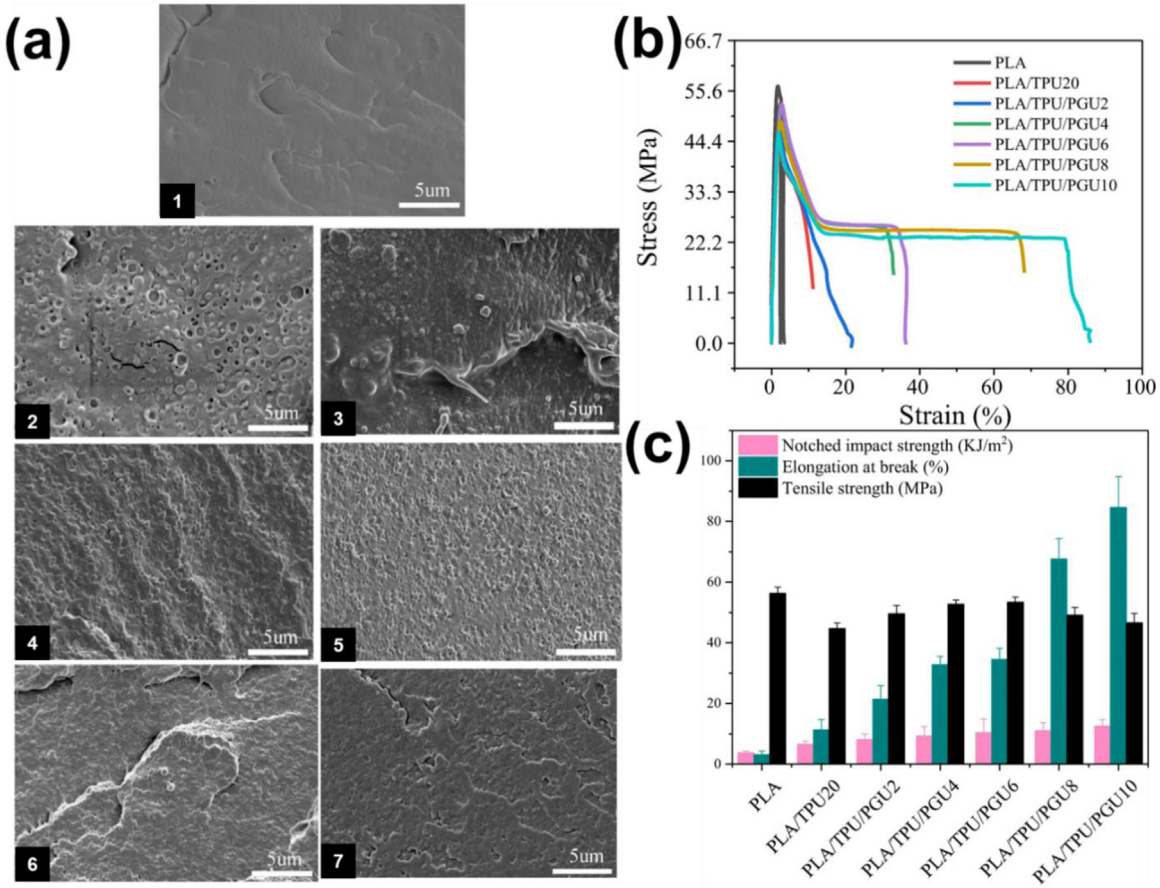

Fig. 18. (a) SEM micrographs (cryo-fractured surface). (1) PLA, (2) PLA/TPU20, (3) PLA/TPU/PGU2, (4) PLA/TPU/PGU4, (5) PLA/TPU/PGU6, (6) PLA/TPU/PGU8, (7) PLA/TPU/PGU10. Tensile properties of the blends. (b) stress-strain curves, and (c) Tensile strength, Elongation at break, and impact strength of the blends [134], Copyright 2020. Adapted with permission from Springer Nature.

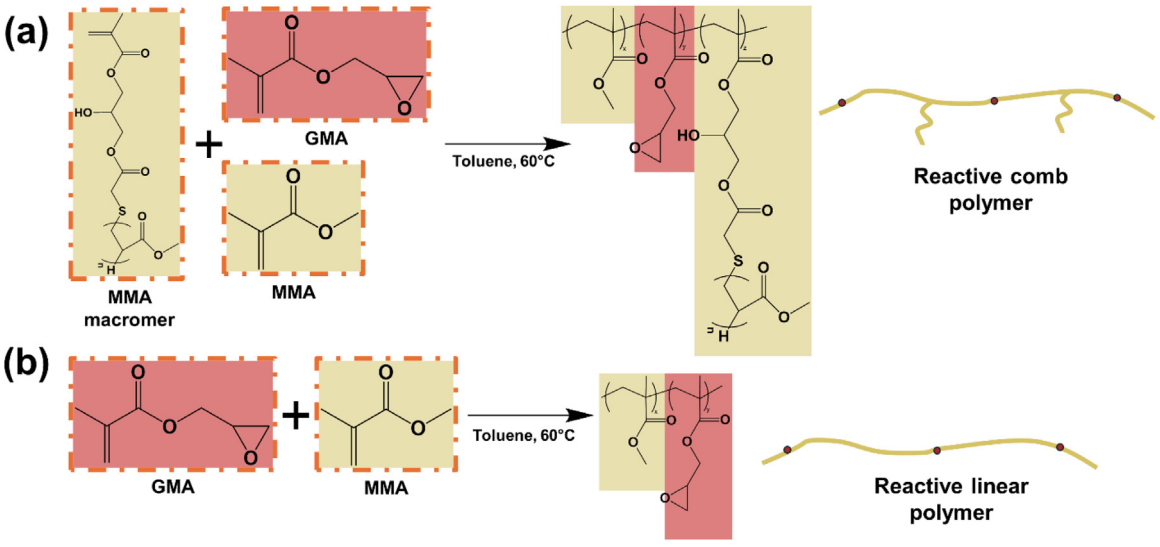

Fig. 19. Synthesis of reactive comb (RC) and reactive Linear (RL) Polymers [142], Copyright 2015. Adapted with permission from American Chemical Society.

lizers in an immiscible poly (L-lactic acid)/poly(vinylidene fluoride) (PLLA/PVDF) system [132]. In comparison to their linear analogs, incorporating just 1 wt % of RC polymers with suitably long side chains markedly decreased the size and improved the uniformity of the PVDF dispersed phase within the PLLA matrix (Fig. 20). The RC-compatibilized blends also showed a notable increase in fracture strain, as illustrated in Fig. 20a–b. This enhanced compatibilization efficiency was attributed to the presence of PMMA side chains, which stabilized the RC polymers at the immiscible blend interface, a finding supported by transmission electron microscopy analysis.

As noted from the TEM microstructure images of the blends (Fig. 20c–F), the size and size distribution of the PVDF particles (dark particles) decreased with the addition of the RL and RC

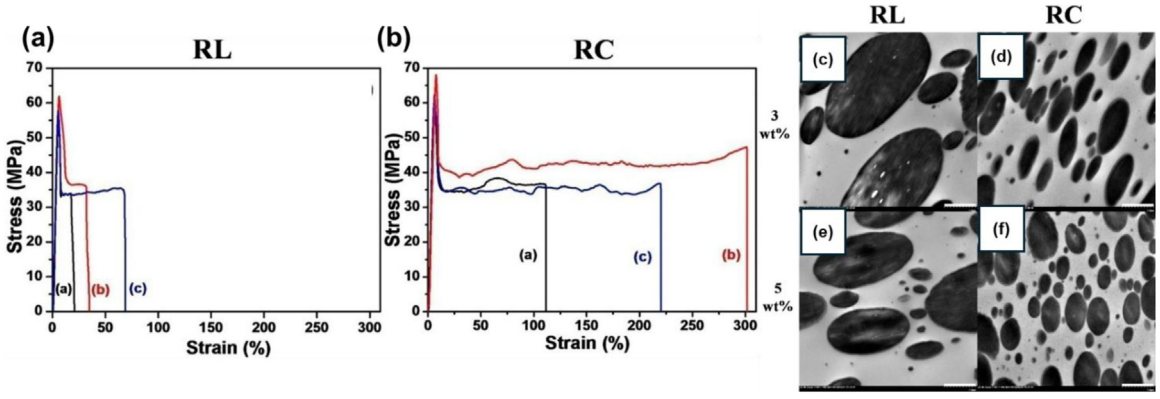

Fig. 20. Stress–strain curves of PLLA/PVDF blends compatibilized by (a) RL, (b) RC polymers. TEM images (c) PLLA/PVDF/L-0–1–9 (50/50/3), (d) PLLA/PVDF/C-1–1–8(S-2400) (50/50/3), (e) PLLA/PVDF/L-0–1–9 (50/50/5), and (f) PLLA/PVDF/C-1–1–8(S-2400) (50/50/5) [142], Copyright 2015. Adapted with permission from American Chemical Society.

copolymer compatibilizers. It was apparent that the particles were more uniformly distributed with the use of RC compatibilizer compared to RL. In addition, the PVDF phase was deformed into an ellipsoid, likely attributed to the ratio of the shear stress and the interfacial tension, The study further shows that the stability of the compatiblizers at the interface was determined by the balance of the reactivity of the epoxide groups with the PLLA phase and the miscibility of the polymethyl methacrylate (PMMA) (as shown in Fig. 19) with the PVDF phase; otherwise, they were likely to escape from the interface. Thus, the better performance of the RC polymers on compatibilization was mainly due to their better interfacial stability, described by the capillary number (Ca) shown in Eq. (8).

Stress–strain results (Fig. 20a–b) from mechanical property tests show that the uncompatibilized blend of the ductile PVDF and brittle PLLA results in the specimen fracturing at a strain value of only 5.9 %. On the contrary, the incorporation of the RL or RC compatibilizing co-polymers led to remarkable enhancement in the ductility of the PLLA/PVDF blends. With similar wt % incorporation of the RL and RC into the blend, the fracture strain of the blends compatibilized by RC was at least three times higher than that by RL, with variations in strain hardening. This variation can be explained by the existence of side chains that counterbalance some of the weakening interaction between the PMMA backbone and the PVDF phase.

In a separate study, Dong et al. investigated the use of a reactive comb compatibilizer for an immiscible blend of poly(l-lactic acid)/acrylonitrile-butadiene-styrene) system (PLLA/ABS) [143] . Results of the study showed that the use of RC co-polymer compatibilizers caused a notable improvement in the interfacial adhesion between the two phases. The strong interfacial adhesion and asymmetric thermal shrinkage were crucial for toughening rigid/rigid polymer blends. Similar to other block and branched compatibilizers, the efficiency of comb polymers as compatibilizers is also dependent on the molecular structures, such as length of side chains, and presence of reactive groups. Overall, compared to linear co-polymers, branched comb polymers are superior in enhancing the compatibilization efficiency ascribed to their superior interfacial adhesion property [143,144].

4.2. Reactive compatibilization

In reactive compatibilization, a third fraction is formed (in-situ) during the melt blending of biopolymer fractions. The copolymer is synthesized at the interface of immiscible phases and acts as a compatibilizer. This method involves the formation of covalent or ionic bonds between the immiscible phases, thus enhancing interfacial adhesion[118].

One of the primary advantages of in situ compatibilizer synthesis is that it eliminates the problems associated with the transport of compatibilizers (pre-prepared) to the interface of immiscible polymers. The selection of biopolymer fractions, composition of blend, reactive agents, and processing conditions dictate the success of reactive compatibilization. The selected functionalities should react fast during mixing, thus minimizing mass transfer constraints [118,145]. The processing conditions (residence time, shear rate, and temperature) should balance reaction rates, minimize degradation, and promote homogeneity [146,147].

For a system of immiscible biopolymers with appropriate reactive agents and optimized processing conditions, the in situ block or grafted copolymers could enhance interfacial adhesion, mechanical properties, and improve the morphology of the blends. It is worth noting that biopolymers can be sensitive to temperature or other process variables, hence, the process variables should be optimized for each respective system [118,119,147,148].

In a study by Carrillo et al., the in situ compatibilization of block terpolymer of PHBV, PLA, and PBAT was carried out [146]. The reaction mechanism for the in situ compatibilization has been outlined in Fig. 21. The effect of low-functionality epoxy-based styrene–acrylic oligomer (ESAO) as a compatibilizer on the material properties of the immiscible blend was studied. As is apparent from Fig. 21, the addition of ESAO to the terpolymer resulted in a ductile specimen, ideal for application in flexible packaging materials. However, the remainder of the specimens exhibited brittle behavior (Fig. 21).

Guan et al. studied the in situ compatibilization of PLA/PBAT blends utilizing an epoxy copolymer (MDO_1G_3) via reactive compatibilization [149]. The immiscible blend of PLA/PBAT demonstrated large PBAT domains, with an average particle size of 3.7 μm (**Fig. 22a1-a3**). The specimens consisting of compatibilizer (MDO_1G_3) had smaller PBAT domains, with sizes of 2.6 μm (0.25 wt %) and 1.6 μm (0.5 wt %), respectively. Furthermore, the compatibilized blends accounted for the higher storage modulus (G′) and loss modulus (G″) values, stemming from the formation of an internal elastic network. Also, the higher complex viscosity values recorded for the compatibilized polymers could be attributed to the grafted structure inhibiting the molecular chains from untangling, as presented in *Fig. 22g*

A groundbreaking advancement in reactive compatibilization is dynamic compatibilization, which has been successfully applied to hybrid bioplastics and blends of bio-based and petrochemical-based plastics. The challenge with mixed plastics lies in their incompatibility during recycling processes, which underscores the need for innovative compatibilization methods [150].

Cai et al. introduced a method using pre-crosslinked PBAT, prepared by mixing PBAT with initiator BIBP and cross-linker TAIC,

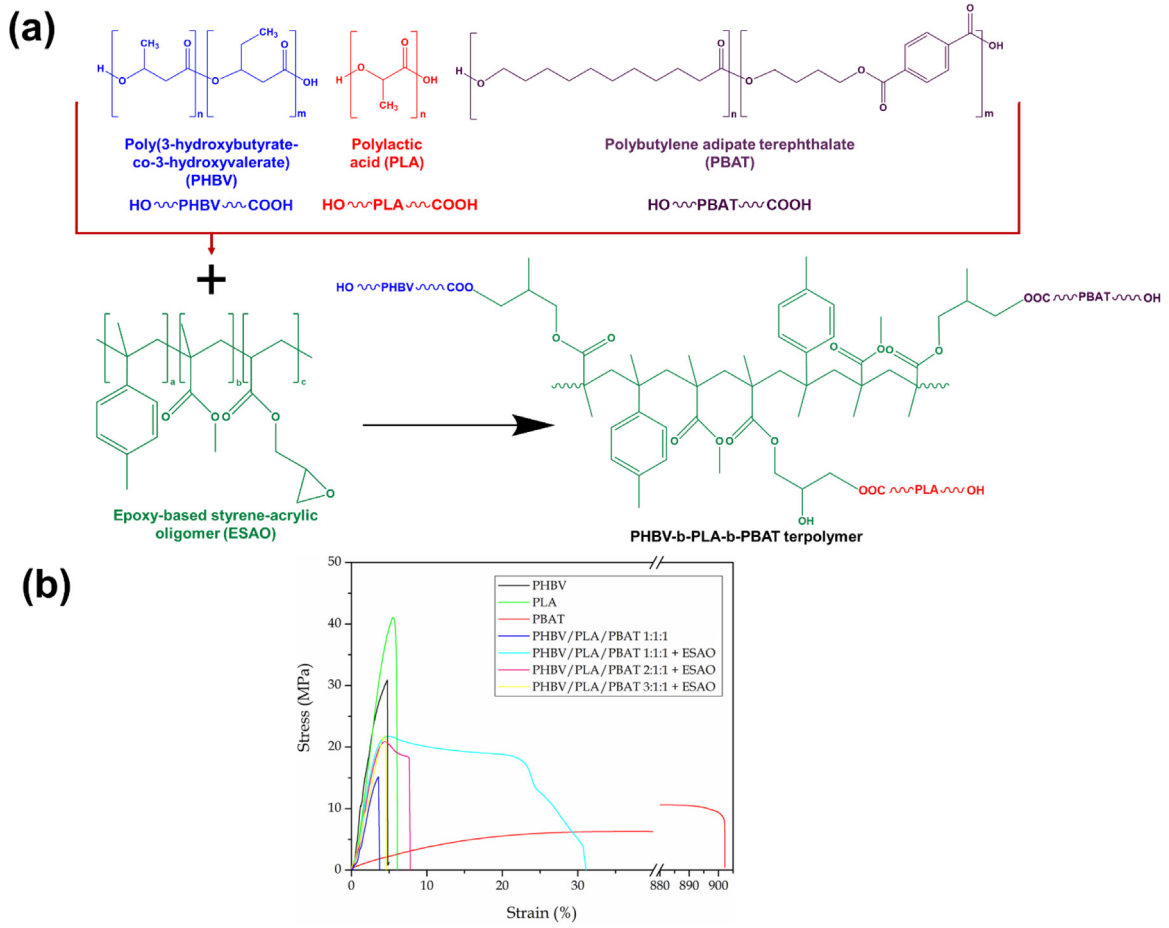

Fig. 21. (a) Reaction mechanism for in situ synthesis of block terpolymer of PHBV, PLA, and PBAT and (b) Stress-strain curves of the blends [146], Copyright 2019. Adapted with permission from Springer Nature.

to enhance PLA/PBAT blend [141]. PBAT is a promising toughening agent for addressing the brittleness of PLA, which limits its applications. However, poor compatibility between PLA and PBAT often leads to phase separation at higher PBAT contents, diminishing the toughening effect. Morphological analyses (Fig. 23) reveal that TAIC improves compatibility by reducing PBAT domain size, blurring interfaces, and transitioning PBAT from spherical to irregular and striped phases. The crosslinked PBAT effectively absorbs impact energy, but excessive TAIC (>0.3 %) leads to over-crosslinking, reducing elasticity, and impairing impact strength due to poor dispersion. By optimizing TAIC levels, the blend achieves better energy transfer and improved toughness, overcoming the limitations of conventional PLA/PBAT blends [151].

In 2023, Clarke et al. introduced a novel strategy to improve the compatibility of immiscible mixed plastic waste, enabling its reuse [152]. They advanced the concept of universal static crosslinkers (USCs) by designing universal dynamic crosslinkers (UDCs), which convert plastic mixtures into recyclable thermosetting materials. Unlike USCs, UDCs form graft multiblock copolymers (gMBCPs), which enhance compatibility by reducing interfacial tension and bridging non-miscible polymers. The approach was successfully applied to hybrid bioplastics such as PLLA/PE and P3HB/PE, where UDCs improved surface homogeneity, eliminated phase separation (Fig. 24), and enhanced mechanical properties like strength and toughness due to strong interfacial adhesion [152].

4.3. Solid particle-induced compatibilization

Another compatibilization strategy involves the use of solid particles (e.g., microparticle and nanoparticle fillers) in the compatibilization of immiscible biopolymer blends. In particle-induced compatibilization, micro-and nanoparticles can be selectively introduced in the blend, either in one blend component fraction or at the interface of the blend components. This preferential dispersion of the solid particle could significantly improve the viscoelastic and mechanical properties of the blends, thus aiding in homogenizing the morphology. Due to the effectiveness, cost efficacy, and simplicity of this compatibilization route, it has garnered significant interest in compatibilizing immiscible blends [118,153,154].

As illustrated in Fig. 25, the localization of nanofiller solid particles inside the blend impacts the material properties. The preferential dispersion of nanofillers at the interface between the immiscible polymer fractions results in a homogeneous morphology where the phase stays separated due to physical jamming and/or steric hindrance. There exist coupling interactions between the immiscible fractions, due to the high surface area of the nanofillers [118,156]. Moreover, the selective incorporation of nanofillers in one phase results in the nanofillers retarding the relation dynamics and hence preserving the morphology [118,157–159].

Nanofillers used for blend stabilization can be categorized based on their geometries: 1-dimensional (graphene nanoplatelets, layered silicates), 2-dimensional (carbon nanotubes), and 3-dimensional (carbon black, metal oxides). The phase morphology of the immiscible blends could be optimized by preferential localization of nanofillers, optimization of filler types, and processing conditions [117,118]. In addition to such stabilization, the use of nanofillers could improve gas barrier, flame retardancy, heat resistance, UV barrier properties, morphology, and mechanical properties [153,158].

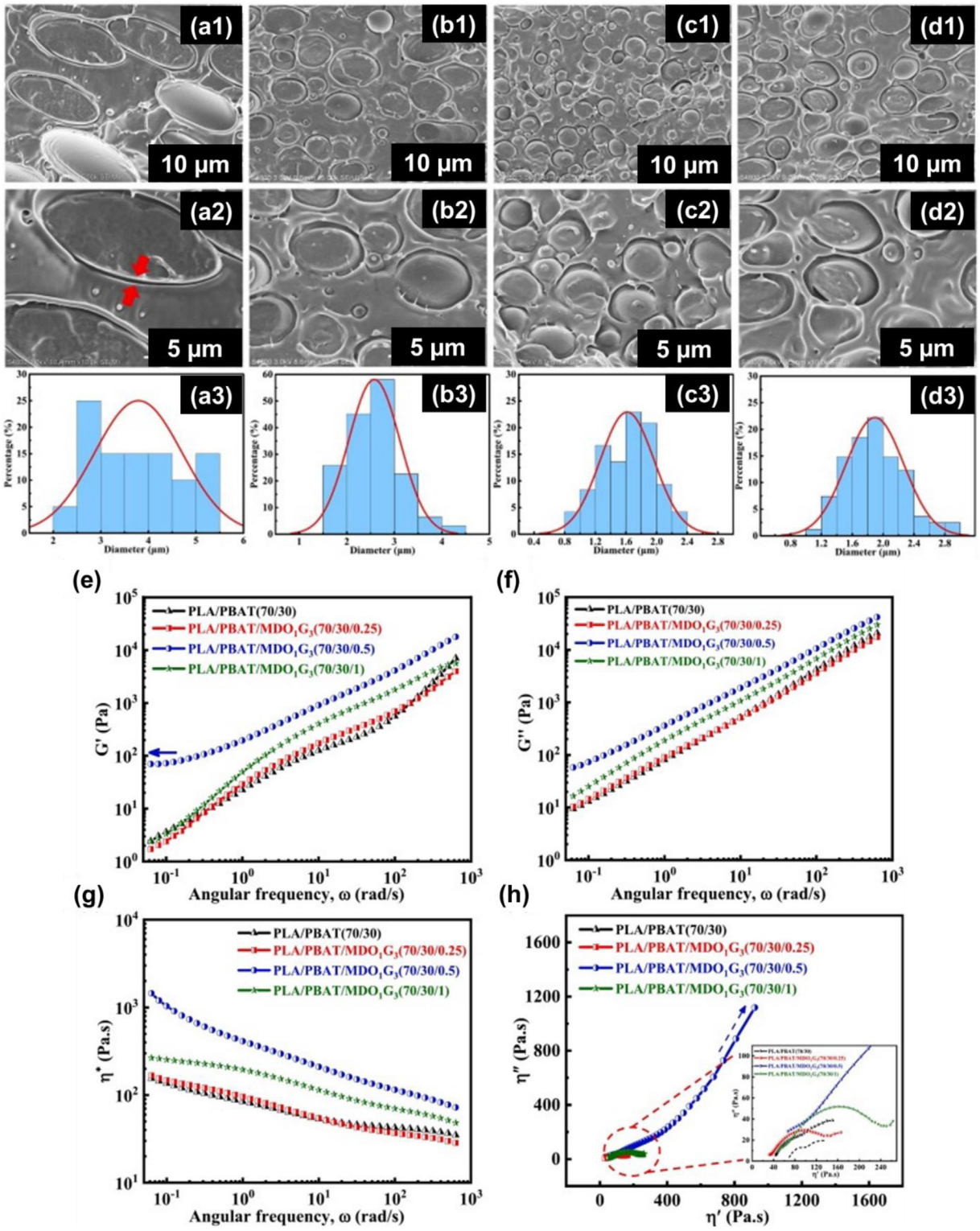

Fig. 22. SEM micrographs of the PLA/PBAT (70/30) blends without and with compatibilizers. (a1, a2) pristine blend, (b1, b2) 0.25 wt % MDO1G3, (c1, c2) 0.5 wt % MDO1G3, (d1, d2) 1 wt % MDO1G3, (a3-d3) particle size distribution curves, Properties of PLA/PBAT/MDO_1G_3 blends. (e) Storage modulus, (f) loss modulus, (g) complex viscosity, and (h) cole-cole curves of the [149], Copyright 2024. Adapted with permission from Elsevier Science Ltd.

In a study by Zembouai et al., the effect of the addition of fillers Sepiolite (SP) and Cloisite 30B (C30B) on the PHBV/PLA blend morphology and material properties was explored [160]. To investigate the effect of nanofiller dispersion on the viscoelastic properties of the blends, a frequency sweep analysis was undertaken. As illustrated in Fig. 26, the complex viscosity and storage modulus values of the filled blends were higher than the baseline PHBV/PLA samples. This was attributed to the strong polymer-filler interactions and their homogeneous dispersion in the matrix. Furthermore, the SEM micrographs confirmed viscoelastic observations. As is apparent from Fig. 26a, the PHBV/PLA blend exhibited biphasic morphology and poor interfacial adhesion. However, the blends consisting

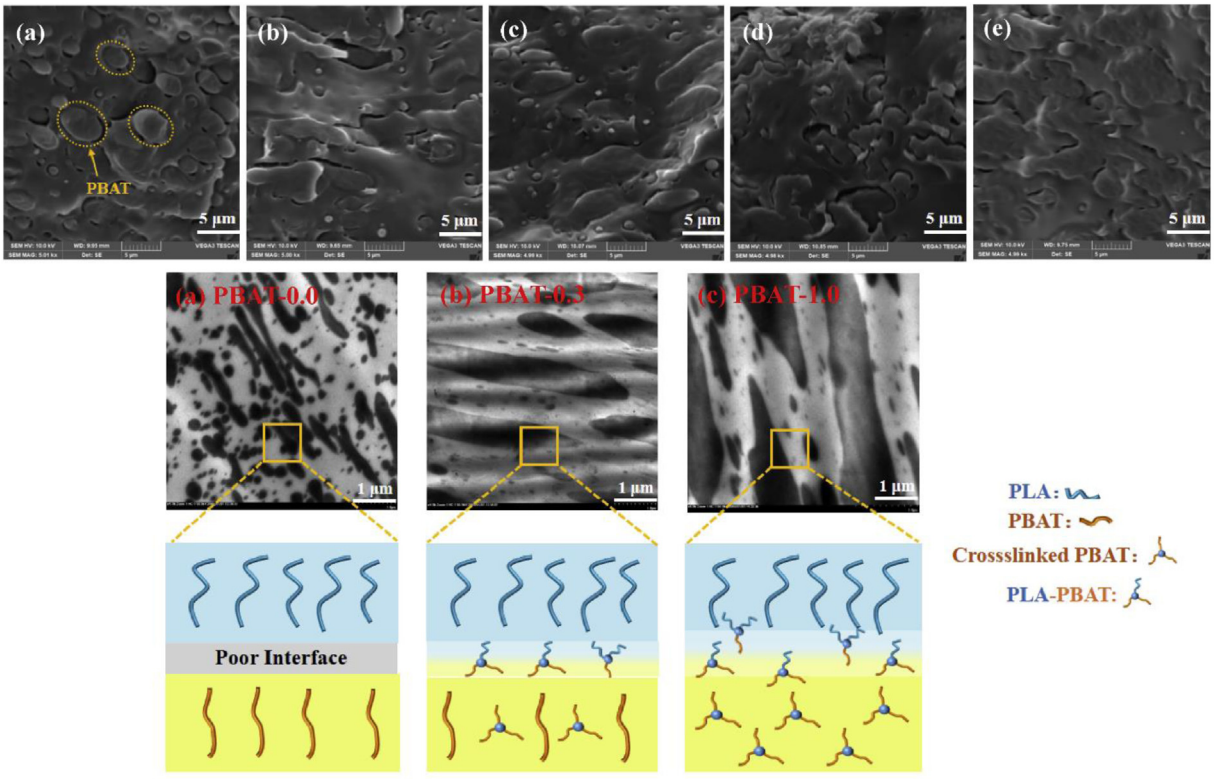

Fig. 23. SEM micrographs. (a) PLA/PBAT, (b) PLA/PBAT-0.1, (c) PLA/PBAT-0.3, (d) PLA/PBAT-0.5, (e) PLA/PBAT-1.0. TEM micrographs. (a) PLA/PBAT, (b) PLA/PBAT-0.3, and (c) PLA/PBAT-1.0 with a constant content of 30 wt % PBAT [151], Copyright 2023. Adapted with permission from Elsevier Science Ltd.

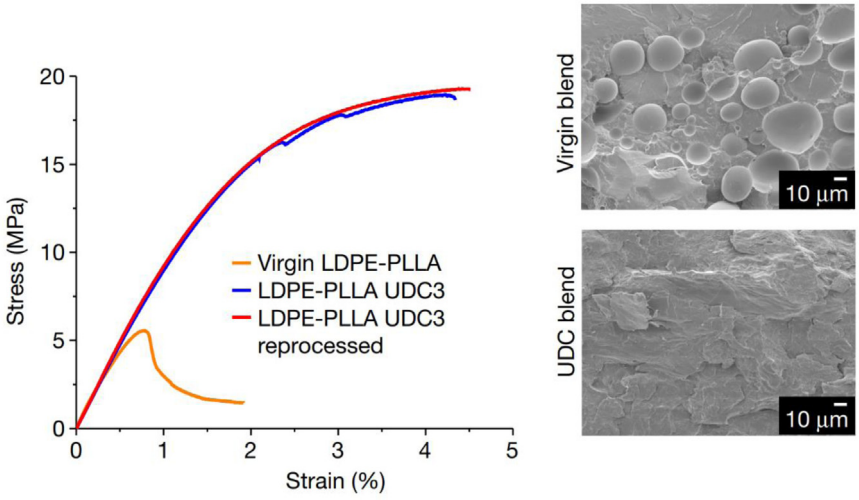

Fig. 24. Dynamic compatibilization of PLLA/LDPE with UDC [152], Copyright 2023. Adapted with permission from Nature.

of both C30B and SP demonstrated homogeneous morphology, as evidenced from Fig. 26d–e. Other studies on compatibilization of immiscible polymeric blends have been tabulated (Table 4).

The use of Janus colloidal nanoparticles, with heterogenous surface composition, formed in situ at polymer–polymer interface of immiscible polymers blends can also provide potent compatibilization benefits [170–172]. This is because Janus nanoparticles can offer an inherent Pickering effect with amphipathy, which allows them to be lodged exclusively at the polymer-polymer interface [173]. The Janus nanoparticles can be formed in situ or be prefabricated. An example of in situ formed Janus nanoparticles as compatibilizers of polymer blends is reported in the work of Wang et al. [170]. In this work, the researchers grafted PLLA chains onto P((S-co-GMA)-g-MMA) during melt mixing that led to the formation of several Janus nanoparticles with a shell structure consisting of PLLA and PMMA hemispheres (as shown in Fig. 27). These Janus nanoparticles migrate to the PLLA/PVDF interface, and acted as effective compatibilizers for the immiscible PLLA/PVDF blends. As a result, remarkable improvement in ductility of the Janus nanoparticle compatibilized blend was observed after 10 min of melt mixing, with an elongation at break reaching 320 %. In comparison, the blend without the Janus nanoparticle exhibited only 5 %, and the sample mixed for just 0.5 min achieves 8 %. This notable enhancement in mechanical properties suggests that the interfacial Janus nanoparticles effectively compatibilized the PVDF/PLLA blend. However, when the mixing duration is extended to 15 min,

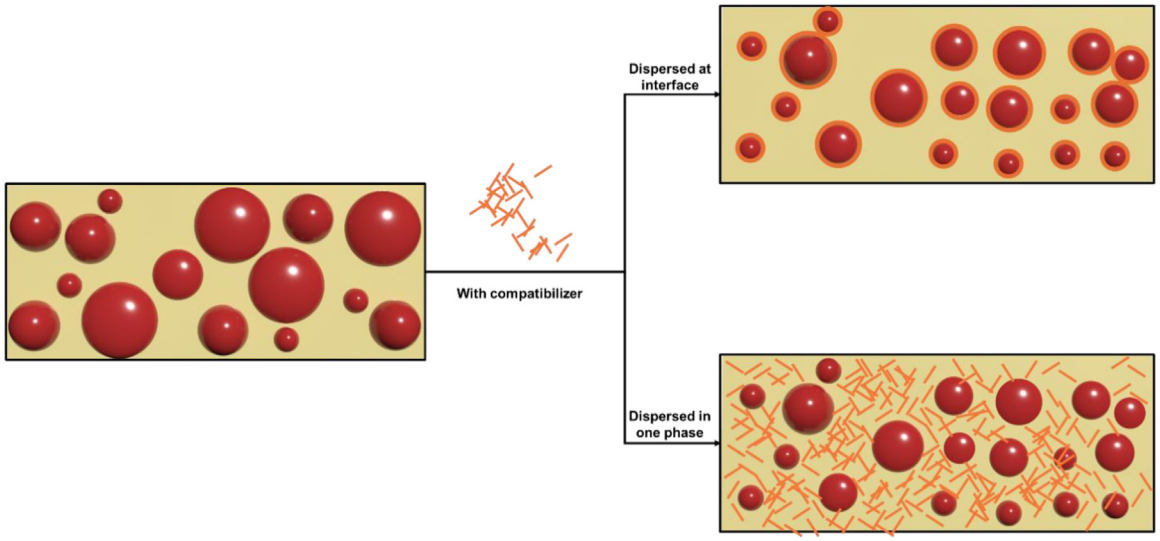

Fig. 25. Main strategies of filler-induced compatibilization by preferential dispersion of filler in one of the two polymer phases, and at the interface of the phases [155], Copyright 2020. Adapted with permission from Elsevier Science Ltd.

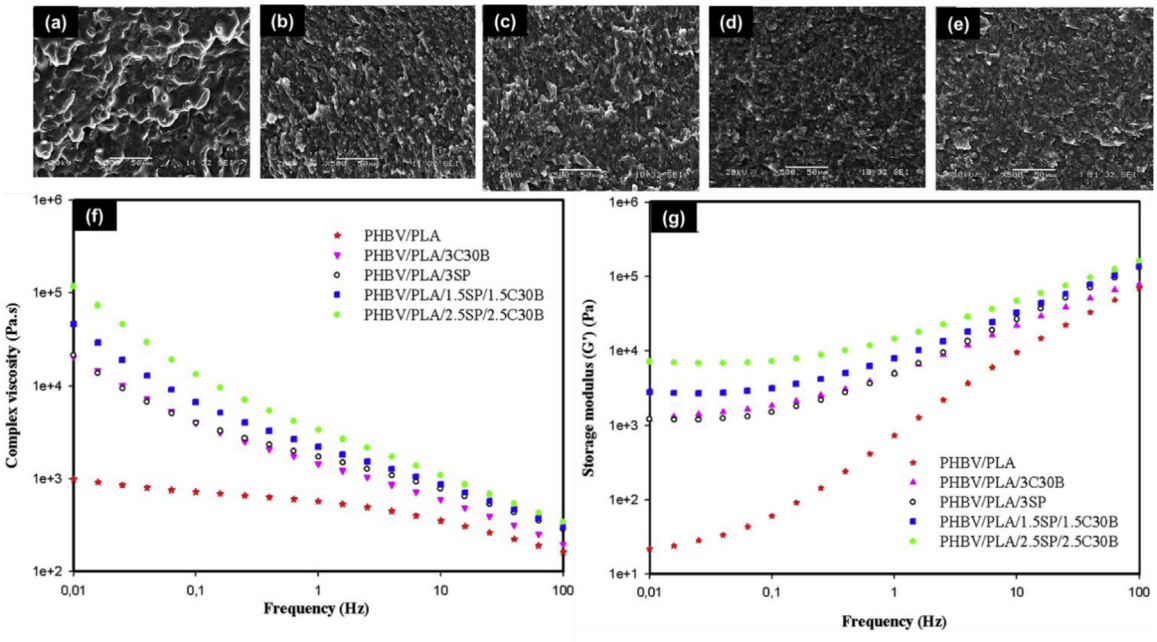

Fig. 26. SEM micrographs. (a) PHBV/PLA, (b) PHBV/PLA/3C30B, (c) PHBV/PLA/3SP, (d) PHBV/PLA/1.5SP/1.5C30B and (e) PHBV/PLA/2.5SP/2.5C30B. Frequency sweep data. (f) complex viscosity vs frequency, and (g) storage modulus vs frequency [160], Copyright 2018. Adapted with permission from Elsevier Science Ltd.

Table 4
Other studies on compatibilization of biopolymer blends.

Polymer	Second polymer phase	Type of compatibilization	Compatibilizer	Material properties to enhance	Ref.
Starch	Zein protein	Non-reactive compatibilization	1–butyl–3-methyl imidazolium chloride ([BMIM]Cl) ionic liquid	Mechanical and viscosity properties	[161]
PLA	NR	Reactive compatibilization	Modified NR	Tensile strength and toughness	[162]
PHBV	PBAT, PLA	Reactive compatibilization	ESAO (Epoxy-based styrene-acrylic oligomer)	Barrier and mechanical properties	[146]
PLA	PBAT	Non-reactive compatibilization	PLA-PBAT-PLA triblock copolymer	Mechanical properties and thermal properties	[163]
PLLA	PBS	Reactive compatibilization	PLLA-block-poly(glycidyl methacrylate)(PLLA-b-PGMA)	Tensile strength, toughness, and viscoelastic properties	[164]
Starch	PBS	Non-reactive compatibilization	Starch-g-PBS	Interfacial adhesion	[165]
PLA	Novatein	Reactive compatibilization	PLA-g-itaconic anhydride	Morphology of PLA and foamability	[166]
PLA	PBAT	Filler-induced compatibilization	Carbon nanotubes (CNTs)	Conductivity (electrical) and impact strength	[167]
PLA	Starch	Non-reactive compatibilization	PLA-g-starch	Tensile properties and morphology	[168]
PLA	ENR	Reactive compatibilization	ENR-g-MA graft copolymer	Thermal stability and impact strength	[169]

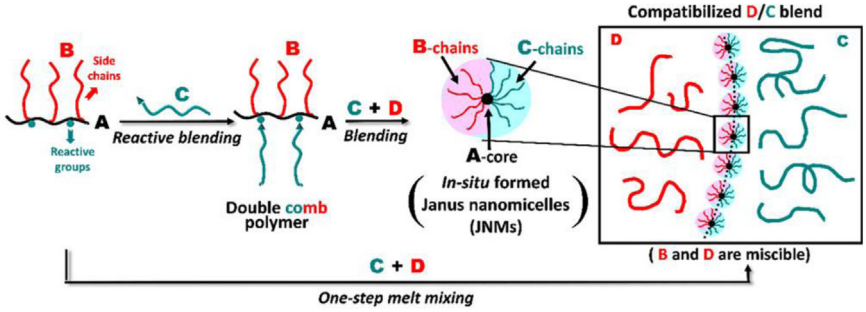

Fig. 27. Proposed Formation of *in Situ* Formed JNMs for Compatibilizers in Immiscible Polymer Blends [170], Copyright 2015. Adapted with permission from American Physical Society.

the elongation at break decreases to approximately 140 %. This reduction is attributed to the migration of most nano micelles into the PLLA phase, resulting in fewer Janus nanoparticles remaining at the interface to promote compatibilization between the two polymer phases.

Some studies show that the compatibilizing performance of the Janus particles for immiscible blends can be considerably superior to other compatibilizers, such as linear block copolymers[135,174]. This is because the Janus particles are located at the interface, even at high temperature and shear, due to their high adsorption energy associated with enthalpic energy [135]. Nevertheless, it is important to note that the fabrication of Janus nanoparticles is still at a lab scale and prohibitively expensive. In addition, for their effective use as a compatibilizer, a relatively large concentration (usually > 8 wt %) needs to be used. Furthermore, intense polymer melt compounding processes that entails high shear, temperature, or ultrasound, or supercritical conditions are needed to anchor the Janus nanoparticles at the interface of the immiscible polymer blends to obtain the intended benefits.

5. Environmental impacts of bioplastic blends

Bioplastics are often regarded as environmentally friendly alternatives to conventional plastics due to their potential to reduce plastic pollution and dependency on fossil fuels [107]. These materials are typically derived from renewable resources and are intended to have lower carbon footprints throughout their entire lifecycle. However, the overall environmental impact of bioplastics is complex and influenced by two critical factors, degradation and recyclability [14,175]. Addressing these challenges is essential for bioplastics to serve as a genuine solution to the global issue of plastic pollution.

5.1. Degradability

Bioplastics and their blends are increasingly being used in numerous commodity and engineering applications [176]. At the end of their life cycle, these materials should ideally be recycled or disintegrate either in the natural environment or within composting facilities. While the degradability of individual bioplastics has been widely studied, degradable bioplastics can be categorized into four main types:

(i) Photodegradable bioplastics: Contain light-sensitive groups in their backbone that degrade under ultraviolet radiation, which enables subsequent bacterial degradation [177].
(ii) Bio-based bioplastics: Made entirely from renewable agricultural and forestry resources, such as corn starch, soybean protein, and cellulose, with minimal or no chemical modifications [178]. Such bioplastics are mostly biodegradable in the natural environment.
(iii) Compostable bioplastics: These bioplastics, e.g., PLA, PBAT, decompose at the same rate as other compostable materials in specific environments without leaving harmful residues, meeting standards for biodegradability, disintegration, and ecotoxicity [179].
(iv) Biodegradable bioplastics: These bioplastics, such as PHA and PEG, are fully degradable by microorganisms into biogases and biomass, primarily carbon dioxide and water, without leaving any toxic residues and supporting sustainability [180].

Biodegradation occurs through two distinct mechanisms depending on the bioplastic's structure and environment. The first, hydro-biodegradation, involves abiotic or biotic hydrolysis followed by bioassimilation, common in hetero-chain bioplastics like cellulose, starch, PLA, and PHA [181,182]. This process can be accelerated by photooxidation, making these bioplastics suitable for applications like cosmetic and hygiene products but less ideal for agricultural or packaging films [182]. The second, oxo-biodegradation, involves peroxidation followed by bioassimilation of low-molecular-weight products, primarily in carbon-chain polymers. Antioxidants regulate peroxidation to maintain mechanical properties for extended periods, with degradation triggered by environmental factors like light or heat. The rate of overall degradation is determined by the slower peroxidation step, as bioassimilation occurs rapidly once oxidation products form [183]. In case of bioplastic blends, hydro-biodegradable pathway would generally be the dominant, at a rate faster than oxo-biodegradation [184]. Reliable real-world predictions should be based on laboratory standards and field trials [185,186].

As plastic waste pollution poses a significant global environmental challenge, biodegradable plastics have emerged as a potential solution. As noted, these plastics are often blended to enhance their functional properties for commercial applications, yet there has been a lack of studies on their environmental fate and degradation behavior [118]. The degradation rates of bioplastic blends are greatly influenced by the choice of constituent polymers, processing conditions, compatibilizers, additives, and surrounding conditions [187]. The presence of amorphous regions in a blend favors enzymatic degradation, as the amorphous region molecules are less densely packed compared to their crystalline counterparts. Thus, additives known to enhance the crystallinity of the blends could render the formulations less prone to degradation [188]. Further, the addition of plasticizers in formulations could result in reduced degradation, primarily, due to plasticizer moieties forming a protective layer around the polymer chains [189,190]. Narancic et al. investigated the biodegradability of some major bioplastics in the market and their blends to better understand their environmental fate [191]. They demonstrated that blending non-home compostable PLA with home compostable PCL (80:20) produced home compostable material with uniformly dispersed spherical PCL droplets in the continuous PLA matrix (Fig. 28). In contrast,

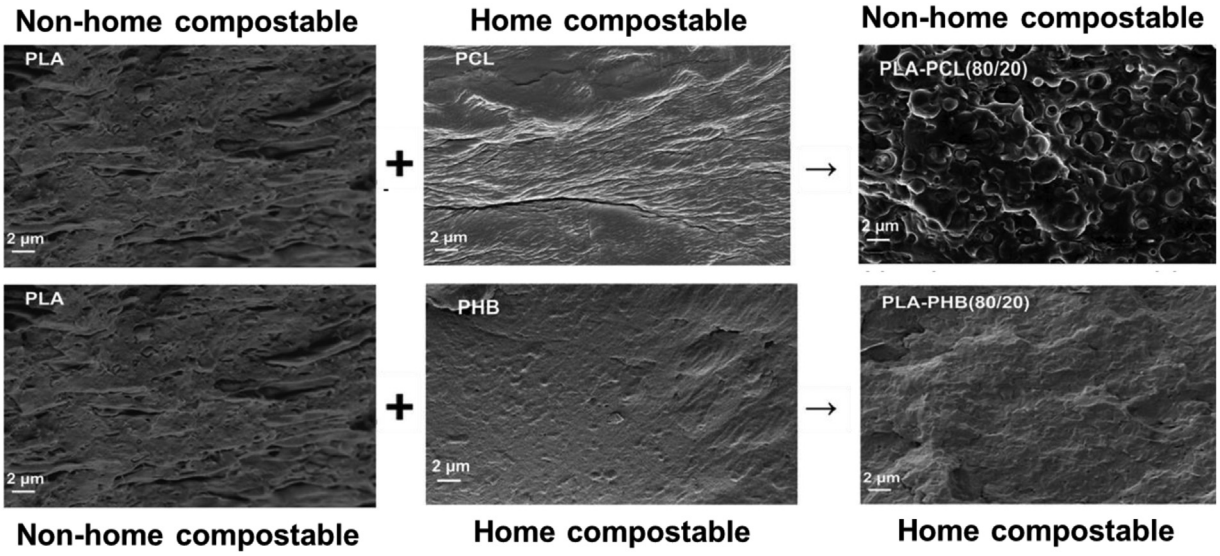

Fig. 28. SEM micrograph of the fracture surfaces of neat biodegradable polymers (PLA, PCL, and PHB), the home compostable PLA–PCL (80/20) blend, and the non-home compostable PLA–PHB (80/20) blend [191], Copyright 2018. Adapted with permission from American Physical Society.

Table 5
Biodegradation performance of bioplastics and their blends in managed and unmanaged environments [191].

	Managed environment				Unmanaged environments		
Bioplastics	Industrial composting	Anaerobic digestion	Home composting	Marine	Fresh water	Anaerobic aq. digestion	Soil
PLA-PCL (80/20)	Pass	Pass	Pass	Fail	Fail	Fail	Fail
PLA-PBS (80/20)	Pass	Fail	Fail	Fail	Fail	Fail	Fail
PLA-PHB (80/20)	Pass	Pass	Fail	Fail	Fail	Fail	Fail
PLA-PHO (85/15)	Pass	Pass	Fail	Fail	Fail	Fail	Fail
PHB-PHO (85/15)	Pass	Pass	Pass	Fail	Fail	Pass	Pass
PHB-PCL (60/40)	Pass	Pass	Pass	Fail	Fail	Fail	Pass
PHB-PBS (50/50)	Pass	Fail	Pass	Fail	Fail	Fail	Fail
PCL-PHO (85/15)	Pass	Pass	Pass	Fail	Fail	Fail	Fail
PCL-TPS (70/30)	Pass	Pass	Pass	Fail	Fail	Fail	Pass
PLA	Pass	Pass	Fail	Fail	Fail	Fail	Fail
PCL	Pass	Pass	Pass	Fail	Fail	Fail	Pass
PBS	Pass	Fail	Fail	Fail	Fail	Fail	Fail
PHO	Pass	Fail	Fail	Fail	Fail	Fail	Fail
PHB	Pass	Pass	Pass	Pass	Pass	Pass	Pass
TPS	Pass	Pass	Pass	Pass	Pass	Pass	Pass

the PLA–PHB (80:20) blend lacked distinct morphological structures and failed to achieve home compostability, highlighting the importance of blend morphology in biodegradability [191].

Table 5 summarized the biodegradation performance of bioplastics and their blends across three managed environments (Controlled Industrial Composting Conditions [ISO 14,855], High-Solids Anaerobic Digestion [AD; ISO 15,985], and Controlled Composting at Ambient Temperature [ISO 14,855 at 28 °C] or Home Composting) and four unmanaged environments (Soil [ISO 17,556], Marine [ASTM D6691], Freshwater [ISO 14,851], and Anaerobic Aqueous Digestion [ISO 14,853]). The results in the table highlight the challenges in assessing the biodegradability of bioplastic blends, as these blended forms are the most likely configurations to appear in the marketplace [191].

In a study by Palai et al., TPS and poly(butylene succinate-co-adipate) (PBSA) incorporating PLA films were extrusion blown and their biodegradation behavior in soil was studied [192]. The extrusion-blown film specimens of neat PLA, PLA/PBSA, and PLA/TPS underwent soil burial for 90 days. As apparent from Fig. 29a, the PLA/TPS film accounted for the highest rate of degradation (40.6 %). This degradation (biotic and abiotic) was attributed to the hydrophilicity of TPS, which resulted in better soil water penetration into the film. This was followed by an 8.6 % weight loss by PLA/PBSA film and 5.8 % by virgin PLA film. These results were synchronous with SEM micrographs, as presented in Fig. 29c–h.

Literature reveals that further investigation into the degradability of bioplastic blends is needed due to their complexity [187]. More specifically, the impact of compatibilizers on the degradation and overall environmental attributes of bioplastic blends requires further attention [119]. This knowledge can guide the design and applications of these materials to support sustainable end-of-life management and minimize environmental impact. For instance, prioritizing biodegradable plastics that degrade in diverse unmanaged environments may be beneficial for applications with higher environmental exposure, such as coastal packaging and marine plastics.

5.2. Recyclability

Bioplastics can be considered the future of 'green polymers'; therefore, their recycling makes it possible to retain the entire carbon content and save primary resources. The low environmental impact of the bioplastics would be compromised if the recycling of industrial wastes cannot be achieved [176]. The recycling of bioplastics and their composites can be accomplished through dif-

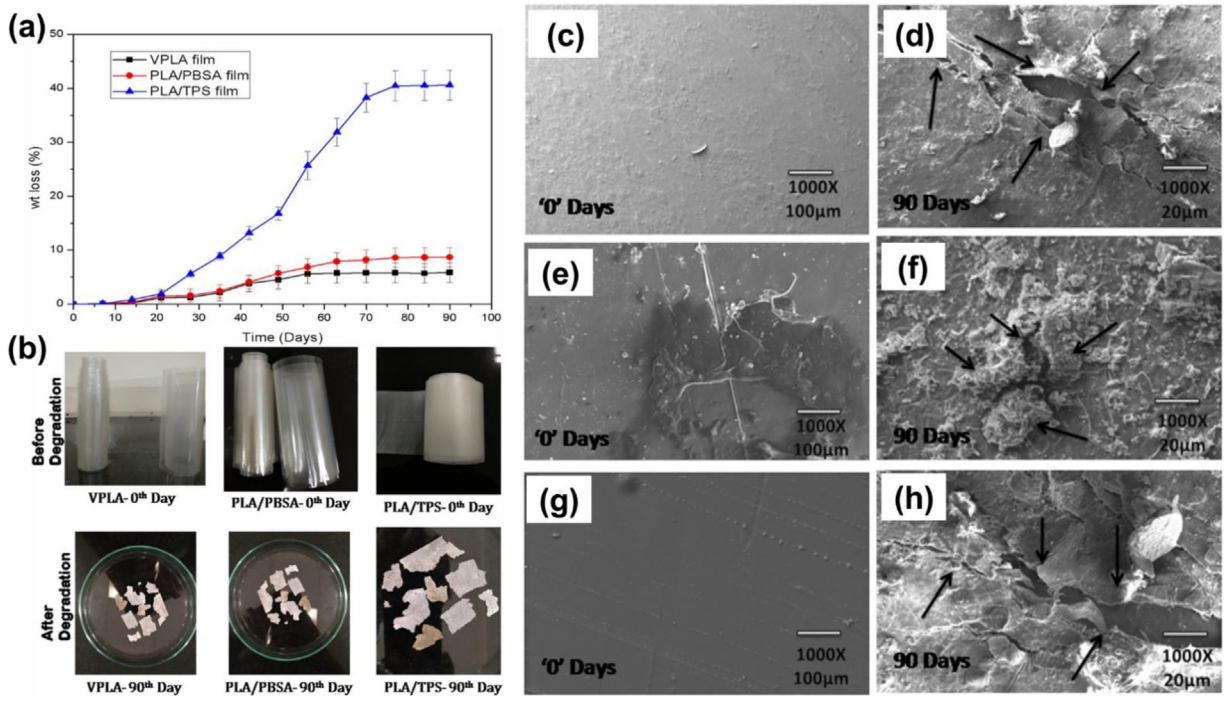

Fig. 29. (a) wt % loss of films, (b) Photographic evidence of films (pre and post 90-day burial. (c)-(h) SEM micrographs [192], Copyright 2021. Adapted with permission from Springer Nature.

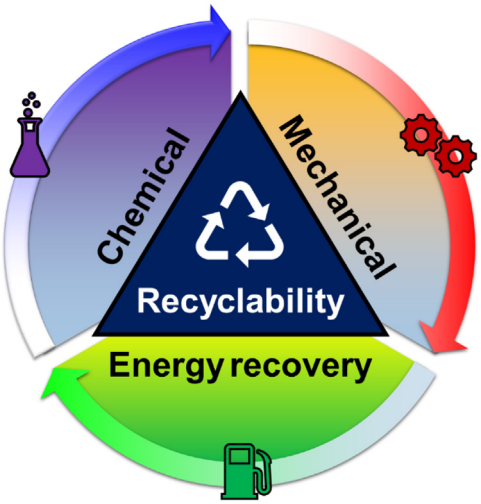

Fig. 30. Various pathways for biopolymer recycling.

ferent pathways, namely, mechanical recycling, chemical recycling, and energy recovery (Fig. 30). Due to its simplicity, mechanical recycling is the most favorable recycling technique under consideration for bioplastics . However, in some cases, the recycled polymer materials could exhibit inferior material properties to their unprocessed counterparts, which can be attributed to material deterioration during the life cycle of the material, process induced molecular chain session, and the presence of potential impurities [183]. Given the thermal sensitivity of biopolymers and their blends, the applicability of mechanical recycling should be evaluated on a case-to-case basis to ensure process efficiency and material integrity.

Mechanical recycling is often simulated through multiple extrusion cycles. In a study by Farias et al., a PLA/PHB (70/30 wt %) bioplastic blend was mechanically recycled five times to assess its performance retention [193]. The dispersed PHB moieties in the PLA matrix exhibited immiscibility with partial interactions between the polymer phases. However, post recycling (>thrice), the PHB moieties dispersed homogeneously in the PLA matrix, as illustrated in Fig. 31a–d, likely attributed to the significant reduction in viscosity through multiple recycling that helps with the moiety dispersion. It was interesting to note that chain scission and degradation of the blend components were not observed in Fourier transform infrared (FTIR) results, and unfortunately, the study did not conduct molecular weight analysis via gel permeation chromatography. On the other hand, higher crystallinity, lower cold crystallization temperature, and lower glass transition temperature (Tg) were observed for the reprocessed blend samples, which could be caused by the nucleating action of the finely dispersed PHB after the reprocessing leading to higher crystallinity. Overall, the increased crystallinity during reprocessing counteracted the observed viscosity decrease, which helped maintain the tensile properties and toughness of the recycled blend. Thus, such sustainable blends can be recycled at least five times without substantial loss of their thermomechanical properties.

Beyond bioplastic blends, the recycling of hybrid bioplastic blends, combination of bio-based and petro-based plastics, is equally essential. Hybrid bioplastics are designed to enhance the material properties of bioplastics such as durability, flexibility, and cost-effectiveness [196–198]. However, their complex composition often poses significant challenges for recycling, such as the varying degradation rates, melting points, and chemical interactions complicate separation and processing. In addition to intentional bioplastic – petrochemical derived plastic blends, the presence of biopolymers in existing post-consumer plastic recycling streams further underscores the importance of advancing recycling knowledge for bioplastic blends [176]. For instance, one significant challenge in recycling of hybrids arises from PLA, widely used in packaging due to its biodegradable properties, which frequently contaminates PET recycling streams. PLA bottles, often indistinguishable from PET bottles by consumers, inadvertently contaminate PET recycling streams. PLA's immiscibility with PET and its

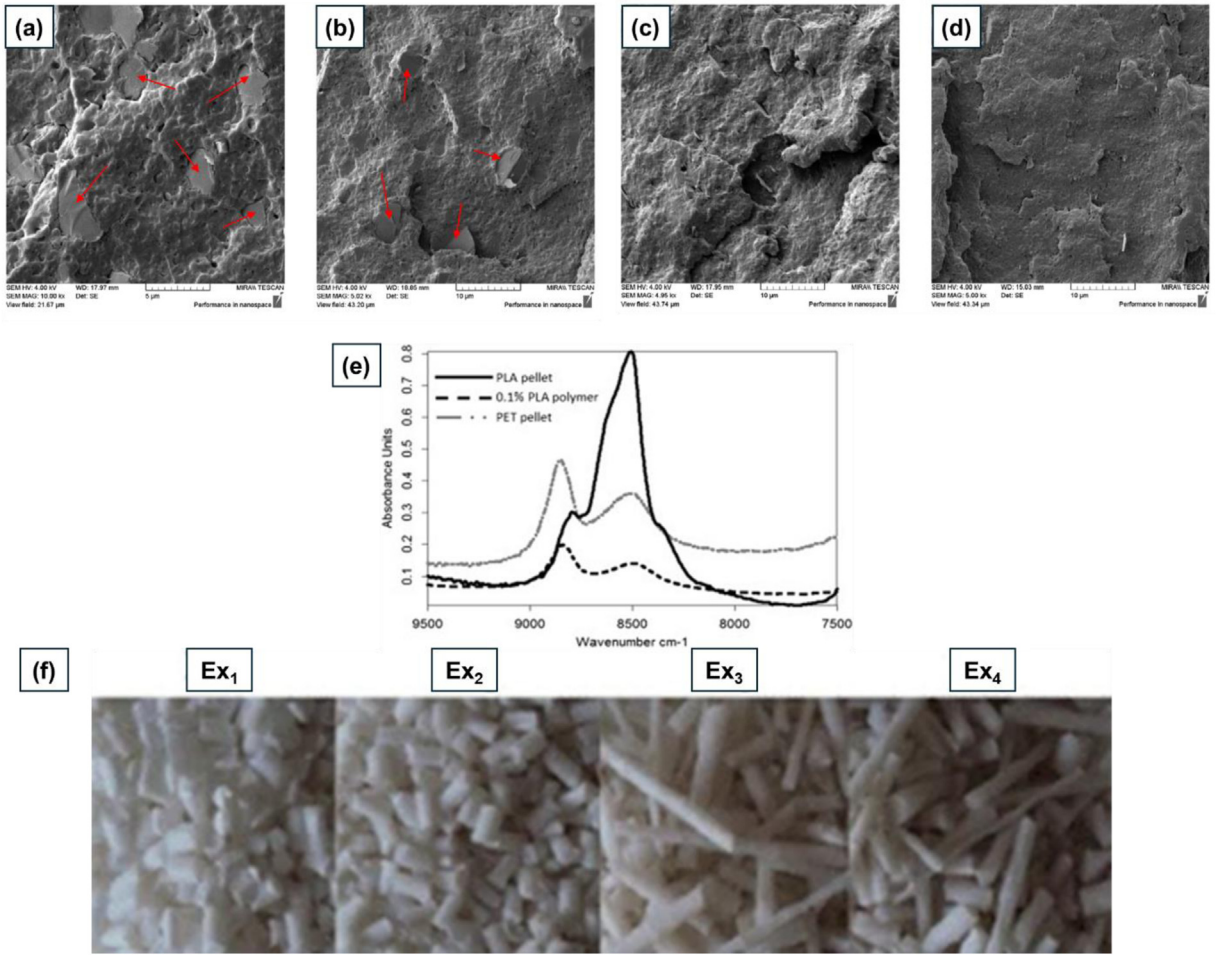

Fig. 31. SEM micrographs of PHB/PLA specimens. (a) baseline, (b) recycled-1 time, (c) recycled-3 times, and (d) recycled-5 times [193]), Copyright 2022. Adapted with permission from John Wiley & Sons Inc. (e) Near-infrared reflectance spectra of PLA, PET, and 0.1 % PLA-contaminated PET [194], Copyright 2014. Adapted with permission from Elsevier Science Ltd. (f) Color change of PLA/PS hybrid bioplastic blend after multiple recycling [195], Copyright 2011. Adapted with permission from Springer Nature.

lower melting point cause severe quality issues, such as rheological disruptions and cloudiness in recycled PET, even at trace levels (<0.1 %). Shear viscosity measurements indicated that PLA reduces the viscosity of the system, with water intensifying hydrolytic chain scission. Rheological analysis further demonstrated that even small amounts of PLA negatively impact PET's processing performance in applications such as spinning and blow molding [199].

A study by Jubinville et al. evaluated the recycling of hybrid blends composed of PLA and low concentrations of either polypropylene (PP) or low-density polyethylene (LDPE) that maintained the total biopolymer content above 89 wt % [14]. The recycling (up to five times) was conducted via a melt compounding process to elucidate the impact of PP and LDPE on the flow and thermomechanical properties of the resulting recycled hybrid material. Results of the study demonstrated that the PLA hybrid with LDPE subjected to recycling underwent crosslinking, noted from an increase in melt viscosity and increase in the zero-shear viscosity ratio of the blended polymers. In contrast, the PP-containing PLA hybrid demonstrated reduced viscosity, likely attributed to temperature and shear mediated chain scission. As a result, the PLA/LDPE system retained thermomechanical properties as opposed to the PLA/PP system, which demonstrated property deterioration.

Despite advanced sorting technologies, the complete elimination of PLA contamination remains unachievable, jeopardizing product consistency. In-line near-infrared spectroscopy (Fig. 31e) has been shown to be a potential solution for real-time detection of PLA contamination [194]. Hamad et al. investigated the impact of recycling on the rheological and mechanical properties of a PLA/PS hybrid bioplastic blend, finding that repeated processing reduces viscosity, degrades appearance (Fig. 31f) and mechanical properties. This is due to both the reduction in chain length and the increase in crystallinity, suggesting that PLA/PS waste is suitable for reuse as an additive in further compounding processes [195].

Further, chemical recycling entails depolymerizing the biopolymers into smaller hydrocarbon molecules (monomers) and utilizing the obtained units in an identical or another polymerization route [188]. Although it demonstrates various advantages over mechanical recycling, chemical recycling is more cost-intensive and environmentally taxing [200].

Lastly, plastic waste management offers two primary energy recovery options. Incineration, widely favored by local authorities, generates thermal energy by burning hydrocarbon or bioplastic polymers. This method of recycling is often considered an option of last resort due to the release of pollutants and often toxic chemicals during incineration [188,200,201]. An alternative is conversion through pyrolysis or hydrogenation, which breaks down polymer waste into low-molecular-weight hydrocarbons used as fuel or feedstocks [183]. The recyclability of many bioplastic blends remains underexplored, posing challenges for their integration into conventional waste streams. Therefore, advancing knowledge on

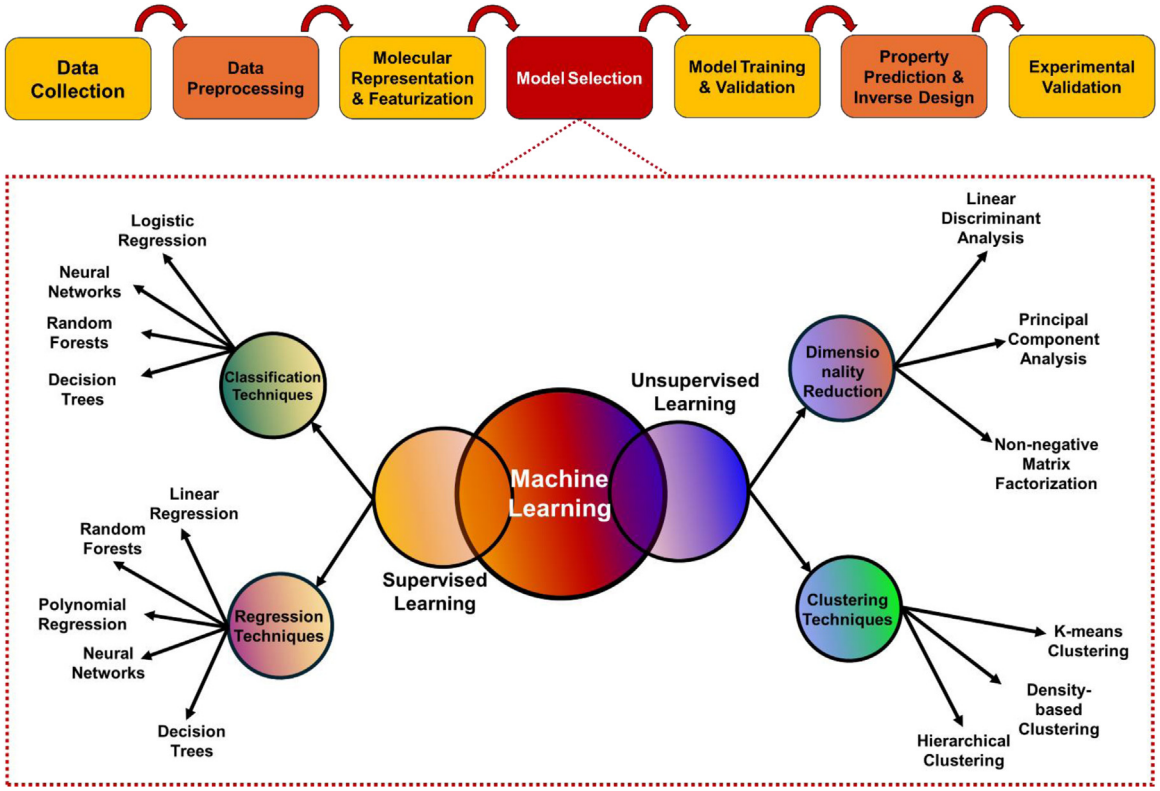

Fig. 32. Basic ML workflow initiating from data collection to model selection from various available options and concluding to experimental validation of the predicted properties.

these materials is essential to minimize their environmental impact and support a sustainable, circular economy.

6. Use of AI methods in the modeling, design, and manufacturing of bioplastic blends

In recent times, the extensive implementation of artificial intelligence (AI) methods in various industries has been observed [202]. The rise in the utilization of AI in the prediction of material properties stems from the advancements in machine learning (ML) techniques and the availability of high-quality data for training models. This has, in turn, enhanced the ability of models to predict material properties (thermal, mechanical, optical), design novel materials, and aid in material discovery [202–204]. While ML's use in "materials informatics" to link material properties with chemical and physical structures is well-established, its application in "process informatics" to optimize production processes is still emerging in the polymer industry. Moreover, the integration of "polymer informatics" in conjunction with AI/ML methods is being regarded as a major advancement in the field [205,206]. To bridge the gap between material property prediction and real-time manufacturing optimization, the utilization of approaches like Physics-Informed Machine Learning (PIML) and Digital Twins is essential [207–209]. While PIML aids in embedding physical laws into AI models, Digital Twins create virtual replica of physical manufacturing processes. This amalgamation results in continuous monitoring and on-the-fly process condition adjustments.

A basic ML workflow for accelerating the design of biopolymer blends has been outlined (Fig. 32). The process initiates with data collection, where experimental, literature-mined, and computationally derived data is collected and pre-processed (cleaning, standardization, and validation)[206,210]. Post selecting the appropriate model, the selected model is trained on a subset of data and validated for accuracy on another unseen data set. Once trained and validated, the respective model can be employed as a powerful predictive tool, primarily aiding in reduction of resource-intensive initial experimentation. For instance, Takada et al. applied random forest regression, a decision tree-based machine learning algorithm, to optimize the impact strength of a PPS/elastomer blend [211].

In a work by Mulenga et al., the application of computational methods like the rule of hybrid mixture (RoHM), finite element analysis (FEA), and artificial neural networks (ANN) in modeling the tensile properties of natural fiber-reinforced composites was reviewed [212]. The significant complications associated with plastic composite systems were highlighted. As illustrated in Fig. 33, an ANN model, with three input nodes and four output nodes, for the prediction of mechanical properties of a natural fiber-reinforced composite material has been presented. In this ANN model, the three input nodes process the data through two hidden layers (six nodes each) interconnected via neurons. Hence, the model outputs tensile strength, impact strength, flexural strength, and hardness.

In a work by Gu et al., convolutional neural networks were employed to design stiff and soft segments of bioinspired composites [213]. The design classified as best by the ML model was denoted as ML-opt and the lowest toughness design was designated ML-min. As illustrated in Fig. 34b, the strain field exhibited by ML-opt was more uniformly distributed in comparison to the lowest toughness (ML-min) specimen. Similar observations were recorded in Fig. 34c**.** Overall, it was inferred that the ML model was able to recognize the design patterns leading to specimens demonstrating low and high toughness.

In the case of bioplastics and their blends and composites, the application of AI is even more nascent due to the added complexity of these materials, such as biodegradability and unique processing challenges [214]. Ebrahimzade et al. successfully monitored

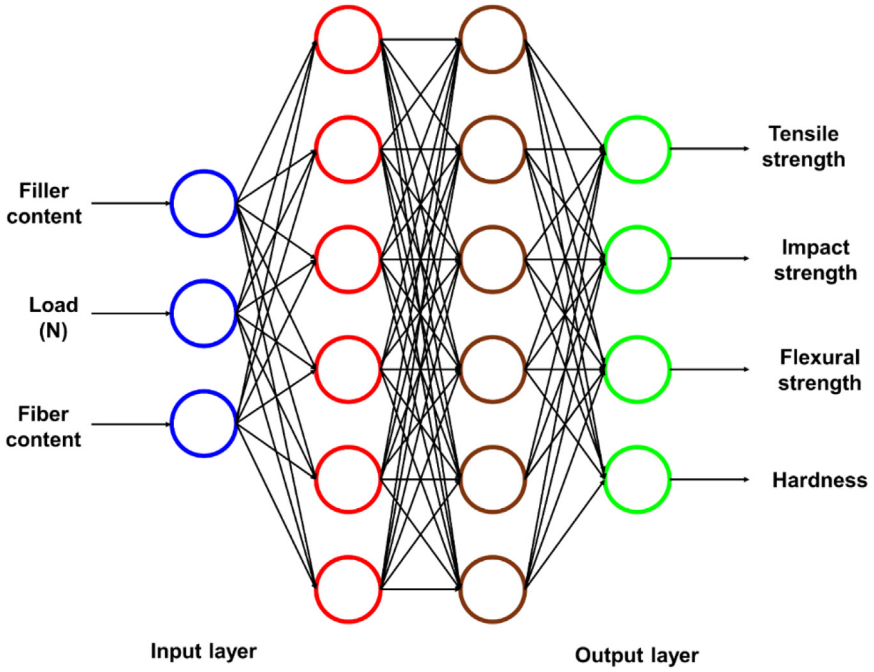

Fig. 33. An ANN model for predicting mechanical properties of natural fiber-reinforced composites [212], Copyright 2021. Adapted with permission from Multidisciplinary Digital Publishing Institute.

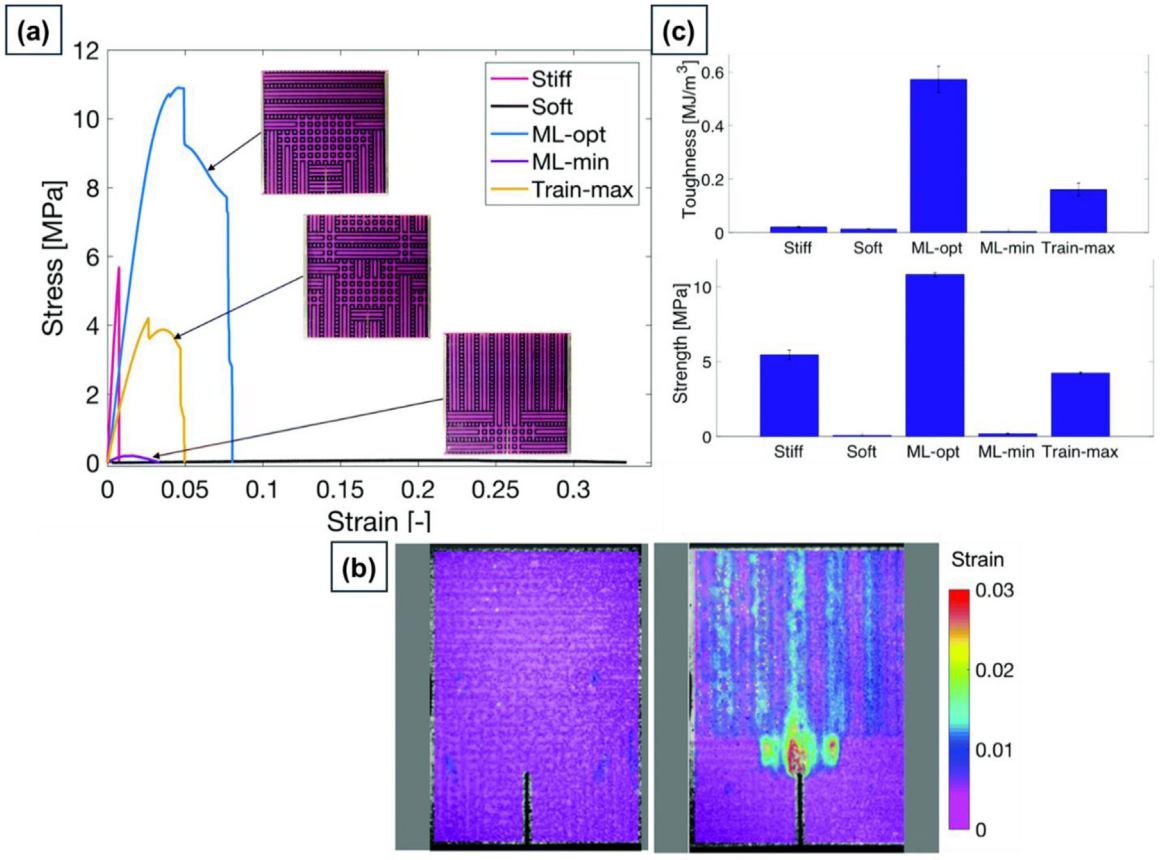

Fig. 34. a). Stress-strain curves, b) Strain field plots, c) Toughness and strength values [213], Copyright 2018. Adapted with permission from The Royal Society of Chemistry.

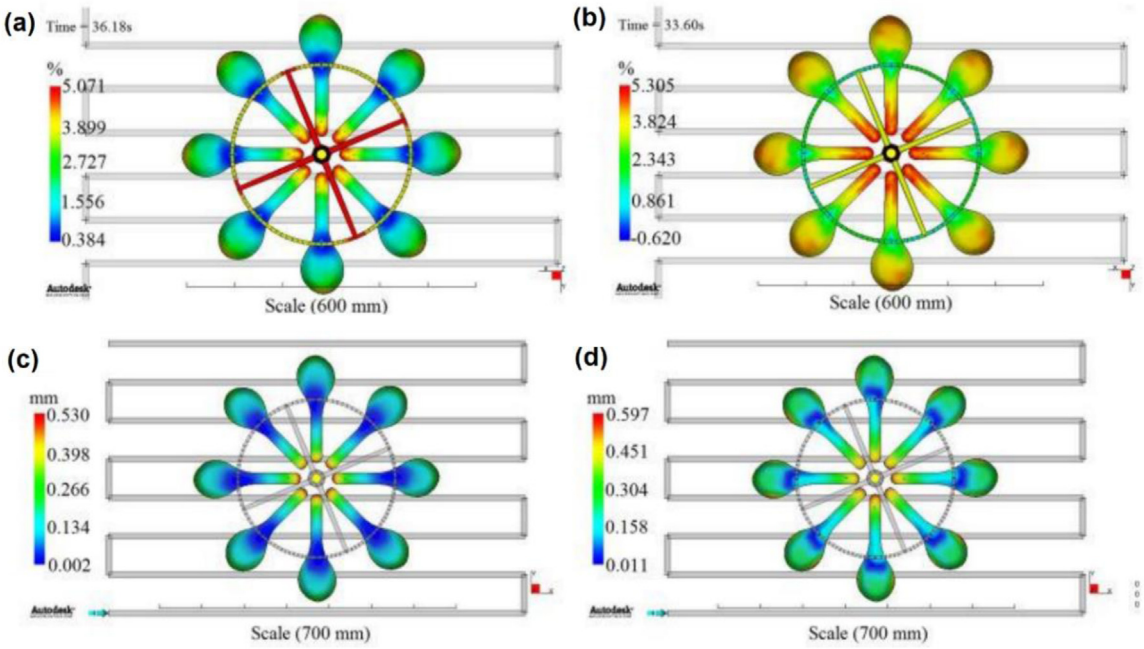

Fig. 35. Shrinkage. (a) PLA-TPU, (b) PLA-TPS. **W**arpage. (c) PLA-TPU, (d) PLA-TPS [219], Copyright 2016. Adapted with permission from Elsevier Science Ltd.

the kinetics of methane production during the anaerobic digestion (AD) of starch-based bioplastics using multi-layer perceptron artificial neural network (MLP-ANN), addressing limitations of commonly used First-order and Gompertz models in bioplastic fermentation modeling [215]. Ibarra-Perez et al. explored the application of ML techniques to predict the composition and mechanical properties of seaweed bioplastics using sparse data from scientific literature [216]. Chen et al. showcased AI and robotics' potential in accelerating the discovery of biodegradable plastic substitutes with programmable properties. An automated robot prepared 286 nanocomposite films to train a support-vector machine, followed by 14 active learning loops to produce 135 more samples and build an accurate ANN. The model predicts material properties and designs substitutes tailored to user needs. The substitutes exhibit comparable properties to petrochemical plastics, with added biodegradability and environmental benefits [217].

In another work, Wang et al. used AI to optimize PLLA/fiber PGA bioplastic composite's crystallinity, enhancing performance by analyzing crystallization time, temperature, and PGA content with ML methods like ANN, as well as Adaptive Neuro-Fuzzy Inference Systems (ANFIS) and Least-Squares Support Vector Regression (LSSVR) [218]. Moreover, Oliaei et al. discussed the integration of a feed-forward back-propagation ANN to optimize the processing and properties of PLA-TPS bioplastic blend and a hybrid bioplastic blend of PLA-TPU to minimize defects like warpage and shrinkage while improving quality and cost-efficiency. Using well-established software (Autodesk Moldflow®), the injection molding process was simulated, and an artificial neural network was developed for pattern recognition and optimization. This approach was conducted in parallel with and compared to the Taguchi Design of Experiments. Fig. 35 indicates the volumetric shrinkage behavior and deflection (warpage) of PLA-TPU and PLA-TPS in the same process conditions, with red regions indicating the highest defect. The results revealed that PLA-TPU demonstrated superior performance in minimizing defects, making it the most stable and efficient option [219].

Wang et al. employed six different AI classes to estimate the relative crystallinity of PLLA/PGA bioplastic blends, a crucial factor for enhancing mechanical performance and stability, as a function of crystallization time, temperature, and PGA content. The models include the multilayer perceptron neural network (MLPNN), recurrent neural network (RNN), cascade feedforward neural network (CFFNN), adaptive neuro-fuzzy inference system with subtractive clustering (ANFIS2), c-means clustering (ANFIS3) membership functions, and least-squares support vector regression (LSSVR). The results showed that CFFNN with one hidden layer and nine neurons provided the most accurate predictions [196].

In a work by Kuenneth et al., deep learning was employed to design and predict the properties of PHA-based bioplastics based on available experimental data for a diverse set of nearly 23,000 homo- and copolymer chemistries. The model identified 14 promising bioplastic blends that could replace common plastics used for packaging, bottles, and more (Fig. 36). They also explored possible ways to produce these bioplastics using microbes or chemical methods [220].

Undoubtedly, data-driven approaches have significantly reduced the reliance on trial-and-error experimentation, offering considerable savings in both time and resources. Despite progress, challenges remain in terms of scalability, cost reduction, and achieving desired material properties [221]. In the context of bioplastics, while AI is revolutionizing material discovery, but numerous limitations need to be addressed. Accurate prediction of the properties of bioplastics or their blends requires training the ML model with high-quality datasets, an absence of which could result in unreliable predictions. The unavailability of high-quality data in sufficient quantity is one of the most significant limitations encountered by the polymer machine learning community [206,222–224]. Consequently, most of the data employed in material/polymer science is categorized as "small data" (comprising tens to hundreds of data points) [206]. Further, insufficient sample sizes and high feature dimensions could result in model overfitting or underfitting [212].

This lack of reliable data can be addressed through in-house experimental data generation and literature-sourced data mining [206,224]. Additionally, utilization of robotic platforms for high-throughput experimentation can automate the data collection process, performing repetitive tasks and generating consistent, reliable, and high precision data [224,225]. Moreover, the in-house generated data can be augmented by systematic data sourcing

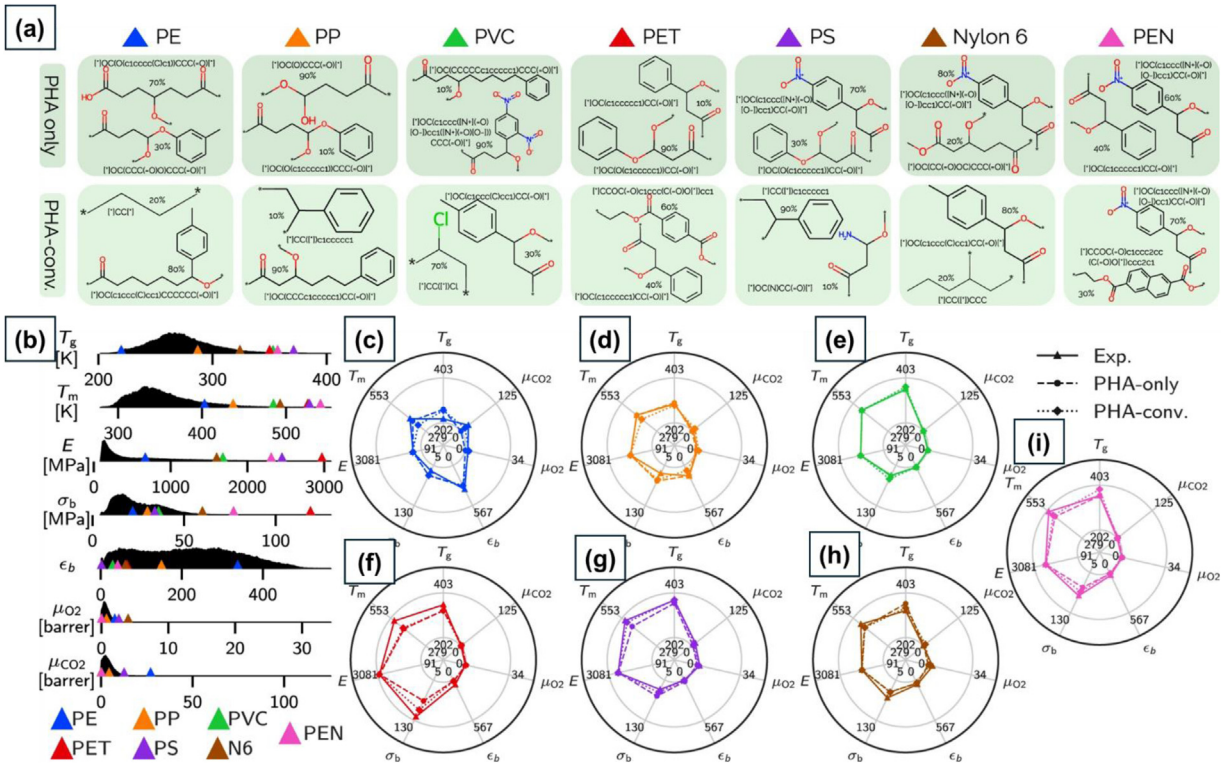

Fig. 36. (a) Bio-replacements (PHA-only and PHA-conventional) for seven commodity plastics. (b) Property density profiles. (c–i) Property radar charts for each commodity plastic comparing experimental properties (triangles with solid lines) to predicted properties of bio-replacements PHA-only (circles with dashed lines) and PHA-conventional (diamonds with dotted lines) [220], Copyright 2022. Adapted with permission from Nature.

from various polymer databases such as PubChem, CROW, Khazana, and PI1m [206,226–229].

Further, some predicted data could be difficult to interpret. To enhance the interpretability of AI predictions, the employment of transparent models like decision trees and random forests is recommended. For more complex models like deep neural networks, the use of post-hoc techniques are essential for explaining predictions. SHAP (Shapley Additive exPlanations) can be used to analyze the effect of each input feature on model's output predictions. Moreover, the complex interplay between multiple variables can be visualized employing Partial Dependence Plots (PDPs) [230,231]. Additionally, potential biases in the models could undermine the reliability of the predictions, rendering them unsuitable for practical application. These biases can be identified by scrutinizing data distributions and using interpretability tools like SHAP [230]. Mitigation of potential biases in models can be ensured by data resampling, augmentation, and diverse data sourcing. Post mitigation, the model could be validated employing Out-of-Distribution (OOD) testing, experimental synthesis and verification of the AI-predicted materials [232]. Addressing these limitations is essential to fully harness the transformative potential of AI in bioplastic blend development.

7. Concluding remarks

This review has provided a comprehensive overview of polymer blends, a practical way for fabricating cost-effective and high-performance materials with tailored properties. By combining the unique material properties of constituent polymeric moieties, new materials exhibiting better mechanical and thermal properties, minimal phase separation, and cost efficacy could be formulated. The thermodynamic interactions, process kinematics, morphology development, and compatibilization strategies for immiscible polymer blends were discussed. Further, the challenges pertaining to biopolymer blends, including recycling methods, end-of-life biodegradability, and cost-effectiveness were addressed. The integration of artificial intelligence in various domains, including material science for computational material discovery and property prediction employing ANN was presented.

By synergizing the principles of blend morphology, employing compatibilization techniques, addressing end-of-life management, and incorporating the transformative power of artificial intelligence (AI), the next-generation of sustainable polymer blends could be designed. Lastly, development of models utilizing small data for accurate predictions and design of compatibized blends without compromising end-of-life options are key research area for future of bioplastic blends.

Declaration of competing interest

The authors declare that they have no known competing financial interests or personal relationships that could have appeared to influence the work reported in this paper.

CRediT authorship contribution statement

Rohan Shorey: Writing – review & editing, Writing – original draft, Investigation, Conceptualization. **Elnaz Esmizadeh:** Writing – review & editing, Writing – original draft, Methodology, Investigation. **Tizazu H. Mekonnen:** Writing – review & editing, Writing – original draft, Validation, Supervision, Project administration, Investigation, Formal analysis, Conceptualization.

Data availability

No data was used for the research described in the article.

Acknowledgments

We appreciate the financial support of the Natural Sciences and Engineering Research Council of Canada (NSERC) and the National Research Council of Canada. This research was conducted in part thanks to funding from the Canada Research Chairs Program to Tizazu H. Mekonnen.

References

[1] Rosenboom JG, Langer R, Traverso G. Bioplastics for a circular economy. Nat Rev Mater 2022;7:117–37. doi:10.1038/s41578-021-00407-8.
[2] Nanda S, Patra BR, Patel R, Bakos J, Dalai AK. Innovations in applications and prospects of bioplastics and biopolymers: a review. Env Chem Lett 2021;20:379–95. doi:10.1007/S10311-021-01334-4.
[3] Di Bartolo A, Infurna G, Dintcheva NT. A review of bioplastics and their adoption in the circular economy. Polymers 2021;13:1229. doi:10.3390/POLYM13081229.
[4] Muthuraj R, Valerio O, Mekonnen TH. Recent developments in short- and medium-chain- length polyhydroxyalkanoates: production, properties, and applications. Int J Biol Macromol 2021;187:422–40. doi:10.1016/J.IJBIOMAC.2021.07.143.
[5] European Bioplastics. Bioplastics market development update 2023. https://www.european-bioplastics.org/bioplastics-market-development-update-2023-2/; 2025 [accessed 04 June 2025].
[6] Statista. Global bioplastic production capacities by material 2023. https://www.statista.com/statistics/678775/production-capacity-distribution-of-bioplastics-worldwide-by-material/; 2025 [accessed 08 March 2025].
[7] Plastics Engineering. Bioplastics Market Trends and Forecasts to 2028. https://www.plasticsengineering.org/2024/12/bioplastics-market-trends-and-forecasts-to-2028-007648/#!; 2025 [accessed 10 December 2025].
[8] Statista. Distribution of the bioplastics production capacity worldwide in 2023, by region. https://www.statista.com/statistics/678811/production-capacity-distribution-of-bioplastics-worldwide-by-region/; 2025 [accessed 04 June 2025].
[9] Rech A, Daugaard AE. Thermoprocessing biopolymers and Bio-waste-based materials. ACS Sustain Resour Manag 2024;2:4–28. doi:10.1021/ACSSUSRESMGT.4C00332.
[10] Esmizadeh E, Gupta A, Asrat S, Mekonnen TH. Crystallization and performance evolution of PHBV nanocomposites through annealing: the role of surface modification of CNCs. Polymers 2024;308:127352. doi:10.1016/J.POLYMER.2024.127352.
[11] Shorey R, Mekonnen TH. Sustainable paper coating with enhanced barrier properties based on esterified lignin and PBAT blend. Int J Biol Macromol 2022;209:472–84. doi:10.1016/J.IJBIOMAC.2022.04.037.
[12] Tadele DT, Trinh BM, Mekonnen TH. PBAT/corn zein ester blends: rheology, morphology, and physicochemical properties. Polymers 2023;283:126258. doi:10.1016/J.POLYMER.2023.126258.
[13] Crawford EA, Mekonnen TH. Effects of chain extension and clay reinforcement on PLA nanocomposite foams. React Funct Polym 2025;209:106183. doi:10.1016/J.REACTFUNCTPOLYM.2025.106183.
[14] Jubinville D, Lee HS, Mekonnen T. High-biocontent polymer blends and their wood plastic composites: blending, compatibilization, and their recyclability. App Compos Mater 2024;31:1625–44. doi:10.1007/S10443-024-10253-W.
[15] Mekonnen T, Mussone P, Khalil H, Bressler D. Progress in bio-based plastics and plasticizing modifications. J Mater Chem A 2013;1:13379–98. doi:10.1039/C3TA12555F.
[16] Cl La Fuente Arias, neiwa Kubo MTK, Tadini CC, Augusto PED. Bio-based multilayer films: a review of the principal methods of production and challenges. Crit Rev Food Sci Nutr 2023;63:2260–76. doi:10.1080/10408398.2021.1973955.
[17] Cucina M, de Nisi P, Tambone F, Adani F. The role of waste management in reducing bioplastics' leakage into the environment: a review. Bioresour Technol 2021;337:125459. doi:10.1016/J.BIORTECH.2021.125459.
[18] Willemse RC, Ramaker EJJ, Van Dam J, Posthuma De Boer A. Morphology development in immiscible polymer blends: initial blend morphology and phase dimensions. Polymers 1999;40:6651–9. doi:10.1016/S0032-3861(99)00038-5.
[19] Ravati S, Poulin S, Piyakis K, Favis BD. Phase identification and interfacial transitions in ternary polymer blends by ToF-SIMS. Polymers 2014;55:6110–23. doi:10.1016/J.POLYMER.2014.09.013.
[20] Paul D. Polymer blends volume 1. 1st ed. Amsterdam: Elsevier; 2012.
[21] Kamal MR, Khoshkava V. Effect of cellulose nanocrystals (CNC) on rheological and mechanical properties and crystallization behavior of PLA/CNC nanocomposites. Carbohydr Polym 2015;123:105–14. doi:10.1016/J.carbpol.2015.01.012.
[22] White RP, Lipson JEG, Higgins JS. How pure components control polymer blend miscibility. Macromolecules 2012;45:8861–71. doi:10.1021/MA3018124.
[23] Akkapeddi MK, Utracki LA. Commercial polymer blends. In: Polymer blends handbook. Dordrecht: Kluwer Academic Publishers; 2002. p. 1023–116.
[24] Pisharath S, Wong SC. Development of the morphology and crystalline state due to hybridization of reinforced toughened nylon containing a liquid-crystalline polymer. J Polym Sci B Polym Phys 2003;41:549–59. doi:10.1002/POLB.10421.
[25] Ogunsona E, D'Souza NA. Characterization and mechanical properties of foamed poly(ε-caprolactone) and Mater-Bi blends using CO2 as blowing agent. J Cell Plast 2015;51:245–68. doi:10.1177/0021955x14537658.
[26] Xanthos M, Dangli SS. Compatibilization of polymer blends by reactive processing. Polym Eng Sci 1991;31:929–35. doi:10.1002/pen.760311302.
[27] Coleman M, Painter P. Miscible polymer blends: background and guide for calculations and design. DEStech Publications, Inc; 2006.
[28] Quayle OR. The Parachors of organic compounds. An interpretation and catalogue. Chem Rev 1953;53:439–589. doi:10.1021/cr60166a003.
[29] Utracki L, Wilkie C. Polymer blends handbook. 2nd Ed. Springer; 2002.
[30] Ajitha AR, Thomas S. Introduction: polymer blends, thermodynamics, miscibility, phase separation, and compatibilization. compatibilization of polymer blends: micro and nano scale phase morphologies, interphase characterization, and properties. Elsevier; 2020. p. 1–29. doi:10.1016/B978-0-12-816006-0.00001-3.
[31] Sarikhani K, Jeddi K, Thompson RB, Park CB, Chen P. Effect of pressure and temperature on interfacial tension of poly lactic acid melt in supercritical carbon dioxide. Thermochim Acta 2015;609:1–6. doi:10.1016/J.TCA.2015.04.005.
[32] Ito EN, Ueki MM, Bretas RES, Hage E. Interfacial tension of PBT/SAN blends by the drop retraction method. Mater Res 2008;11:165–9. doi:10.1590/S1516-14392008000200009.
[33] Virgilio N, Desjardins P, L'Espérance G, Favis BD. Modified interfacial tensions measured in situ in ternary polymer blends demonstrating partial wetting. Polymers 2010;51:1472–84. doi:10.1016/J.polymer.2010.01.017.
[34] Virgilio N, Desjardins P, L'Espérance G, Favis BD. In situ measure of interfacial tensions in ternary and quaternary immiscible polymer blends demonstrating partial wetting. Macromolecules 2009;42:7518–29. doi:10.1021/MA9005507.
[35] Son Y. Comparative measurement of interfacial tension by transient dynamic methods. J Appl Polym Sci 2006;99:1910–18. doi:10.1002/APP.22670.
[36] Palmer G, Demarquette NR. Evaluation of imbedded fiber retraction phenomenological models for determining interfacial tension between molten polymers. Polymers 2005;46:8169–77. doi:10.1016/J.POLYMER.2005.06.047.
[37] Luciani A, Champagne MF, Utracki LA. Interfacial tension in polymer blends.1. Theory. Macromol Symp 1998;126:307–21. doi:10.1002/masy.19981260125.
[38] Antonoff G. On the validity of Antonoff's rule. J Phys Chem 1942;46:497–9. doi:10.1021/J150418A009.
[39] Wisian-Neilson P. Book Reviews: physical Properties of Polymers Handbook. J Am Chem Soc 1997;119:4096 96. doi:10.1021/JA965747X.
[40] Wu S. Polymer interface and adhesion. Polym Interface Adhes 2017:1–630. doi:10.1201/9780203742860/polymer-interface-adhesion-souheng-wu.
[41] Biresaw G, Carriere CJ. Interfacial tension of poly(lactic acid)/polystyrene blends. J Polym Sci B Polym Phys 2002;40:2248–58. doi:10.1002/POLB.10290.
[42] Wu S. Calculation of interfacial tension in polymer systems. Polym Sci C: Polym Symp 1971;34:19–30. doi:10.1002/POLC.5070340105.
[43] Gale M. Compounding with single-screw extruders. Adv Polym Techn 1997;16:251–62. doi:10.1002/(SICI)1098-2329(199711)16:4.
[44] Formela K, Zedler Hejna A, Tercjak A. Reactive extrusion of bio-based polymer blends and composites–current trends and future developments. Express Polym Lett 2018;12:24–57. doi:10.3144/EXPRESSPOLYMLETT.2018.4.
[45] Jamalzadeh M, Sobkowicz MJ. Reactive extrusion of post-irradiated poly(ethylene terephthalate) to improve the interfacial interactions in compounding with its immiscible polyethylene blends. Polym Eng Sci 2024;64:1796–811. doi:10.1002/PEN.26659.
[46] Wang S, Daelemans L, Fiorio R, Gou M, DR D'hooge, De Clerck K, et al. Improving mechanical properties for extrusion-based additive manufacturing of poly(Lactic Acid) by annealing and blending with poly(3-Hydroxybutyrate). Polymers 2019;11:1529. doi:10.3390/POLYM11091529.
[47] Selvakumar M, Bhat DK, Renganathan NG. Miscibility of polymethylmethacrylate and polyethyleneglycol blends in tetrahydrofuran. J Appl Polym Sci 2009;111:452–60. doi:10.1002/APP.29113.
[48] Chella R, Ottino JM. Stretching in some classes of fluid motions and asymptotic mixing efficiencies as a measure of flow classification. Arch Ration Mech Anal 1985;90:15–42. doi:10.1007/BF00281585.
[49] Cardinaels R, Moldenaers P. Morphology development in immiscible polymer blends. In: Guo Q. polymer morphology: principles, characterization, and processing. Wiley; 2016. p. 348–73. doi:10.1002/9781118892756.CH19.
[50] Banerjee R, Ray SS. Role of rheology in morphology development and advanced processing of thermoplastic polymer materials: a review. ACS Omega 2023;8:27969–8001. doi:10.1021/ACSOMEGA.3C03310.
[51] Utracki LA, Shi ZH. Development of polymer blend morphology during compounding in a twin-screw extruder. Part I: droplet dispersion and coalescence—A review. Polym Eng Sci 1992;32:1824–33. doi:10.1002/PEN.760322405.
[52] Naser AZ, Deiab I, Defersha F, Yang S. Expanding poly(lactic acid) (PLA) and polyhydroxyalkanoates (PHAs) applications: a review on modifications and effects. Polymers 2021;13:4271. doi:10.3390/POLYM13234271.
[53] Ohkoshi I, Abe H, Doi Y. Miscibility and solid-state structures for blends of poly[(S)-lactide] with atactic poly[(R,S)-3-hydroxybutyrate]. Polymers 2000;41:5985–92. doi:10.1016/S0032-3861(99)00781-8.
[54] Iannace S, Ambrosio L, Huang SJ, Nicolais L. Poly(3-hydroxybutyrate)-co-(3-hydroxyvalerate)/Poly-L-lactide blends: thermal and mechanical properties. J Appl Polym Sci 1994;54:1525–35. doi:10.1002/APP.1994.070541017.
[55] Cheng H, Li Y, Zhang Y, Yu Y, Yu M, Han C, et al. Ternary blends from biodegradable poly(L-lactic acid), poly(ε-caprolactone) and poly(vinyl ac-

etate) with balanced properties. J Polym Res 2023;30:1–14. doi:10.1007/S10965-023-03564-2.
[56] Sivalingam G, Karthik R, Madras G. Blends of poly(ε-caprolactone) and poly(vinyl acetate): mechanical properties and thermal degradation. Polym Degrad Stab 2004;84:345–51. doi:10.1016/j.polymdegradstab.2004.01.011.
[57] Hay JN, Sharma L. Crystallisation of poly(3-hydroxybutyrate)/polyvinyl acetate blends. Polymers 2000;41:5749–57. doi:10.1016/S0032-3861(99)00807-1.
[58] Li X, Yang P, Zhu Z, You Z, Zhang W, Zhang T, et al. Sol-gel condensation of temperature sensitive and shape stabilized phase change materials for thermal energy storage. Thermochim Acta 2020;693. doi:10.1016/j.tca.2020.178758.
[59] Takhulee A, Takahashi Y. Vao-soongnern V. Molecular simulation and experimental studies of the miscibility of polylactic acid/polyethylene glycol blends. J Polym Res 2016;24:1–10. doi:10.1007/S10965-016-1174-3.
[60] Sheth M, Ananda Kumar R, Davé V, Gross RA, Mccarthy SP. Biodegradable polymer blends of poly (lactic acid) and poly (ethylene glycol). J Appl Polym Sci 1997;66:1495–505. doi:10.1002/(SICI)1097-4628(19971121)66:8.
[61] Sungsanit K, Kao N, Bhattacharya SN. Properties of linear poly(lactic acid)/polyethylene glycol blends. Polym Eng Sci 2012;52:108–16. doi:10.1002/PEN.22052.
[62] Yeganeh J, Goharpey F, Foudazi R. Can only rheology be used to determine the phase separation mechanism in dynamically asymmetric polymer blends (PS/PVME)? RSC Adv 2012;2:8116–27. doi:10.1039/c2ra21307a.
[63] Yeganeh J, Goharpey F, Foudazi R. Anomalous phase separation behavior in dynamically asymmetric LCST polymer blends. RSC Adv 2014;4:12809–25. doi:10.1039/c3ra47299j.
[64] Navas IO, Kamkar M, Arjmand M, Sundararaj U. Morphology evolution, molecular simulation, electrical properties, and rheology of carbon nanotube/polypropylene/polystyrene blend nanocomposites: effect of molecular interaction between styrene-butadiene block copolymer and carbon nanotube. Polymers 2021;13:230. doi:10.3390/POLYM13020230.
[65] Li H, Sundararaj U. Morphology development of polymer blends in extruder: the effects of compatibilization and rotation rate. Macromol Chem Phys 2009;210:852–63. doi:10.1002/MACP.200800543.
[66] Kitayama N, Keskkula H, Paul DR. Reactive compatibilization of nylon 6/styrene–acrylonitrile copolymer blends. Part 1. Phase inversion behavior. Polymers 2000;41:8041–52. doi:10.1016/S0032-3861(00)00156-7.
[67] Li L, Miesch C, Sudeep PK, Balazs AC, Emrick T, Russell TP, et al. Kinetically trapped co-continuous polymer morphologies through intraphase gelation of nanoparticles. Nano Lett 2011;11:1997–2003. doi:10.1021/NL200366Z.
[68] Willemse RC, Posthuma De Boer A, Van Dam J, Gotsis AD. Co-continuous morphologies in polymer blends: the influence of the interfacial tension. Polymers 1999;40:827–34. doi:10.1016/S0032-3861(98)00307-3.
[69] Veenstra H, Van Dam J, Posthuma De Boer A. Formation and stability of co-continuous blends with a poly(ether-ester) block copolymer around its order–disorder temperature. Polymers 1999;40:1119–30. doi:10.1016/S0032-3861(98)00342-5.
[70] Manas-Zloczower I. Mixing and compounding of polymers: theory and practice. 2nd ed. Munich: Carl Hanser Verlag; 2009.
[71] Hagedorn JG, Martys NS, Douglas JF. Breakup of a fluid thread in a confined geometry: droplet-plug transition, perturbation sensitivity, and kinetic stabilization with confinement. Phys Rev Stat Phys Plasmas Fluids Relat Interdiscip Top 2004;69:18. doi:10.1103/PHYSREVE.69.056312.
[72] Grace HP. Dispersion phenomena in high viscosity immiscible fluid systems and application of static mixers as dispersion devices in such systems. Chem Eng Commun 1982;14:225–77. doi:10.1080/00986448208911047.
[73] García-Masabet V, Pérez OS, Cailloux J, Abt T, Sánchez-Soto M, Carrasco F, et al. PLA/PA bio-blends: induced morphology by extrusion. Polymers 2019;12:10. doi:10.3390/POLYM12010010.
[74] Wu S. Formation of dispersed phase in incompatible polymer blends: interfacial and rheological effects. Polym Eng Sci 1987;27:335–43. doi:10.1002/pen.760270506.
[75] Chen H, Sundararaj U, Nandakumar K. Modeling of polymer melting, drop deformation, and breakup under shear flow. Polym Eng Sci 2004;44:1258–66. doi:10.1002/pen.20121.
[76] Lin B, Mighri F, Huneault MA, Sundararaj U. Parallel breakup of polymer drops under simple shear. Macromol Rapid Commun 2003;24:783–8. doi:10.1002/MARC.200350026.
[77] Lin B, Sundararaj U, Mighri F, Huneault MA. Erosion and breakup of polymer drops under simple shear in high viscosity ratio systems. Polym Eng Sci 2003;43:891–904. doi:10.1002/PEN.10073.
[78] Horiuchi S, Matchariyakul N, Yase K, Kitano T. Morphology development through an interfacial reaction in ternary immiscible polymer blends. Macromolecules 1997;30:3664–70. doi:10.1021/MA9615258.
[79] Fortelný I. Coalescence in polymer blends: solved and open problems. Macromol Symp 2001;158:137–48. doi:10.1002/1521-3900(200008)158:1<137::AID-ASY137>3.0.CO;2-S.
[80] Wang H, Zinchenko AZ, Davis RH. The collision rate of small drops in linear flow fields. J Fluid Mech 1994;265:161–88. doi:10.1017/S0022112094000790.
[81] Jeelani SAK, Hartland S. Effect of interfacial mobility on thin film drainage. J Colloid Interface Sci 1994;164:296–308. doi:10.1006/JCIS.1994.1171.
[82] Janssen JMH, Meijer HEH. Dynamics of liquid-liquid mixing: a 2-zone model. Polym Eng Sci 1995;35:1766–80. doi:10.1002/PEN.760352206.
[83] Fortelný I. An analysis of the origin of coalescence suppression in compatibilized polymer blends. Eur Polym J 2004;40:2161–6. doi:10.1016/J.EURPOLYMJ.2004.05.017.
[84] Wong ACY, Lam F. Study of selected thermal characteristics of polypropylene/polyethylene binary blends using DSC and TGA. Polym Test 2002;21:691–6. doi:10.1016/S0142-9418(01)00144-1.
[85] Hubo S, Delva L, Van Damme N, Ragaert K. Blending of recycled mixed polyolefins with recycled polypropylene: effect on physical and mechanical properties. AIP Conf Proc 2016:1779. doi:10.1063/1.4965586.
[86] Grizzuti N, Buonocore G, Iorio G. Viscous behavior and mixing rules for an immiscible model polymer blend. J Rheol 2000;44:149–64. doi:10.1122/1.551073.
[87] Hind RK, McLaughlin E, Ubbelohde AR. Structure and viscosity of liquids camphor+pyrene mixtures. Trans Faraday Soc 1960;56:328–30. doi:10.1039/TF9605600328.
[88] Utracki LA. On the viscosity-concentration dependence of immiscible polymer blends. J Rheol 1991;35:1615–37. doi:10.1122/1.550248.
[89] Ferg EE, Bolo LL. A correlation between the variable melt flow index and the molecular mass distribution of virgin and recycled polypropylene used in the manufacturing of battery cases. Polym Test 2013;32:1452–9. doi:10.1016/J.POLYMERTESTING.2013.09.009.
[90] Bremner T, Rudin A, Cook DG. Melt flow index values and molecular weight distributions of commercial thermoplastics. J Appl Polym Sci 1990;41:1617–27. doi:10.1002/APP.1990.070410721.
[91] Pesaranhajiabbas E, Pal AK, Rodriguez-Uribe A, Mohanty AK, Misra M. Biodegradable polymer blends: studies on performance control through droplet to Co-continuous morphology. ACS Appl Polym Mater 2022;4:5546–56. doi:10.1021/ACSAPM.2C00603.
[92] Willemse RC, Posthuma De Boer A, Van Dam J, Gotsis AD. Co-continuous morphologies in polymer blends: a new model. Polymers 1998;39:5879–87. doi:10.1016/S0032-3861(97)10200-2.
[93] Sarazin P, Roy X, Favis BD. Controlled preparation and properties of porous poly(l-lactide) obtained from a co-continuous blend of two biodegradable polymers. Biomaterials 2004;25:5965–78. doi:10.1016/J.BIOMATERIALS.2004.01.065.
[94] Fortelný I, Jůza J. The effects of copolymer compatibilizers on the phase structure evolution in polymer blends—A review. Materials 2021;14:7786. doi:10.3390/MA14247786.
[95] Porter RS, Wang LH. Compatibility and transesterification in binary polymer blends. Polymers 1992;33:2019–30. doi:10.1016/0032-3861(92)90866-U.
[96] Trinh BM, Tadele DT, Mekonnen TH. Robust and high barrier thermoplastic starch – PLA blend films using starch- graft -poly(lactic acid) as a compatibilizer. Mater Adv 2022;3:6208–21. doi:10.1039/D2MA00501H.
[97] Van Dyk AK, Chatterjee T, Ginzburg VV, Nakatani AI. Shear-dependent interactions in hydrophobically modified ethylene oxide urethane (HEUR) based coatings: mesoscale structure and viscosity. Macromolecules 2015;48:1866–82. doi:10.1021/MA502174X.
[98] Barzykin AV, Seki K, Tachiya M. Kinetics of diffusion-assisted reactions in microheterogeneous systems. Adv Colloid Interface Sci 2001;89–90:47–140. doi:10.1016/S0001-8686(00)00053-1.
[99] Macosko CW, Jeon HK, Hoye TR. Reactions at polymer–polymer interfaces for blend compatibilization. Prog Polym Sci 2005;30:939–47. doi:10.1016/j.progpolymsci.2005.06.003.
[100] Koning C, Van Duin M, Pagnoulle C, Jerome R. Strategies for compatibilization of polymer blends. Prog Polym Sci 1998;23:707–57. doi:10.1016/S0079-6700(97)00054-3.
[101] Kun D, Pukánszky B. Polymer/lignin blends: interactions, properties, applications. Eur Polym J 2017;93:618–41. doi:10.1016/J.eurpolymj.2017.04.035.
[102] Fortelný I, Kamenická D, Kovář J. Effect of the viscosity of components on the phase structure and impact strength of polypropylene/ethylene-propylene elastomer blends. Macromol Mater Eng 1988;164:125–41. doi:10.1002/APMC.1988.051640110.
[103] Taylor GI. The formation of emulsions in definable fields of flow. Proc R Soc L A 1934;146:501–23. doi:10.1098/RSPA.1934.0169.
[104] Kammer H-W. Surface and interfacial tension of polymer melts — Thermodynamic theory of the interface between immiscible polymers. Z Phys Chem 1977;258O:1149–61. doi:10.1515/ZPCH-1977-258153.
[105] Sternberg J, Sequerth O, Pilla S. Green chemistry design in polymers derived from lignin: review and perspective. Prog Polym Sci 2021;113:101344. doi:10.1016/j.progpolymsci.2020.101344.
[106] Upton BM, Kasko AM. Strategies for the conversion of lignin to high-value polymeric materials: review and perspective. Chem Rev 2016;116:2275–306. doi:10.1021/ACS.chemrev.5B00345.
[107] Shorey R, Salaghi A, Fatehi P, Mekonnen TH. Valorization of lignin for advanced material applications: a review. RSC Sustain 2024;2:804–31. doi:10.1039/D3SU00401E.
[108] Shin BY, S-Il Lee, Shin YS, Balakrishnan S, Narayan R. Rheological, mechanical and biodegradation studies on blends of thermoplastic starch and polycaprolactone. Polym Eng Sci 2004;44:1429–38. doi:10.1002/PEN.20139.
[109] Fenni SE, Wang J, Haddaoui N, Favis BD, Müller AJ, Cavallo D. Nucleation of poly(lactide) partially wet droplets in ternary blends with poly(butylene succinate) and poly(ϵ-caprolactone). Macromolecules 2020;53:1726–35. doi:10.1021/ACSMacromol.9B02295.
[110] Willett JL, Kotnis MA, O'brien GS, Fanta GF, Gordon SH. Properties of starch-graft-poly (glycidyl methacrylate)–PHBV composites. J Appl Polym Sci 1998;70(6):1121–7. doi:10.1002/(SICI)1097-4628(19981107)70:6<1121::AID-PP8>3.0.CO;2-Q.
[111] Li Y, Gancheva T, Estakhrianhaghighi E, Favis BD, Akbarzadeh A. Material extrusion of quaternary co-continuous biopolymers: a strategy for realiz-

ing lightweight cellular solids with high impact toughness. Addit Manuf 2023;77:103805. doi:10.1016/J.ADDMA.2023.103805.
[112] Jaratrotkamjorn R, Khaokong C, Tanrattanakul V. Toughness enhancement of poly(lactic acid) by melt blending with natural rubber. J Appl Polym Sci 2012;124:5027–36. doi:10.1002/APP.35617.
[113] Dil EJ, Arjmand M, Navas IO, Sundararaj U, Favis BD. Interface bridging of multiwalled carbon nanotubes in polylactic Acid/poly(butylene adipate-co-terephthalate): morphology, rheology, and electrical conductivity. Macromolecules 2020;53:10267–77. doi:10.1021/ACS.Macromol.0C01525.
[114] Rosli NA, Ahmad I, Anuar FH, Abdullah I. Effectiveness of cellulosic Agave angustifolia fibres on the performance of compatibilised poly(lactic acid)-natural rubber blends. Cellulose 2019;26:3205–18. doi:10.1007/S10570-019-02262-X.
[115] Gong J, Qiang Z, Ren J. In situ grafting approach for preparing PLA/PHBV degradable blends with improved mechanical properties. Polym Bull 2022;79:9543–62. doi:10.1007/S00289-021-03958-6.
[116] Zhang M, Thomas NL. Blending polylactic acid with polyhydroxybutyrate: the effect on thermal, mechanical, and biodegradation properties. Adv Polym Technol 2011;30:67–79. doi:10.1002/ADV.20235.
[117] Dorigato A, Fredi G. Effect of nanofillers addition on the compatibilization of polymer blends. Adv Ind Eng Polym Res 2024;7:405–27. doi:10.1016/j.aiepr.2023.09.004.
[118] Fredi G, Dorigato A. Compatibilization of biopolymer blends: a review. Adv Ind Eng Polym Res 2024;7:373–404. doi:10.1016/j.aiepr.2023.11.002.
[119] Imre B, Pukánszky B. Compatibilization in bio-based and biodegradable polymer blends. Eur Polym J 2013;49:1215–33. doi:10.1016/J.EURPOLYMJ.2013.01.019.
[120] Charfeddine I, Majesté JC, Carrot C, Lhost O. Surface tension and interfacial tension of polyolefins and polyolefin blends. J Appl Polym Sci 2022;139:51885. doi:10.1002/APP.51885.
[121] Gu L, Macosko CW. Evaluating PE/PLA interfacial tension using ternary immiscible polymer blends. J Appl Polym Sci 2021;138:50623.
[122] Liu J, Li J. Compatibilization effect of nanosilica on polypropylene/polystyrene immiscible blend. J Polym Res 2025;32:1–13. doi:10.1007/S10965-025-04566-Y.
[123] Zhang Z, Zhang J, Cao W, Liu X, Gong L, Zhang X, et al. Design of toughed bio-based polylactide/polyamide 11 blends with regulatable size of dispersed phase and spherulites by interfacial stereocomplex crystallites. Int J Biol Macromol 2024;282:137267. doi:10.1016/J.IJBIOMAC.2024.137267.
[124] Zhang X, Li X, Ji G, Huang J, Li T, Xia B, et al. Compatibilization of poly(lactic acid)/poly(propylene carbonate) blends by star-shaped multi-arm polymer with low molecular weight. Polymers 2024;313:127715. doi:10.1016/J.polymer.2024.127715.
[125] Staffa LH, Veroneze IB, Cruz SA. Exploring interfacial tension role in the laminar morphology development in reactive compatibilized PP/EVOH. J Mater Res 2025;40:69–80. doi:10.1557/S43578-024-01454-X.
[126] Van Puyvelde P, Velankar S, Moldenaers P. Rheology and morphology of compatibilized polymer blends. Curr Opin Colloid Interface Sci 2001;6:457–63. doi:10.1016/S1359-0294(01)00113-3.
[127] Taguet A, Cassagnau P, Lopez-Cuesta JM. Structuration, selective dispersion and compatibilizing effect of (nano)fillers in polymer blends. Prog Polym Sci 2014;39:1526–63. doi:10.1016/J.progpolymsci.2014.04.002.
[128] Laoutid F, Estrada E, Michell RM, Bonnaud L, Müller AJ, Dubois P. The influence of nanosilica on the nucleation, crystallization and tensile properties of PP–PC and PP–PA blends. Polymers 2013;54:3982–93. doi:10.1016/J.polymer.2013.05.031.
[129] Berezkin AV, Kudryavtsev YV. End-coupling reactions in incompatible polymer blends: from droplets to complex micelles through interfacial instability. Macromolecules 2013;46:5080–9. doi:10.1021/MA400700N.
[130] Tang J, Tang W, Yuan H, Jin R. Mechanical behaviors of ethylene/styrene interpolymer compatibilized polystyrene/polyethylene blends. J Appl Polym Sci 2007;104:4001–7. doi:10.1002/APP.26031.
[131] Gani L, Tencé-Girault S, Milléquant M, Bizet S, Leibler L. Co-continuous nanostructured blend by reactive blending: incorporation of high molecular weight polymers. Macromol Chem Phys 2010;211:736–43. doi:10.1002/MACP.200900552.
[132] Imre B, García L, Puglia D, Vilaplana F. Reactive compatibilization of plant polysaccharides and biobased polymers: review on current strategies, expectations and reality. Carbohydr Polym 2019;209:20–37. doi:10.1016/J.carbpol.2018.12.082.
[133] Ryan AJ. Designer polymer blends. Nat Mater 2002;1:8–10 2002 1:1. doi:10.1038/nmat720.
[134] Mo XZ, Wei FX, Tan DF, Pang JY, Lan CB. The compatibilization of PLA-g-TPU graft copolymer on polylactide/thermoplastic polyurethane blends. J Polym Res 2020;27:1–13. doi:10.1007/S10965-019-1999-7.
[135] Walther A, Matussek K, Müller AHE. Engineering nanostructured polymer blends with controlled nanoparticle location using Janus particles. ACS Nano 2008;2:1167–78. doi:10.1021/NN800108Y.
[136] Xu Q, Li K, Wang P, Tian R, Lu C. Fluorescence technique lighting the particle migration in polymers. Macromolecules 2022;55:5840–8. doi:10.1021/ACS.macromol.2C00788.
[137] Zhang CL, Feng LF, Zhao J, Huang H, Hoppe S, Hu GH. Efficiency of graft copolymers at stabilizing co-continuous polymer blends during quiescent annealing. Polymers 2008;49:3462–9. doi:10.1016/j.polymer.2008.06.003.
[138] Xu Y, Thurber CM, Lodge TP, Hillmyer MA. Synthesis and remarkable efficacy of model polyethylene-graft -poly(methyl methacrylate) copolymers as compatibilizers in polyethylene/poly(methyl methacrylate) blends. Macromolecules 2012;45:9604–10. doi:10.1021/ma302187b.
[139] López-Barrón CR, Tsou AH. Strain hardening of polyethylene/polypropylene blends via interfacial reinforcement with Poly(ethylene-cb-propylene) comb block copolymers. Macromolecules 2017;50:2986–95. doi:10.1021/acs.macromol.7b00264.
[140] Self JL, Zervoudakis AJ, Peng X, Lenart WR, Macosko CW, Ellison CJ. Linear, Graft, and beyond: multiblock copolymers as next-generation compatibilizers. JACS Au 2022;2:310–21. doi:10.1021/jacsau.1c00500.
[141] Coltelli MB, Mallegni N, Rizzo S, Fiori S, Signori F, Lazzeri A. Compatibilization of poly(Lactic acid) (PLA)/plasticized cellulose acetate extruded blends through the addition of reactively extruded comb copolymers. Molecules 2021;26 2006. doi:10.3390/molecules26072006.
[142] Dong W, Wang H, He M, Ren F, Wu T, Zheng Q, et al. Synthesis of reactive comb polymers and their applications as a highly efficient compatibilizer in immiscible polymer blends. Ind Eng Chem Res 2015;54:2081–9. doi:10.1021/ie503645a.
[143] Dong W, He M, Wang H, Ren F, Zhang J, Zhao X, et al. PLLA/ABS blends compatibilized by reactive comb polymers: double tg depression and significantly improved toughness. ACS Sustain Chem Eng 2015;3:2542–50. doi:10.1021/acssuschemeng.5b00740.
[144] Li Y, Dong W, Wang H. Reactive comb compatibilizers for immiscible polymer blends. In: Beyer G, Hopmann C, editors. Reactive extrusion: principles and applications. Wiley; 2017. p. 271–97. doi:10.1002/9783527801541.ch10.
[145] Al-Itry R, Lamnawar K, Maazouz A. Rheological, morphological, and interfacial properties of compatibilized PLA/PBAT blends. Rheol Acta 2014;53:501–17. doi:10.1007/S00397-014-0774-2.
[146] Quiles-Carrillo L, Montanes N, Lagaron JM, Balart R, Torres-Giner S. In Situ compatibilization of biopolymer ternary blends by reactive extrusion with low-functionality epoxy-based styrene–Acrylic oligomer. J Polym Env 2019;27:84–96. doi:10.1007/S10924-018-1324-2.
[147] Calderón BA, McCaughey MS, Thompson CW, Barinelli VL, Sobkowicz MJ. Evaluating the influence of specific mechanical energy on biopolymer blends prepared via high-speed reactive extrusion. ACS Appl Polym Mater 2019;1:1410–19. doi:10.1021/ACSAPM.9B00177.
[148] Al-Itry R, Lamnawar K, Maazouz A. Reactive extrusion of PLA, PBAT with a multi-functional epoxide: physico-chemical and rheological properties. Eur Polym J 2014;58:90–102. doi:10.1016/J.eurpolymj.2014.06.013.
[149] Guan J, Zhang C, Xu P, Niu D, Yang W, Zhang X, et al. Biodegradable reactive compatibilizers for efficient in-situ compatibilization of poly (lactic acid)/poly (butylene adipate-terephthalate) blends. Int J Biol Macromol 2024;262:130029. doi:10.1016/J.IJBIOMAC.2024.130029.
[150] Tan Y, Cheng Y, Xu J, Wang H. Catalytic chemical recycling and upcycling of polyolefin plastics. Giant 2024;19:100307. doi:10.1016/J.GIANT.2024.100307.
[151] Cai K, Liu X, Ma X, Zhang J, Tu S, Feng J. Preparation of biodegradable PLA/PBAT blends with balanced toughness and strength by dynamic vulcanization process. Polymers 2024;291:126587. doi:10.1016/J.polymer.2023.126587.
[152] Clarke RW, Sandmeier T, Franklin KA, Reich D, Zhang X, Vengallur N, et al. Dynamic crosslinking compatibilizes immiscible mixed plastics. Nature 2023;616:731–9 2023 616:7958. doi:10.1038/s41586-023-05858-3.
[153] Salzano De Luna M, Filippone G. Effects of nanoparticles on the morphology of immiscible polymer blends – Challenges and opportunities. Eur Polym J 2016;79:198–218. doi:10.1016/J.eurpolymj.2016.02.023.
[154] Pegoretti A, Dorigato A. Polymer composites: reinforcing fillers. Encycl Polym Sci Technol 2019:1–72. doi:10.1002/0471440264.PST130.PUB2.
[155] Li Y, Zhang K, Nie M, Wang Q. Chapter 19 - application of compatibilized polymer blends in packaging. In: Compatibilization of polymer blends: micro and nano scale phase morphologies, interphase characterization, and properties. Elsevier; 2019. p. 539–61. doi:10.1016/B978-0-12-816006-0.00019-0.
[156] Shahdan D, Rosli NA, Chen RS, Ahmad S. A feasible compatibilization processing technique for improving the mechanical and thermal performance of rubbery biopolymer/graphene nanocomposites. Polymers 2022;14. doi:10.3390/POLYM14225009.
[157] Ahmadzadeh Y, Babaei A, Goudarzi A. Assessment of localization and degradation of ZnO nano-particles in the PLA/PCL biocompatible blend through a comprehensive rheological characterization. Polym Degrad Stab 2018;158:136–47. doi:10.1016/J.POLYMDEGRADSTAB.2018.10.007.
[158] Fredi G, Karimi Jafari M, Dorigato A, Bikiaris DN, Checchetto R, Favaro M, et al. Multifunctionality of reduced graphene oxide in bioderived polylactide/poly(Dodecylene Furanoate) nanocomposite films. Molecules 2021;26:2938. doi:10.3390/MOLECULES26102938.
[159] Fredi G, Karimi Jafari M, Dorigato A, Bikiaris DN, Pegoretti A. Improving the thermomechanical properties of poly(lactic acid) via reduced graphene oxide and bioderived poly(decamethylene 2,5-furandicarboxylate). Materials 2022;15:1316. doi:10.3390/MA15041316.
[160] Zembouai I, Kaci M, Zaidi L, Bruzaud S. Combined effects of Sepiolite and Cloisite 30B on morphology and properties of poly(3-hydroxybutyrate-co-3-hydroxyvalerate)/polylactide blends. Polym Degrad Stab 2018;153:47–52. doi:10.1016/J.POLYMDEGRADSTAB.2018.04.017.
[161] Leroy E, Jacquet P, Coativy G, Reguerre AL, Lourdin D. Compatibilization of starch-zein melt processed blends by an ionic liquid used as plasticizer. Carbohydr Polym 2012;89:955–63. doi:10.1016/j.carbpol.2012.04.044.
[162] Ozbay C, Gumus OY. Enhanced strength and toughness of polylactic acid by blending with modified natural rubber having acetate pendant group. J Elast Plast 2023;55:653–76. doi:10.1177/00952443231166143.

[163] Ding Y, Lu B, Wang P, Wang G, Ji J. PLA-PBAT-PLA tri-block copolymers: effective compatibilizers for promotion of the mechanical and rheological properties of PLA/PBAT blends. Polym Degrad Stab 2018;147:41–8. doi:10.1016/j.polymdegradstab.2017.11.012.
[164] Zhang B, Sun B, Bian X, Li G, Chen X. High melt strength and high toughness PLLA/PBS blends by copolymerization and in situ reactive compatibilization. Ind Eng Chem Res 2017;56:52–62. doi:10.1021/ACS.IECR.6B03151.
[165] Suchao-In K, Koombhongse P, Chirachanchai S. Starch grafted poly(butylene succinate) via conjugating reaction and its role on enhancing the compatibility. Carbohydr Polym 2014;102:95–102. doi:10.1016/J.CARBPOL.2013.11.001.
[166] Walallavita AS, Verbeek CJR, Lay MC. Biopolymer foams from Novatein thermoplastic protein and poly(lactic acid). J Appl Polym Sci 2017;134:45561. doi:10.1002/APP.45561.
[167] Urquijo J, Aranburu N, Dagréou S, Guerrica-Echevarría G, Eguiazábal JI. CNT-induced morphology and its effect on properties in PLA/PBAT-based nanocomposites. Eur Polym J 2017;93:545–55. doi:10.1016/J.EURPOLYMJ.2017.06.035.
[168] Yang X, Finne-Wistrand A, Hakkarainen M. Improved dispersion of grafted starch granules leads to lower water resistance for starch-g-PLA/PLA composites. Compos Sci Technol 2013;86:149–56. doi:10.1016/J.COMPSCITECH.2013.07.013.
[169] Musa L, Krishna Kumar N, Abd Rahim SZ, Mohamad Rasidi MS, Watson Rennie AE, Rahman R, et al. A review on the potential of polylactic acid based thermoplastic elastomer as filament material for fused deposition modelling. J Mater Res Technol 2022;20:2841–58. doi:10.1016/J.JMRT.2022.08.057.
[170] Wang H, Dong W, Li Y. Compatibilization of immiscible polymer blends using in situ formed Janus nanomicelles by reactive blending. ACS Macro Lett 2015;4:1398–403. doi:10.1021/acsmacrolett.5b00763.
[171] Chen D, Wang H, Li Y. Reactive compatibilization: formation of double-grafted copolymers by in situ binary grafting and their compatibilization effect. ACS Appl Mater Interfaces 2017;9:33091–9. doi:10.1021/acsami.7b08699.
[172] Wang H, Yang X, Fu Z, Zhao X, Li Y, Li J. Rheology of Nanosilica-compatibilized immiscible polymer blends: formation of a “heterogeneous network” facilitated by interfacially anchored hybrid Nanosilica. Macromolecules 2017;50:9494–506. doi:10.1021/acs.macromol.7b02143.
[173] Gong L, Hu Z, Chen Y, Zhang J, Cao W, Liu X, et al. Role of stereoregularity of polylactide on the microstructure and mechanical properties of reactive polylactide/poly(ε-Caprolactone)/triisocyanate bio-polyester blends. J Polym Sci 2025;63:2521–34. doi:10.1002/pol.20250032.
[174] Qiao H, Yang B, Zheng B, Chen M, Cardinaels R, Moldenaers P, et al. Janus nanoparticles as efficient interface compatibilizer in blends of polylactide and elastomers: importance of interfacial relaxation on toughening. J Rheol 2024;68:765–83. doi:10.1122/8.0000826.
[175] La Mantia FP, Morreale M, Botta L, Mistretta MC, Ceraulo M, Scaffaro R. Degradation of polymer blends: a brief review. Polym Degrad Stab 2017;145:79–92. doi:10.1016/j.polymdegradstab.2017.07.011.
[176] Soroudi A, Jakubowicz I. Recycling of bioplastics, their blends and biocomposites: a review. Eur Polym J 2013;49:2839–58. doi:10.1016/J.eurpolymj.2013.07.025.
[177] Ataeian P, Trinh BM, Mekonnen TH. Effect of pro-oxidants on the aerobic biodegradation, disintegration, and physio-mechanical properties of compostable polymers. J Appl Polym Sci 2024;141:e54970. doi:10.1002/APP.54970.
[178] Chang BP, Trinh BM, Tadele DT, Bandara N, Mekonnen TH. Natural antioxidant and antimicrobial agents and processing technologies for the design of active food packaging polymers. Polym Rev 2023;63:961–1013. doi:10.1080/15583724.2023.2234464.
[179] Trinh BM, Chang BP, Mekonnen TH. The barrier properties of sustainable multiphase and multicomponent packaging materials: a review. Prog Mater Sci 2023;133:101071. doi:10.1016/J.PMATSCI.2023.101071.
[180] Bezirhan Arikan E, Duygu Ozsoy HA. Review: investigation of bioplastics. J Civ Eng Arch 2015;9:188–92. doi:10.17265/1934-7359/2015.02.007.
[181] Tertyshnaya YV, Podzorova MV, Khramkova AV, Ovchinnikov VA, Krivandin AV. Structural rearrangements of polylactide/natural rubber composites during hydro- and biotic degradation. Polymers 2023;15:1930. doi:10.3390/POLYM15081930.
[182] Zaaba NF, Jaafar M. A review on degradation mechanisms of polylactic acid: hydrolytic, photodegradative, microbial, and enzymatic degradation. Polym Eng Sci 2020;60:2061–75. doi:10.1002/PEN.25511.
[183] Scott G‘. Gr.een’ polymers. Polym Degrad Stab 2000;68:1–7. doi:10.1016/S0141-3910(99)00182-2.
[184] Atiwesh G, Mikhael A, Parrish CC, Banoub J, Le TAT. Environmental impact of bioplastic use: a review. Heliyon 2021;7:e07918. doi:10.1016/J.heliyon.2021.E07918.
[185] Yu Y, Flury M. Unlocking the potentials of biodegradable plastics with proper management and evaluation at environmentally relevant concentrations. Npj Mater Sustain 2024;2:1–7 2024 2:1. doi:10.1038/s44296-024-00012-0.
[186] Piao Z, Asantewaa A, Boakye A, Yao Y. Environmental impacts of biodegradable microplastics. Nat Chem Eng 2024;1:661–9 2024 1:10. doi:10.1038/s44286-024-00127-0.
[187] Folino A, Pangallo D, Calabrò PS. Assessing bioplastics biodegradability by standard and research methods: current trends and open issues. J Env Chem Eng 2023;11:109424. doi:10.1016/j.jece.2023.109424.
[188] Samir A, Ashour FH, Hakim AAA, Bassyouni M. Recent advances in biodegradable polymers for sustainable applications. Npj Mater Degrad 2022;6:1–28 2022 6:1. doi:10.1038/s41529-022-00277-7.
[189] Zimmermann L, Göttlich S, Oehlmann J, Wagner M, Völker C. What are the drivers of microplastic toxicity? Comparing the toxicity of plastic chemicals and particles to Daphnia magna. Env Pollut 2020;267:115392. doi:10.1016/J.ENVPOL.2020.115392.
[190] Withana PA, Yuan X, Im D, Choi Y, Bank MS, Lin CSK, et al. Biodegradable plastics in soils: sources, degradation, and effects. Env Sci Process Impacts 2025. doi:10.1039/D4EM00754A.
[191] Narancic T, Verstichel S, Reddy Chaganti S, Morales-Gamez L, Kenny ST, De Wilde B, et al. Biodegradable plastic blends create new possibilities for end-of-life management of plastics but they are not a panacea for plastic pollution. Env Sci Technol 2018;52:10441–52. doi:10.1021/ACS.EST.8B02963.
[192] Palai B, Mohanty S, Nayak SK. A comparison on biodegradation behaviour of polylactic acid (PLA) based blown films by incorporating thermoplasticized starch (TPS) and poly (Butylene Succinate-co-Adipate) (PBSA) biopolymer in soil. J Polym Env 2021;29:2772–88. doi:10.1007/s10924-021-02055-z.
[193] Farias NC, Major I, Devine D, Brennan Fournet M, Pezzoli R, Farshbaf Taghinezhad S, et al. Multiple recycling of a PLA/PHB biopolymer blend for sustainable packaging applications: rheology-morphology, thermal, and mechanical performance analysis. Polym Eng Sci 2022;62:1764–74. doi:10.1002/pen.25962.
[194] McLauchlin AR, Ghita O, Gahkani A. Quantification of PLA contamination in PET during injection moulding by in-line NIR spectroscopy. Polym Test 2014;38:46–52. doi:10.1016/J.polymertesting.2014.06.007.
[195] Hamad K, Kaseem M, Deri F. Effect of recycling on rheological and mechanical properties of poly(lactic acid)/polystyrene polymer blend. J Mater Sci 2011;46:3013–19. doi:10.1007/S10853-010-5179-8/METRICS.
[196] Hamad K, Kaseem M, Deri F, Hamad K, Kaseem M, Deri F. Preparation and characterization of binary and ternary blends with poly(Lactic Acid), polystyrene, and acrylonitrile-butadiene-styrene. J Biomater Nanobiotechnol 2012;3:405–12. doi:10.4236/JBNB.2012.33040.
[197] Verhoogt H, Ramsay BA, Favis BD. Polymer blends containing poly(3-hydroxyalkanoate)s. Polymers 1994;35:5155–69. doi:10.1016/0032-3861(94)90465-0.
[198] Wang XL, Yang KK, Wang YZ. Properties of starch blends with biodegradable polymers. J Macromol Sci C: Polym Rev 2003;43:385–409. doi:10.1081/MC-120023911.
[199] La Mantia FP, Botta L, Morreale M, Scaffaro R. Effect of small amounts of poly(lactic acid) on the recycling of poly(ethylene terephthalate) bottles. Polym Degrad Stab 2012;97:21–4. doi:10.1016/J.polymdegradstab.2011.10.017.
[200] Lamberti FM, Román-Ramírez LA, Wood J. Recycling of bioplastics: routes and benefits. J Polym Env 2020;28:2551–71 2020 28:10. doi:10.1007/S10924-020-01795-8.
[201] Grigore ME. Methods of recycling, properties and applications of recycled thermoplastic polymers. Recycling 2017;2:24. doi:10.3390/recycling2040024.
[202] Papadimitriou I, Gialampoukidis I, Vrochidis S, Kompatsiaris I. AI methods in materials design, discovery and manufacturing: a review. Comput Mater Sci 2024;235:112793. doi:10.1016/j.commatsci.2024.112793.
[203] Wei J, Chu X, Sun XY, Xu K, Deng HX, Chen J, et al. Machine learning in materials science. InfoMat 2019;1:338–58. doi:10.1002/inf2.12028.
[204] Mueller T, Kusne AG, Ramprasad R. Machine learning in materials science. Rev Comput Chem 2016;29:186–273. doi:10.1002/9781119148739.CH4.
[205] Alafeef M, Srivastava I, Pan D. Machine learning for precision breast cancer diagnosis and prediction of the nanoparticle cellular internalization. ACS Sens 2020;5:1689–98. doi:10.1021/ACSSensors.0C00329/suppl_file/SE0C00329_SI_001.PDF.
[206] Ge W, De Silva R, Fan Y, Sisson SA, Stenzel MH. Machine learning in polymer research. Adv Maters 2025;37:2413695. doi:10.1002/adma.202413695.
[207] Raissi M, Perdikaris P, Karniadakis GE. Physics-informed neural networks: a deep learning framework for solving forward and inverse problems involving nonlinear partial differential equations. J Comput Phys 2019;378:686–707. doi:10.1016/J.JCP.2018.10.045.
[208] Malashin I, Tynchenko V, Gantimurov A, Nelyub V, Borodulin A. Physics-informed neural networks in polymers: a review. Polymers 2025;17:1108 1108 2025;17. doi:10.3390/polym17081108.
[209] da Silva LRR, Pimenov DY, da Silva RB, Ercetin A, Giasin K. Review of applications of digital twins and industry 4.0 for machining. J Manuf Mater Process 2025;9:211. doi:10.3390/jmmp9070211.
[210] Yan C, Li G. The rise of machine learning in polymer discovery. Adv Intell Syst 2023;5:2200243. doi:10.1002/aisy.202200243.
[211] Takada S, Suzuki T, Takebayashi Y, Ono T, Yoda S. Machine learning assisted optimization of blending process of polyphenylene sulfide with elastomer using high speed twin screw extruder. Sci Rep 2021;11:1–9 2021 11:1. doi:10.1038/s41598-021-03513-3.
[212] Mulenga TK, Ude AU, Vivekanandhan C. Techniques for modelling and optimizing the mechanical properties of natural fiber composites: a review. Fibers 2021;9:1–17. doi:10.3390/fib9010006.
[213] Gu GX, Chen CT, Richmond DJ, Buehler MJ. Bioinspired hierarchical composite design using machine learning: simulation, additive manufacturing, and experiment. Mater Horiz 2018;5:939–45. doi:10.1039/C8MH00653A.
[214] Malashin I, Martysyuk D, Tynchenko V, Gantimurov A, Semikolenov A, Nelyub V, et al. Machine learning-based process optimization in biopolymer manufacturing: a review. Polymers 2024;16:3368. doi:10.3390/POLYM16233368.
[215] Ebrahimzade I, Ebrahimi-Nik M, Rohani A, Tedesco S. Towards monitoring

biodegradation of starch-based bioplastic in anaerobic condition: finding a proper kinetic model. Bioresour Technol 2022;347:126661. doi:10.1016/J.BIORTECH.2021.126661.
[216] Ibarra-Pérez D, Faba S, Hernández-Muñoz V, Smith C, Galotto MJ, Garmulewicz A. Predicting the composition and mechanical properties of seaweed bioplastics from the scientific literature: a machine learning approach for modeling sparse data. Appl Sci 2023;13:11841. doi:10.3390/APP132111841/S1.
[217] Chen T, Pang Z, He S, Li Y, Shrestha S, Little JM, et al. Machine intelligence-accelerated discovery of all-natural plastic substitutes. Nat Nanotechnol 2024;19:782–91 2024 19:6. doi:10.1038/s41565-024-01635-z.
[218] Wang J, Ayari MA, Khandakar A, Chowdhury MEH, Zaman SMAU, Rahman T, et al. Estimating the relative crystallinity of biodegradable polylactic acid and polyglycolide polymer composites by machine learning methodologies. Polymers 2022;14:527. doi:10.3390/POLYM14030527/S1.
[219] Oliaei E, Heidari BS, Davachi SM, Bahrami M, Davoodi S, Hejazi I, et al. Warpage and shrinkage optimization of injection-molded plastic spoon parts for biodegradable polymers using Taguchi, ANOVA and Artificial Neural Network methods. J Mater Sci Technol 2016;32:710–20. doi:10.1016/J.JMST.2016.05.010.
[220] Kuenneth C, Lalonde J, Marrone BL, Iverson CN, Ramprasad R, Pilania G. Bioplastic design using multitask deep neural networks. Commun Mater 2022;3:1–10 2022 3:1. doi:10.1038/s43246-022-00319-2.
[221] Sofian A, Sun X, Gupta VK, Berenjian A, Xia A, Ma Z, et al. Advances, synergy, and perspectives of machine learning and biobased polymers for energy, fuels, and biochemicals for a sustainable future. Energy Fuels 2024;38:1593–617. doi:10.1021/ACS.energyfuels.3C03842.
[222] Cencer MM, Moore JS, Assary RS. Machine learning for polymeric materials: an introduction. Polym Int 2022;71:537–42. doi:10.1002/PI.6345.
[223] Meyer TA, Ramirez C, Tamasi MJ, Gormley AJ. A user's guide to machine learning for polymeric biomaterials. ACS Polym Au 2023;3:141–57. doi:10.1021/ACSPOLYMERSAU.2C00037.
[224] Martin TB, Audus DJ. Emerging trends in machine learning: a polymer perspective. ACS Polym Au 2023;3:239–58. doi:10.1021/ACSpolymersau.2C00053.
[225] Stach E, DeCost B, Kusne AG, Hattrick-Simpers J, Brown KA, Reyes KG, et al. Autonomous experimentation systems for materials development: a community perspective. Matter 2021;4:2702–26. doi:10.1016/J.MATT.2021.06.036.
[226] Hu B, Lin A, Brinson LC. ChemProps: a RESTful API enabled database for composite polymer name standardization. J Cheminform 2021;13:1–13. doi:10.1186/S13321-021-00502-6.
[227] Huan TD, Mannodi-Kanakkithodi A, Kim C, Sharma V, Pilania G, Ramprasad R. A polymer dataset for accelerated property prediction and design. Sci Data 2016;3:1–10. doi:10.1038/sdata.2016.12.
[228] Ma R, Liu Z, Zhang Q, Liu Z, Luo T. Evaluating polymer representations via quantifying structure-property relationships. J Chem Inf Model 2019;59:3110–19. doi:10.1021/ACS.JCIM.9B00358.
[229] Chi M, Gargouri R, Schrader T, Damak K, Maâlej R, Sierka M. Atomistic descriptors for machine learning models of solubility parameters for small molecules and polymers. Polymers 2022;14:26. doi:10.3390/POLYM14010026.
[230] Miccio LA. Understanding polymers through transfer learning and explainable AI. Appl Sci 2024;14:10413. doi:10.3390/APP142210413.
[231] Oviedo F, Ferres JL, Buonassisi T, Butler KT. Interpretable and explainable machine learning for materials science and chemistry. Acc Mater Res 2022;3:597–607. doi:10.1021/ACCOUNTSMR.1C00244.
[232] Tang H, Yue T, Li Y. Uncertainty quantification in machine learning for polymer properties: a benchmark study. ChemRxiv 2025. doi:10.26434/CHEMRXIV-2024-7LGGJ-V2.